Selective production of difluorodimethyl ether from chlorodifluoromethane – A kinetic study using a well-mixed batch absorber

Rasmika Prithipal

[BSc. Eng]

In fulfillment of the requirements for the degree

Master of Science in Engineering, Chemical Engineering,

University of KwaZulu-Natal

March 2013

Name of supervisor: Prof. D. Ramjugernath

Name of co-supervisor: Prof. M. Starzak

As the candidate's Supervisor I agree/do not agree to the submission of this thesis.

_____ _____

Prof. D. Ramjugernath Prof. M. Starzak

DECLARATION

I ……. declare that

(i) The research reported in this dissertation, except where otherwise indicated, is my original work.

(ii) This dissertation has not been submitted for any degree or examination at any other university.

(iii) This dissertation does not contain other persons' data, pictures, graphs or other information, unless specifically acknowledged as being sourced from other persons.

(iv) This dissertation does not contain other persons' writing, unless specifically acknowledged as being sourced from other researchers. Where other written sources have been quoted, then:

a) their words have been re-written but the general information attributed to them has been referenced;

b) where their exact words have been used, their writing has been placed inside quotation marks, and referenced.

(v) Where I have reproduced a publication of which I am an author, co-author or editor, I have indicated in detail which part of the publication was actually written by myself alone and have fully referenced such publications.

(vi) This dissertation/thesis does not contain text, graphics or tables copied and pasted from the Internet, unless specifically acknowledged, and the source being detailed in the dissertation/thesis and in the References sections.

Signed:_____

Acknowledgements

To my parents, Anil and Lalitha Prithipal, and my sister, Arisha Prithipal, thank you for your love, support, and words of encouragement.

I would like to thank Prof D. Ramjugernath for affording me the opportunity to work on this project. Sincere thanks to Prof M. Starzak for his time, constant guidance and knowledge throughout the project. I would also like to thank Dr. David Lokhat for his assistance and guidance. It is greatly appreciated. Many thanks extend to Prof. J.D. Raal for his assistance with the thermodynamic derivation and to Dr. Daniel Teclu for kindly imparting his knowledge of solution chemistry. I would like to also thank the technical staff at the School of Chemical Engineering: Rekha Maharaj, Sadha Naidoo, Dudley Naidoo, Merlien Reddy, Danny Singh, Thobekile Mofokeng, Preyothen Nayager and as well the workshop staff, for their much needed assistance, experience and willingness to help. Sincere gratitude is expressed towards the Pollution Research Group: Dr. K.M. Foxon, Mr. C.J. Brouckaert and Kavisha Nandhlal for the dissolved oxygen probe used in this project. I am also thankful to Bilal Kazi for kindly assisting me in the laboratory. To all my friends, thank you for your great company and the good laughs we shared through trying days.

Lastly I would like to thank the National Research Foundation (NRF) for their financial support.

ABSTRACT

The gas-liquid reaction between chlorodifluoromethane (R-22) and methanol, in the presence of sodium hydroxide, was investigated in an isothermal, stirred, semi-batch reactor. The objective of the study was to develop a model for the reaction and to identify the kinetic parameters. Reactor temperature was varied from 283 to 303 K, with inlet R-22 partial pressures between 40.5 and 60.8 kPa (absolute). Solutions containing sodium hydroxide concentrations of between 1.5 and 2.5 $mol \cdot dm^{-3}$ were charged into the reactor prior to each experiment. Preliminary investigations using the R-22-methanol system revealed that stainless steel was an inappropriate choice of material for the reactor as it displayed catalytic tendencies toward trimethyl orthoformate formation. Consequently, the reactor was constructed from glass and was equipped with an internal cooling coil, a single heating jacket and a temperature control unit. Liquid samples that were withdrawn from the reactor were degassed under vacuum to remove residual chlorodifluoromethane, and thereby inhibit further reaction. Spectrophotometry was used to analyze the liquid samples to determine the concentration of chloride ions in solution. The products obtained were difluorodimethyl ether (major product) and trimethyl orthoformate (by-product) as well as sodium chloride and sodium fluoride salts. Difluorodimethyl ether is a potential replacement for ozone depleting CFC refrigerants. A Box-Behnken experimental design was used to investigate the effect of reaction conditions on the product distribution. Variations in the reaction temperature, initial concentration of sodium hydroxide and inlet partial pressure of R-22 were considered.

The modeling of the gas-liquid reactions was based on the α-dehydrohalogenation mechanism. Since gas solubility in a liquid decreases in the presence of dissolved salts, the "salting-out" effect on mass transfer was included in the reactor model. Sechenov coefficients for sodium chloride and sodium fluoride were combined to give a salt Sechenov coefficient K_{salt}. It was known from the literature that the presence of precipitated salts causes inefficient mixing and inhibits mass transfer, particularly in this system due to the relatively low salt solubilities in methanol. This mixing effect was also included in the appropriate mass transfer terms of the reactor model. The experimental data was fitted to a proposed kinetic scheme. Kinetic parameters for each of the proposed reactions, the Sechenov 'salting out' coefficients and the mixing parameter were obtained through the use of a non-linear, least-squares optimization algorithm. For the kinetic study, activation energies of 89.12 and 45.83 $kJ \cdot mol^{-1}$ were obtained for the difluorodimethyl ether and trimethyl orthoformate formation reactions, respectively, with a Sechenov salt coefficient of 0.712 and a mixing parameter of 22.43.

TABLE OF CONTENTS

List of Figures

CHAPTER 1

CHAPTER 2

CHAPTER 3

CHAPTER 4

CHAPTER 5

APPENDIX F

List of Tables

CHAPTER 2

CHAPTER 3

CHAPTER 4

CHAPTER 5

APPENDIX B

APPENDIX C

APPENDIX D

APPENDIX E

NOMENCLATURE

A	Absorbance	%
A	Pre-exponential factor	-
A_c	Surface area of coil	m^2
A_i	Peak area	m^2
C	Concentration	$mol \cdot dm^{-3}$
C^*	Oxygen saturated concentration	$mol \cdot dm^{-3}$
C_0	Initial concentration at zero time	$mol \cdot dm^{-3}$
C_p	Heat capacity	$J \cdot mol^{-1} \cdot K^{-1}$
d_b	Average bubble size	m
d_c	Coil tube diameter	m
d_{imp}	Impeller diameter	m
d_t	Tank diameter	m
D	Diffusivity	$m^2 \cdot s^{-1}$
E_a	Activation energy	$kJ \cdot mol^{-1}$
E_A	Enhancement factor	-
F	Faraday's constant	$C \cdot mol^{-1}$
g	Gravitational acceleration	$m^2 \cdot s^{-1}$
Ha	Hatta number	-
h_i	Heat transfer coefficient	$W \cdot m^{-2} \cdot K^{-1}$
H^{cc}	Concentration-based Henry's law constant	-
H^{pc}	Henry's law constant or partition coefficient	$dm^3 \cdot kPa \cdot mol^{-1}$
H_f	Enthalpy of formation	$kJ \cdot mol^{-1}$
H_r	Enthalpy of reaction	$kJ \cdot mol^{-1}$
H_s	Enthalpy of solution	$kJ \cdot mol^{-1}$
K	Sechenov coefficient	-
k_1	Reaction rate constant for reaction 1	$(dm^3 \cdot mol^{-1})^2 \cdot min^{-1}$
k_2	Reaction rate constant for reaction 2	$(dm^3 \cdot mol^{-1}) \cdot min^{-1}$
k_l	Thermal conductivity	$W \cdot m^{-1} \cdot K^{-1}$
k_L	Liquid-side mass transfer coefficient	$m \cdot min^{-1}$
$k_L a$	Volumetric mass transfer coefficient	min^{-1}
k_M	Mass transfer coefficient	min^{-1}
k_{probe}	Sensor lag constant	min^{-1}

L	Length of coil	m
m	Mixing parameter	–
$\dot{m}$	Mass flow rate of coolant	$kg \cdot s^{-1}$
M	Molecular mass	$g \cdot mol^{-1}$
$\dot{n}$	Molar flow rate	$mol \cdot min^{-1}$
$n_{\pm}$	Valence of cation/anion	-
N	Impeller speed	rps
P	Power	W
P_i	Partial pressure	Pa
Q	Volumetric flow rate	$m^3 \cdot min^{-1}$
Q_r	heat rate	W
r	Rate of reaction	$mol \cdot dm^{-3} \cdot min^{-1}$
R	Universal gas constant	$J \cdot mol^{-1} \cdot K^{-1}$
R_i	Net rate of change for component *i*	$mol \cdot dm^{-3} \cdot min^{-1}$
S	Selectivity	%
t	Time	min
T	Transmittance (Section 4.3.)	%
T	Temperature	K
U	Overall heat transfer coefficient	$W \cdot m^{-2} \cdot K^{-1}$
V	Volume	dm^3
V^m	Molar volume of mixture	$dm^3 \cdot mol^{-1}$
V^s	Superficial gas velocity	$m \cdot s^{-1}$
x	Mole fraction	-
X	Conversion	%
Y	Yield	%

Greek letters

δ	Film thickness	m
σ	Surface tension	$N \cdot m^{-1}$
π	Pi	-
ρ	Density	$kg \cdot m^{-3}$
Φ	Gas-holdup (dimensionless)	-
σ_i^2	Variance of data point *i*	-
μ	Solvent viscosity	Pa·s
χ	Solvent association parameter	-
$\lambda_{\pm}$	Limiting ionic conductances	$(A \cdot cm^{-2})(V \cdot cm^{-1})(g\text{-}equiv \cdot cm^{-3})$
ν	Stoichiometric coefficient	-

Subscripts and Superscripts

b	Bulk phase
G	Gas
L	Liquid
m	Order of reactant 1
n	Order of reactant 2
LM	Logarithmic mean

CHAPTER 1

INTRODUCTION

1.1. Background and motivation

Chlorodifluoromethane (R-22) has been widely used as an industrial and domestic refrigerant since the 1950s (Calm, 2008). The hydro-chlorofluorocarbon (HCFC) molecule exhibits acute stability with an atmospheric lifetime of 15.3 years (Tiwary and Collins, 2010). The chlorine atom in a molecule of R-22 gas reacts with ozone in the stratosphere, causing the destruction of the ozone layer (Halimic et al., 2003).

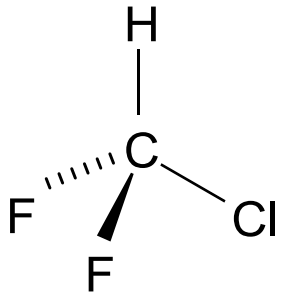

Figure 1-1a). A molecule of R-22

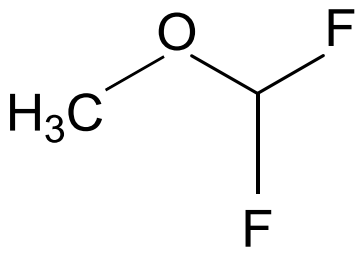

Figure 1-1b). A molecule of difluorodimethyl ether

The potential of R-22 gas to deplete the ozone layer has deemed it unsuitable for use as a general refrigerant. Hydrofluoroethers (HFEs) represent potential alternatives to HCFCs, possessing physical and thermodynamical properties that are suitable for refrigeration applications. HFEs are less stable than R-22 and do not contribute to ozone depletion as they are unlikely to reach the stratosphere. A typical example of this new generation of refrigerants, difluorodimethyl ether, can be conveniently produced via the reaction of R-22 and methanol in the presence of sodium hydroxide. This synthesis also provides a means of converting current reserves of R-22 into a useful product (Nishiumi and Kato, 2003).

The synthesis of difluorodimethyl ether from R-22 and methanol in the presence of sodium hydroxide has formed the basis of numerous studies such as that of Lee et al. (2001) and Nishiumi and Kato (2003). Lee et al. (2001) investigated the effect of reaction temperature, concentration of

base and the chemical nature of the base on the yield of difluorodimethyl ether. The authors found that lower reaction temperatures and base concentrations favoured the formation of difluorodimethyl ether (Lee et al., 2001). They also found that the use of alkali metal carbonates resulted in superior difluorodimethyl ether yields in comparison to the alkali metal hydroxides; however, the synthesis required reaction temperatures well above the normal boiling point of methanol and high pressures (Lee et al., 2001). Kato and Nishiumi (2003) studied the aforementioned reaction at 303 K. A stationary-state reaction model was developed, which included the mass transfer characteristics of the system. An overall volumetric mass transfer coefficient and rate constant were reported only at 303 K. There is a lack of credible kinetic data in the literature for this reaction system over a wider range of operating conditions. Therefore, the collection and analysis of rate data for the reaction of R-22 and methanol in the presence of sodium hydroxide were carried out using a stirred semi-batch gas-liquid reactor. A Box-Behnken experimental design, comprising 12 experiments, was used for the generation of the kinetic data. Reaction temperature, partial pressure of R-22 and initial sodium hydroxide concentration were varied simultaneously according to the design.

1.2. Objectives

The overall objective of the project was to develop a kinetic model for the reaction of R-22 and methanol in the presence of sodium hydroxide and to identify the kinetic parameters. In order to achieve this objective, a number of different tasks had to be carried out. Firstly, the effect of reaction conditions on the product distribution had to be investigated using a statistical experimental design. Apart from yielding important information regarding the most preferable operating range, this stage also served to generate kinetic data for the identification procedures. Next an appropriate mathematical model had to be developed for the three-phase reactor, taking into account gas-liquid interfacial mass transfer as well as reactions in the bulk liquid. Thereafter, the rate data generated using the statistical experimental design had to be critically evaluated and the kinetic parameters of the gas-liquid reactions had to be determined in the temperature range of 283.15 -303.15 K.

1.3. Thesis outline

This chapter has served as a brief introduction to the reaction system considered in this investigation. It has also identified the main objectives associated with this project. Chapter two

provides further detail on fluoroorganic compounds, the chemistry of ozone destruction and the use of fluorinated ethers as replacement refrigerants. In chapter three, the development of the kinetic model and the reactor modeling are presented. The chapter also provides a theoretical understanding of the concepts to be discussed in chapters four and five. Chapter four discusses the equipment used together with the materials and methods that were required. The presentation and discussion of the results is dealt with in chapter five. The conclusions drawn from the research and recommendations for future work are given in chapter six.

CHAPTER 2

LITERATURE REVIEW

2.1. Fluoroorganic compounds: characteristics

The skeletal backbone of most fluorochemical refrigerants is methane and ethane. The elements of concern in the two molecules are carbon (C) and hydrogen (H). Chlorination and/or fluorination of either molecule generate refrigerant groups such as chlorofluorocarbons (CFCs), hydro-chlorofluorocarbons (HCFCs), hydro-fluorocarbons (HFCs) and perfluorocarbons (PFCs) (Whitman et al., 2005). Table 2-1 lists examples of each refrigerant group (Whitman et al., 2005).

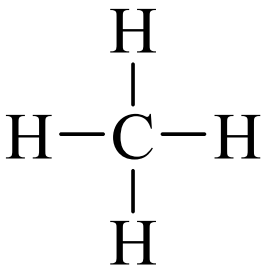

Figure 2-1. Methane molecule

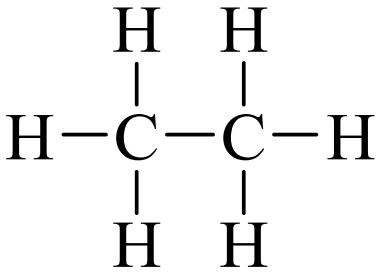

Figure 2-2. Ethane molecule

Table 2-1. Examples of refrigerants that are CFCs, HCFCs and HFCs (Whitman et al., 2005)

Group	Refrigerant name	Chemical Formula
CFCs	R-11	$CCl F_2$
	R-12	CCl_2F_2
	R-113	CCl_2FCClF_2
	R-114	$CClF_2CClF_2$
	R-115	$CClF_2CF_3$
HCFCs	R-22	$CHClF_2$
	R-123	$CHCl_2CF_3$
	R-124	$CHClFCF_3$
	R-142b	CH_3CClF_2
HFCs	R-125	CHF_2CF_3
	R-134a	CH_2FCF_3
	R-23	CHF_3
	R-32	CH_2F_2
	R-143a	CH_3CF_3
	R-152a	CH_3CHF_2

The above-mentioned refrigerants are fluoroorganic compounds. The bond between the carbon and fluorine atom in fluoroorganic compounds is radically stable (Kirsch, 2004). The stability can be attributed to the overlap of the fluorine 2s and 2p orbitals and the respective carbon orbital; as well as the fluorine substituent that blocks the central carbon atom (Kirsch, 2004). The bond is also physically characteristic of a high polarity and electronegativity (Kirsch, 2004). A comparison of physical characteristics between carbon and various halogens is listed in Table 2-2 (Kirsch, 2004).

Table 2-2. Comparison of physical characteristics between carbon and various halogens (Kirsch, 2004)

X	H	F	Cl	Br	I	C
Bond Length C-X / pm	109	138	177	194	213	
Binding energy C-X / kcal·mol^{-1}	98	115.7	77.2	64.3	50.7	~83
Electronegativity	2.2	3.98	3.16	2.96	2.66	2.55
Dipole moment, μ, C-X / D	(0.4)	1.41	1.46	1.38	1.19	-
Van der Waals radius / pm	120	147	175	185	198	-
Atom polarizability, a / 10^{-24} cm^{-3}	0.667	0.557	2.18	3.05	4.7	-

2.2. Chemistry of ozone destruction

Ozone (O_3) is produced by the interaction of sunlight with oxygen (Parker and Morrissey, 2003). It is a rare molecular structure of oxygen, shielding the earth from the ultraviolet radiation generated by the sun. Approximately 90% of the ozone is found in the stratosphere (Parker and Morrissey, 2003). The stratosphere is that part of the atmosphere in which chemical reactions, mainly due to the presence of chlorine radicals, take place (Mohanraj et al., 2009). It stretches from 10 km above the surface of the earth to approximately 50 km beyond (Mohanraj et al., 2009). In this region, a relatively high concentration of ozone can be found.

Chlorofluorocarbons, perfluorocarbons and halofluorocarbons, to list a few, cannot be degraded below the stratosphere because of their acute chemical stability. As a result the compounds enter the stratosphere. Chlorofluorocarbons for example undergo photolytic dissociation in the stratosphere despite showing high stability in the low level atmosphere (Kirsch, 2004). The carbon-chlorine bond terminates releasing the chlorine radical. The chlorine radical is then free to react with ozone (O_3) to form oxygen (O_2) and chlorooxide radicals ($ClO^{\bullet}$). The chlorooxide radical can be converted back into chlorine by reaction with nitrous oxide (NO), nitric oxide (NO_2), atomic oxygen (O) or hydroperoxy radicals ($HOO^{\bullet}$**).** The chlorine radical may also react with methane present in the stratosphere to form HCl, which in turn may react with hydroxyl radicals to re-form the chlorine radical. Figure 2-3 describes graphically the catalytic process by which the ozone is depleted. The catalytic process described was summarized from the literature (Kirsch, 2004).

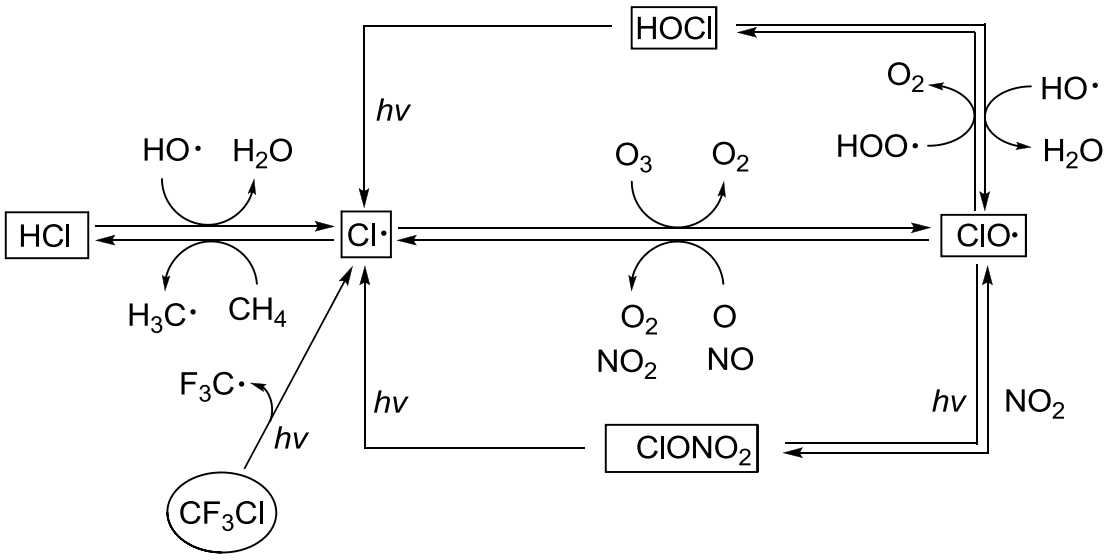

Figure 2-3. Catalytic process instrumental in the depletion of the ozone layer (Kirsch, 2004)

2.2.1. Ozone depleting potential

Ozone depleting potential (ODP) is a relative measure of the magnitude of degradation to the ozone layer by a substance capable of depleting the ozone layer (a gas) (Halimic et al., 2009). The base reference used is trichlorofluoromethane (R-11) with an ODP of 1.0 (Halimic et al., 2009). The ODP of R-22 relative to R-11 is 0.05 (Tiwary and Collins, 2010). Table 2-3 lists the ODP of popular refrigerants (hydrocarbons) and their lifespan in the stratosphere. Of this list, the least harmful refrigerants are HFC-125, HFC-134a, HFC-143a and HFC-152a with no ODP. Carbon tetrachloride is the most harmful refrigerant with an ODP of 1.1. HFEs possess a zero ODP due to the absence of the chlorine atom in these refrigerants.

Table 2-3.Ozone depleting potential and atmospheric lifetime of popular refrigerants (Tiwary and Collins, 2010)

Halocarbon	ODP	Lifetime / years
CFC-11	1.00 (by definition)	60
12	0.9	120
113	0.85	90
114	0.6	200
115	0.37	400
HCFC-22	0.05	15.3
123	0.017	1.6
124	0.02	6.6
HFC-125	0	28.1
134a	0	15.5
HCFC-141b	0.095	7.8
142b	0.05	19.1
HFC-143a	0	41
152a	0	1.7
Carbon tetrachloride (CCl4)	1.1	50
Methyl chloroform (CH_3CCl_3)	0.14	6.3

2.2.2. Global Warming Potential

Global warming potential (GWP) is defined as „the ratio of calculated steady state net infrared flux change forcing at the troposphere for each unit mass of any halocarbon emitted relative to the same for CFC-11" (Banks et al., 2000). Anthropogenic substances emitted into the environment cause the temperature of the earth"s surface to increase. Such a phenomenon is referred to as global warming (Tsai W., 2005). A comparison of the GWP of HFEs listed in Table 2-4 to the GWP of common refrigerants depicted graphically in Figure 2-4 indicates a relatively greater GWP for CFCs and HCFCs. Figure 2-4 illustrates a GWP range between 2000 and 12000 for CFCs and HCFCs whereas Table 2-4 lists a range between 39 and 15600 for HFEs.

Table 2-4. Atmospheric lifetimes and global warming potentials of HFEs (Tsai W., 2005)

HFEs	Atmospheric lifetime (year)[a]	GWP[b]	Degradation products	Reference(s)
HFE-125	165, 165.2	15600, 14000	$CF_3OC(O)F$, CF_2O	[62–64]
HFE-134	24.8, 29.7	5800, 5720	$CHF_2OC(O)F$, CF_2O	[62–64]
HFE-143a	5.7	656	$CF_3OC(O)H$, CO_2	[62,63]
HFE-227me	40, 8	4500	$FC(O)OCF_3$, $CF_3C(O)F$	[5,65,66]
HFE-245mf	2.6, 4.9	649	NA[c]	[10,12,67]
HFE-245mc	2.9, 5.1	697	NA[c]	[10,67]
HFE-254pc	1.4, 2.6	353	NA[c]	[10,67]
HFE-356mec	2.6, 0.94	99	NA[c]	[10,67]
HFE-356mff	0.294	39	CF_3CH_2OCHO	[63,68]
HFE-7000 (HFE-347mcc)	4.7	450	n-$C_3F_7OC(O)H$	[69]
HFE-7100 (HFE-449mccc)	5	410	$C_4F_9OC(O)H$	[70]
HFE-7200 (HFE-569mccc)	0.77	60	$C_4F_9OC(O)CH_3$, $C_4F_9OC(O)H$	[71]
HFE-7500	2.2	100	n-$C_3F_7CF(OC(O)CH_3)CF(CF_3)_2$, n-$C_3F_7CF(OC(O)HCF)(CF_3)_2$	[72]

[a] Estimated values, which can be mainly calculated by the reciprocal of the pseudo-first order rate constant for its removal by OH radicals in the troposphere.
[b] Global warming potential with 100-year time horizon (relative to GWP of $CO_2 = 1$).
[c] Not available.

The atmospheric lifetime of CFCs, HCFCs, HFCs and HFEs is shown graphically in Figure 2-4 (Sekiya and Misaki, 2000).

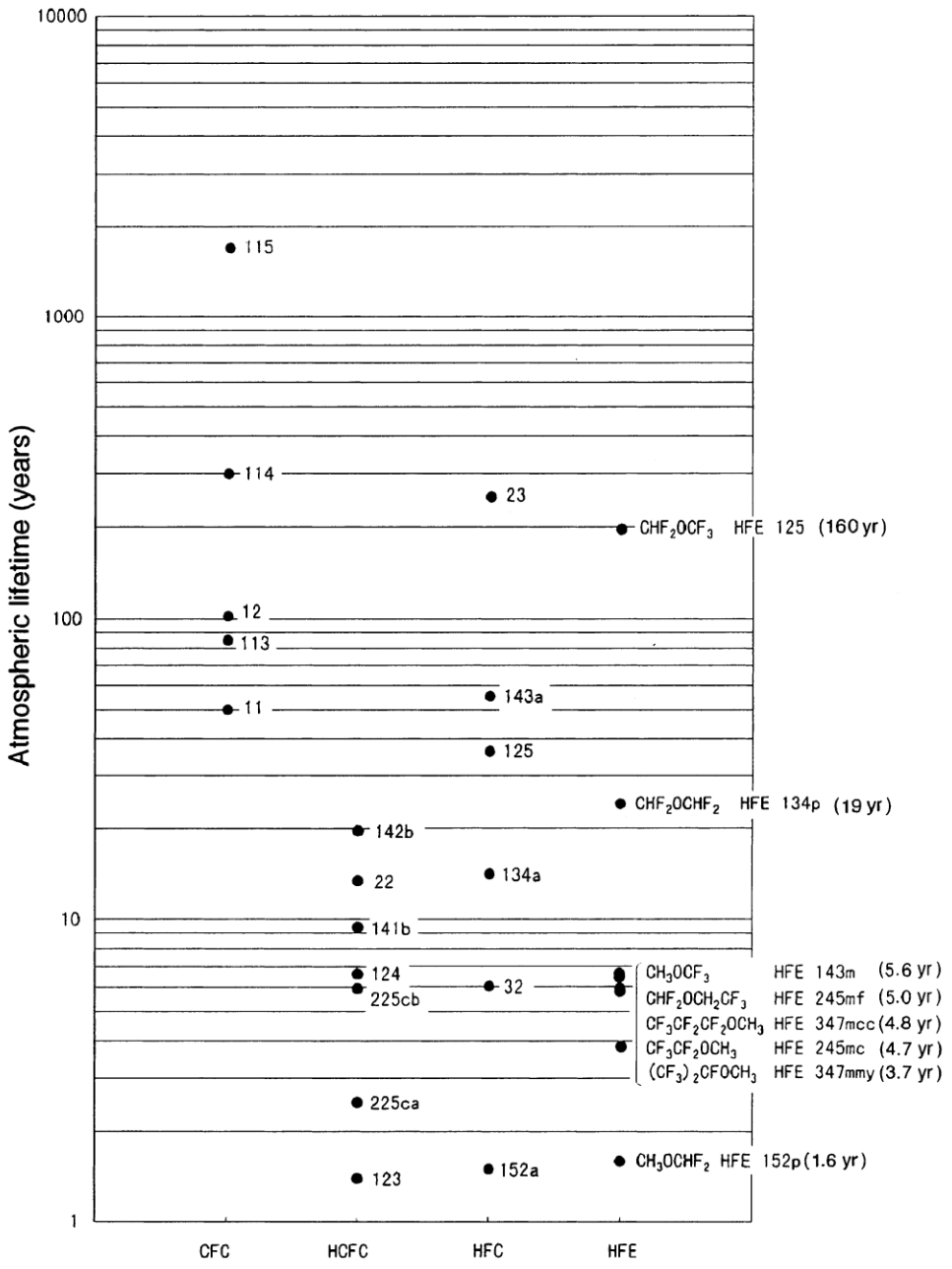

Figure 2-4.Atmospheric lifetimes of CFCs, HCFCs, HFCs and HFEs (Sekiya and Misaki, 2000)

2.3. Properties and Characteristics of refrigerants

A substance, be it a fluoroorganic compound or a natural chemical (such as carbon dioxide), may be categorized as a refrigerant if it exhibits the necessary properties that define a refrigerant. Thermodynamic, physical and chemical properties are all important attributes of a good refrigerant.

2.3.1. Physical Properties

Table 2-5 lists the physical and thermo physical properties that are desirable of a good refrigerant (Sapali, 2009; Mohanraj et al., 2009).

Table 2-5. Physical and thermo physical properties of a good refrigerant (Sapali, 2009; Mohanraj et al., 2009)

Physical Property	Characteristic
Specific volume	Low
Viscosity	Low
Thermal conductivity	High
Dielectric strength	High

2.3.2. Chemical Properties

Chemical properties are important to ensure that refrigeration systems operate safely. The properties listed in Table 2-6 are summarized from the literature (Sapali, 2009; Mohanraj et al., 2009).

Table 2-6. Chemical properties of a good refrigerant (Sapali, 2009; Mohanraj et al., 2009)

Chemical Property	Characteristic
Toxicity	Non-toxic
Flammability	Low, must not be inflammable
Flashpoint	< 294.35 K
Stability	Unreactive with metals, Must be able to withstand the effect of pressure and temperature without decomposition
Corrosiveness	Non-corrosive
Leak detection (smell)	Must be easy to detect a leak

2.3.3. Thermodynamic properties

Table 2-7 lists the thermodynamic properties characteristic of a good refrigerant (Sapali, 2009; Mohanraj et al., 2009).

Table 2-7. Thermodynamic properties of a good refrigerant (Sapali, 2009; Mohanraj et al., 2009)

Thermodynamic Property	Characteristic
Latent heat of evaporation	High
Boiling point	Low
Freezing point	Lower than system temperature
Evaporating pressure	Slightly greater than atmospheric
Condensing pressure	Low
Critical temperature and pressure	Must be greater than condensing temperature

A high latent heat of evaporation is preferable because a lower power requirement implies that less refrigerant can be used to produce greater cooling effects (Sapali, 2009). A freezing point temperature that is lower than evaporating temperature will prevent freezing of the refrigerant (Sapali, 2009; Mohanraj et al., 2009). A low condensing pressure will simplify construction and reduce leakages (Sapali, 2009).

2.3.4. An ideal refrigerant

Table 2-8 lists properties that are characteristic of ideal refrigerants; summarized from the literature (Sapali, 2009).

Table 2-8. Properties of an ideal refrigerant (Sapali, 2009)

Property	Description	Specification
Thermodynamic	ODP	Zero
	GWP	Zero
	Latent heat of evaporation	High
	Critical pressure	High
	Critical temperature	High
	Condensing pressure	High
	Evaporating pressure	High
Chemical	Toxicity	Non-toxic
	Flammability	Non-flammable
	Corrosiveness	Non-corrosive
	Miscibility with oil	Low
Physical	Leak detection	Easy
	Cost and availability	Cheap and available

2.4. Substitution of chlorine containing fluoroorganic compounds with HFEs

Hydrofluoroethers are regarded as the new generation of eco-friendly refrigerants. Their potential as candidate alternatives to CFCs, HCFCs and PFCs was investigated by Sekiya and Misaki (2000) as part of the "development of new refrigerants, blowing agents and cleaning solvents for effective use of energy" initiative. As a part of their investigation, 150 fluorinated ethers were evaluated as alternatives to blowing agents, refrigerants and cleaning solvents. This review is concerned specifically with fluorinated ethers as refrigerant replacements.

It is imperative that the profile of the fluorinated ether not lose the integrity of the physical, chemical and thermodynamic properties of refrigerants. Yet, at the same time, the fluorinated ethers should not pose a threat to the environment unlike the CFC counterparts (Sekiya and Misaki, 2000).

Since the fluorine atom in CFCs provides the basis for good properties and fluorine does not contribute to ozone depletion, it is the fundamental key to an alternative (Sekiya and Misaki, 2000). Fluorinated compounds exhibit all the properties of a suitable refrigerant. Sekiya and Misaki (2000) theorized that in order for compounds to not pose an environmental threat, the compounds must decompose at a faster rate than CFCs. The authors proposed that this is attainable by the introduction of a hydrogen atom into the molecule and the elimination of chloride and bromide ions. The researchers only considered tests on fluorinated ethers with short life spans (between 1 and 5 years). Physical properties such as density, specific heat, surface tension, thermal stability and flammability were investigated (Sekiya and Misaki, 2000). The toxicity of the fluorinated ethers is negligible, and, of the various fluorinated ethers investigated, none has possessed a boiling point close to R-22. However, three fluorinated ethers were discovered that possessed properties similar to R-11 and R-114. These are regarded as suitable alternatives.

2.5. Dechlorination of R-22 with methanol

2.5.1. Reaction schemes

Difluorodimethyl ether can be formed via the reaction of R-22 with methanol in the presence of sodium hydroxide. The actual mechanism of dechlorination has been investigated by a number of authors (Hine and Porter, 1957; Lee et al., 2001; Satoh et al., 1998). The extraction of a halide ion from a halogen containing compound occurs via one of two mechanisms: an S_N2 mechanism or a dehydrohalogenation mechanism. The objective of the research undertaken by Hine and Porter (1957) was to confirm which of the mechanisms applied to chlorodifluoromethane (R-22), and thereby introduce a scheme for the reactions.

The mechanism of the S_N2 reaction is drawn in Figure 2-5. A polar bond exists between carbon and the halogen (Bruice, 2004). The halogen is more electronegative than the carbon. As a result, the halogen and the carbon have partially negative and positive charges, respectively (Bruice, 2004).

A nucleophile (OH^-) is attracted to the electrophile (C) forming a new bond. Simultaneously, the carbon-halogen bond is broken heterolytically (Bruice, 2004).

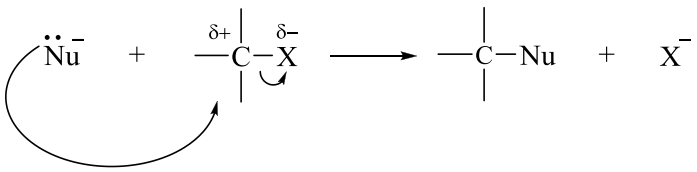

Figure 2-5. Substitution reaction (Bruice, 2004)

Elimination reactions, in particular, the dehydrohalogenation mechanism, involve the simultaneous removal of a halogen (Cl, F, I, Br) and a proton (H) from the alkyl halide (Bruice, 2004). The mechanism for the α-dehydrohalogenation mechanism is drawn in Figure 2-6.

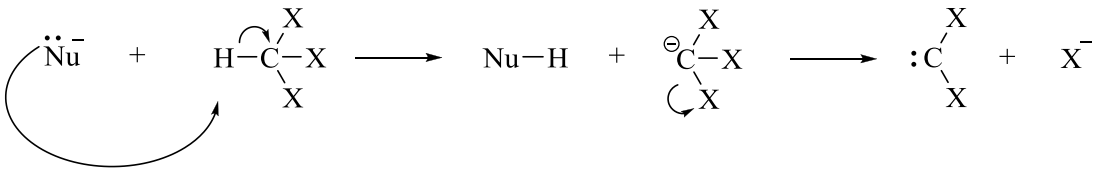

Figure 2-6. Elimination reaction (Bruice, 2004)

In α-eliminations (dehydrohalogenation), the proton and the halide are positioned on the same carbon atom. A nucleophile (OH^-) removes a proton (H), subsequently forming a carbanion. The halogen is then removed from the carbanion, forming a carbene (Bruice, 2004).

Hine and Porter (1957) initially suspected the reaction between R-22 and methanol, in the presence of sodium hydroxide, to occur via the S_N2 mechanism. The authors conducted a test to determine the rate at which the methoxide ion (CH_3O^-) reacts. The approximate rate constant was found experimentally to be 4.5×10^{-6} $dm^3\cdot mol^{-1}\cdot s^{-1}$ at 308.15 K. However, α-fluorine decreases S_N2 reactivity and therefore the authors anticipated a slower reaction (Hine and Porter, 1957). The authors discounted the plausibility of the S_N2 mechanism and considered instead, the α-dehydrohalogenation to form difluoromethylene ($:CF_2$), followed by the reaction to form the only two organic products: difluorodimethyl ether and trimethyl orthoformate. Difluoromethylene formation was considered to be a major reaction. It is an intermediate that reacts further with methanol to produce difluorodimethyl ether and trimethyl orthoformate. The reaction scheme suggested by Hine and Porter (1957) is drawn in Figure 2-7.

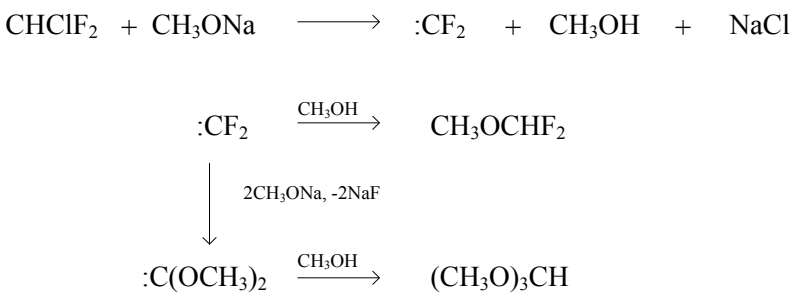

Figure 2-7. Reaction scheme 1 (Hine and Porter, 1957)

Satoh et al. (1998) proposed that trimethyl orthoformate was not produced from difluoromethylene. Rather, it was formed consecutively with difluorodimethyl ether. Figure 2-8 shows the reaction scheme suggested by Satoh et al. (1998). The authors reported that the removal of difluorodimethyl ether, upon formation, will lower the formation of trimethyl orthoformate.

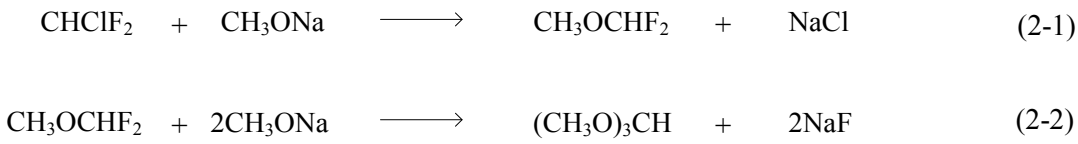

Figure 2-8. Reaction scheme 2 (Satoh et al., 1998)

Lee et al. (2001) investigated this reaction system to confirm the validity of either proposed mechanism. Difluorodimethyl ether was reacted with sodium methoxide (sodium hydroxide in methanol) for 2 hours at 298.15 K. The reaction produced a trace quantity of trimethyl orthoformate, thus strongly proving the mechanism by Satoh et al. (1998) implausible and the scheme by Hine and Porter (1957) plausible. The reaction as shown by Hine and Porter (1957) and rewritten by Lee et al. (2001) is drawn in Figure 2-9.

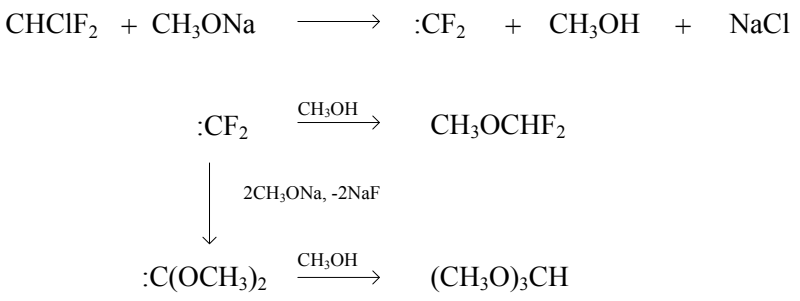

Figure 2-9. Reaction scheme 3 (Lee et al., 2001)

2.5.2. Experimental studies of the production of difluorodimethyl ether from R-22

Satoh et al. (1998) measured the vapour pressure of difluorodimethyl ether, once synthesized from the reaction between R-22 and methanol. Vapour pressures are a good indication of the suitability of a compound as a refrigerant (Satoh et al., 1998). Two sets of apparatus were used for the synthesis of difluorodimethyl ether and the vapour pressure measurements. The initial apparatus was a circulating type system. R-22 emanating from the product stream was constantly recycled through the circuit. Figure 2-10 depicts the circulating system as an excerpt from the original paper. A yield of 70% difluorodimethyl ether was obtained. A by-product was discovered and found to be trimethyl orthoformate. This was confirmed by injection of product and by-product into the GCMS. The analysis provided fragmentation information on the products. The fragmentations of the products are listed in Table 2-9. The authors used the fragmentation spectra to identify the two products. In particular, the M^+ or molecular ion peak gave an indication of the relative formula mass (molecular mass) of the compounds. Other molecular fragments, including the most abundant peak ($[M-H]^+$), were used to piece together the molecular structure.

Table 2-9. Fragmentation details for difluorodimethyl ether and trimethyl orthoformate (Satoh et al., 1998)

	Mass-to-charge ratios (m/z)		
	M^+	**100%, $[M-H]^+$**	**Other**
CH_3OCHF_2	82	81	63, 51, 31
$CH(OCH_3)_3$	105	75	47, 31

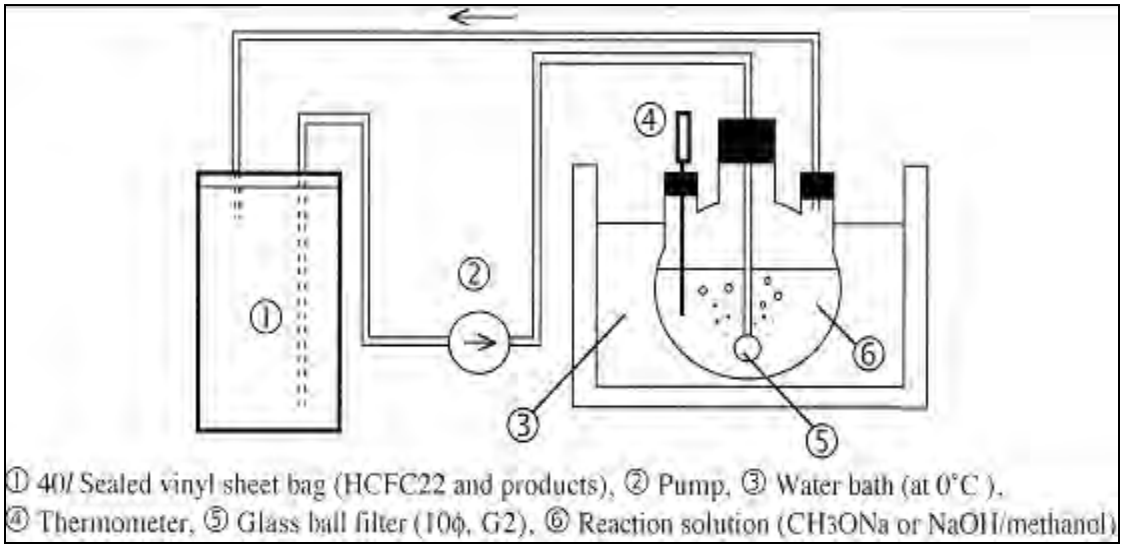

Figure 2-10. Circulating type system (Satoh et al., 1998)

Satoh et al. (1998) reported that the removal of difluorodimethyl ether, immediately after formation would reduce the formation of trimethyl orthoformate. A flow system was therefore commissioned by the authors. Figure 2-11 depicts the excerpt of the apparatus from Satoh et al. (1998). R-22 gas was injected by the vapour pressure, into the reactor containing a solution of sodium hydroxide and methanol, at a rate of 1 $dm^3 \cdot min^{-1}$ (Satoh et al., 1998). The reactor was maintained at 273.15 K in a water bath. The product gas was then cooled as it entered two consecutive cold traps submerged in an ethylene glycol bath at 268.15 K. The first cold trap contained molecular sieve 5A to remove methanol. The second cold trap separated the by-product from the product gas stream. The difluorodimethyl ether gas was liquefied in the third cold trap at 238.15 K.

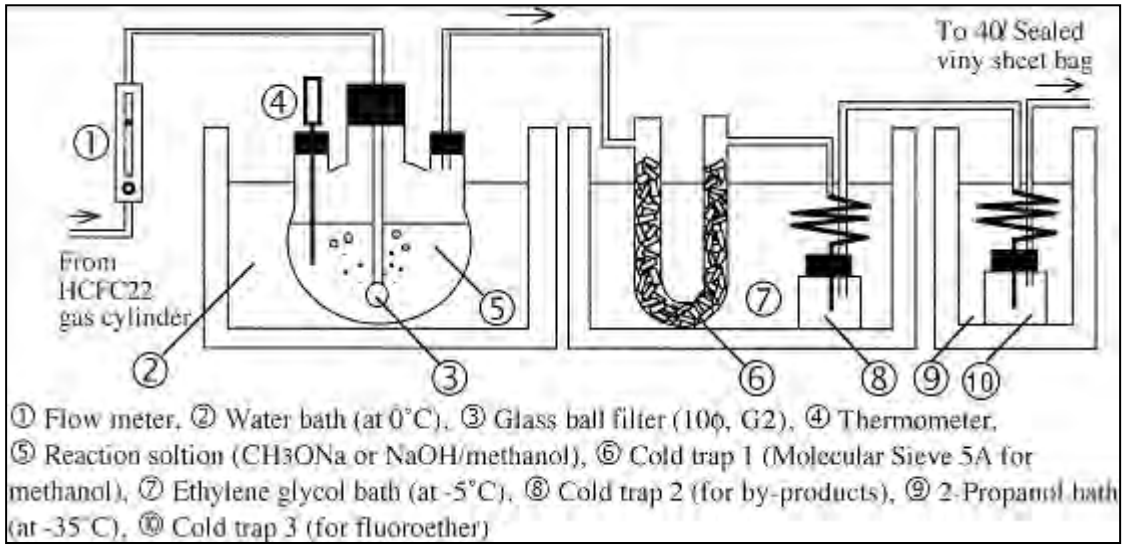

Figure 2-11. Flow type system (Satoh et al., 1998)

The difluorodimethyl ether liquid collected was passed through three distillation steps to obtain a difluorodimethyl ether purity of 94.5% and a yield of 63%. The distillation process shown in Figure 2-12 is an excerpt taken from Satoh et al. (1998). The 2-propanol bath was set at 253.15, 258.15 and 263.15 K for the three steps of distillation.

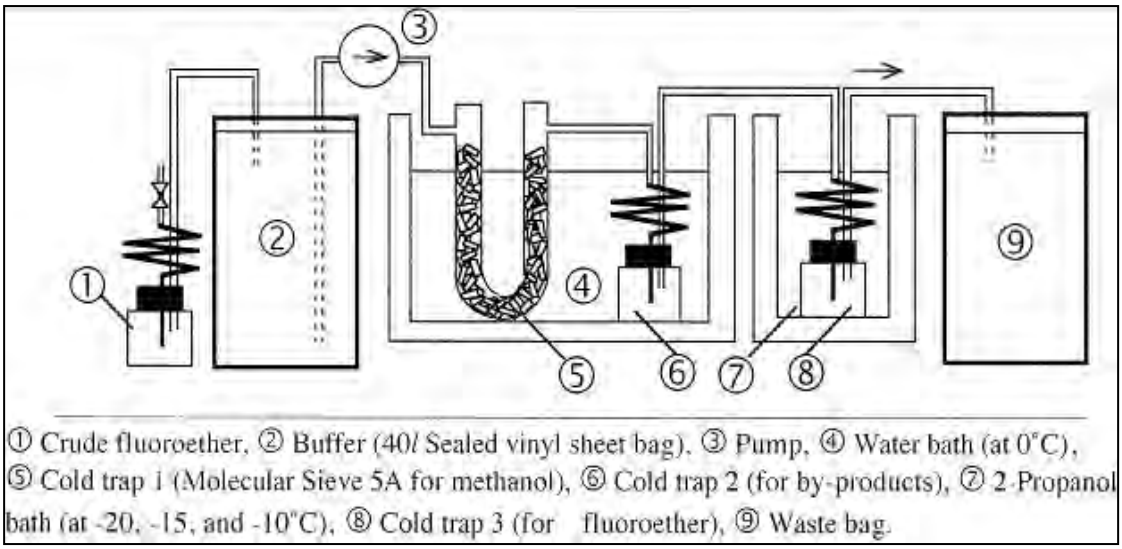

Figure 2-12. Distillation apparatus for the flow type system (Satoh et al., 1998)

The vapour pressure measurements undertaken by the authors involved two sets of apparatus. The first apparatus was valid for the temperature range 260 to 290 K in a water bath. The second apparatus was applicable for temperatures greater than 290 K in an air bath. Temperature was measured with a platinum-resistant thermometer. Pressure was measured with a Bourdon gauge. Between 266 and 393 K, no difluorodimethyl ether decomposition was noticed.

Lee et al. (2001) suggested the use of alkali metal carbonates as a more efficient base system to suppress the formation of trimethyl orthoformate and increase the yield of difluorodimethyl ether. K_2CO_3, Na_2CO_3 and Li_2CO_3 were reported as possible replacements to sodium hydroxide in methanol. The effect of reaction parameters on the formation of trimethyl orthoformate was investigated prior to analyzing the performance of the mentioned bases. The authors observed an increase in difluorodimethyl ether yield with temperature at constant base concentration. A decrease of difluorodimethyl ether yield with base concentration was observed at constant temperature. The author‟s findings show that trimethyl orthoformate formation cannot be suppressed by changes to reaction temperature or sodium methoxide concentration.

Nishiumi and Kato (2003) studied the effect of salt concentration on the dechlorination of R-22 and suggested that the accumulation of sodium chloride in the reactor resulted in less efficient mixing of the NaOH/methanol solution (Nishiumi and Kato, 2003). They noted that the white precipitate of sodium chloride was visible due to the low solubility of sodium chloride in methanol. They postulated that the accumulation of sodium chloride precipitate and the inhibitory effect on mixing reduced the mass transfer rate. A simple model of the reaction system was developed which ignored the production of sodium fluoride. The effect of sodium chloride on the rate of mass transfer was accounted for by the addition of a correction to the mass transfer coefficient. This correction factor was a function of the total salt concentration. It appeared to be satisfactory since the mass transfer coefficient is a function of the intensity of mixing as inferred from the presence of impeller speed in many established mass transfer correlations.

2.6. Analytical methods

2.6.1. Determination of chloride ion concentration

The Mohr method is a classical procedure in the analysis of chloride ion concentration (Murthy, 1995). It is described as an argentometric titration in which silver nitrate is used to precipitate silver chloride. The end-point is detected by the formation of a reddish-brown precipitate, silver chromate, formed by the reaction of an excess of silver ions with chromate (Radojević, 2006). Unfortunately there is no experimental evidence that there is no interference from fluoride ions that may be present in the solution.

The mercurimetric method developed in 1933 by Dubsky used diphenylcarbohydrazine as an indicator for mercuric nitrate titration (Zall et al., 1956). To determine the concentration of the chloride ion by colorimetric means, Barney (1957) suggested the reaction of chloride with mercuric chlorinilate to liberate the acid chlorinilate ion. The downfall of this method is the unavailability of commercial mercuric chlorinilate. It is also an expensive procedure to prepare mercuric chlorinilate.

Ion selective electrodes can also be used for the determination of chloride ion concentration. Table 2-10 lists the available ion selective electrodes, with which chloride ions can be analyzed efficiently and accurately, without interference from fluoride ions. The disadvantage of the ion selective electrode is the high cost.

There are a number of spectrophotometric or colorimetric methods given in the literature for the determination of chloride ion concentration. Most of the available methods summarized in Table 2-11 involve the displacement of a complex ion from an aqueous solution by the chloride ion and the subsequent reaction of the complex ion with another reagent to give a measurable absorbance. The information in Table 2-11 is presented in chronological order.

The spectrophotometric determination of chloride in solution discussed by Zall et al. (1956) was selected as a method of analysis due to the fact that there is no interference from the presence of fluoride ions. The foundation of the method relies on the chloride ion causing the displacement of the thiocyanate group from mercuric thiocyanate. Subsequently, thiocyanate reacts with ferric iron to form iron thiocyanate present as $[Fe(SCN)]^{2+}$. The reaction of Fe^{3+} with SCN^- ions produces a distinct absorbance measurable on a spectrophotometer at 460 nm (Zall et al., 1956).

Table 2-10. Ion-selective electrodes available for chloride analysis

Brand	References	Auxiliary Equipment	Accuracy	Sensitivity	Reproducibility	Interference from F^-
OMEGA CIE	Omega (1993)	pH/mV meter reference electrode ISA	-	-	± 2 %	None
PASCO CIE	PASCO (1996-2012)	ISE amplifier fill solution computer Interface TISAB 1,2,3 (buffer)	-	-	± 2 %	None
THERMO SCIENTIFIC CIE	Thermo Scientific (2008)	Reference electrode Meter stirrer bars	-	-	± 2 %	None

Table 2-11. Spectrophotometric methods in literature for chloride analysis

Authors	Method	Reagents	Interference from F^-
Clarke (1950)	Spectrophotometric	Diphenylcarbazone indicator Mercuric nitrate Potassium chloride sodium hydroxide	-
Zall (1956)	Spectrophotometric	Mercuric thiocyanate Ferric perchlorate Perchloric acid Nitric acid	None
Barney (1957)	Spectrophotometric	Mercuric chlorinate	Present
Chu and Wu (1973)	Spectrophotometric	Mercuric thiocyanate Iron (iii) nitrate Perchloric acid	None
Venkatesan (2010)	Spectrophotometric	Ferric ammonium sulphate Mercuric thiocyanate nitric acid	None

2.6.2. Determination of fluoride ion concentration

A number of titrimetric methods are available to analyze the concentration of fluoride ions. Titrations that use electrodes to detect the endpoint produce more accurate results than titrations in which the endpoint is detected visually (Nichols and Olsen, 1943). Bond and Murray (1952) proposed titration by thorium nitrate to determine fluoride ion concentrations in solution. Sodium alizarin sulphonate indicator was used to detect the endpoint. According to Matuszak and Brown (1945), the solution pH must be 3.3 with acetic acid and must avoid direct sunlight. This was accomplished by reflecting sunlight off a white surface (Bond and Murray, 1952). The titration was not sensitive to temperatures between 278.15 and 313.15 K. For the method to be used, the endpoint must be detected with an electrode, as visual endpoint detection will pose inaccuracies.

Willard and Winter (1933) studied a complex method to titrate soluble silico-fluoride and fluoride with thorium nitrate, in the presence of zirconium alizarin indicator. The authors did not obtain satisfactory results spectrophotometrically (Willard and Winter, 1933).

Nichols and Olsen (1943) investigated the determination of fluoride ion concentration in organic compounds. The process was initiated with the breakdown of the organic compound by sodium peroxide. This caused the carbon-fluorine bond to break, transforming the fluorine in the compound into fluoride ion (Nichols and Olsen, 1943). The fluoride ion was then titrated with cerous nitrate. The authors also corroborated the hypothesis that titration with electrometric endpoint detection was more accurate than visual endpoint detection. The method was attempted potentiometrically by Batchelder and Meloche (1931). The results were unsatisfactory due to adsorption by hydrous cerous fluoride. The chloride ion, present as a maximum of 2000 p.p.m. sodium chloride, did not interfere with the analysis (Nichols and Olsen, 1943). The visual method, using methyl red indicator presented satisfactory results only when used for the same conditions as electrometric detection and with no sodium present (Nichols and Olsen, 1943). The disadvantages of this method, among others are: the expensive equipment required for the electrometric titration and the complex preparation of cerous nitrate.

Table 2-12 reports in chronological order, the titration methods available to analyze the concentration of fluoride ions.

Ion selective electrodes can also be used for the determination of fluoride ion concentration. Table 2-13 lists the available ion selective electrodes and the auxiliary equipment with which fluoride ions can be analyzed efficiently and accurately, without interference from chloride ions. The disadvantage of the ion selective electrode is the high cost.

In the spectrophotometric determination of fluoride ions, the fluoride ion displaces organic ligands from coloured complexes of metal ions such as ferric iron, thorium, titanium and zirconium. The displacement of the metal ion results in the decrease of the absorbance of the reaction mixture. Armstrong (1933) based a colorimetric method on the reaction of ferric iron with fluoride to determine micro quantities of fluorine with interfering ions present. He also tested the replacement of thiocyanate with acetyl acetone, salicylic acid and 8-hydroxy quinoline for the use as iron colour reagents (Armstrong, 1933). Smith and Dutcher (1934) devised a colorimetric method based on the fading action of zirconium-quinalizarin (Armstrong, 1933). Armstrong (1936) developed an accurate procedure based on thorium nitrate titration to analyze micro quantities of fluoride in biological material. A part of the procedure was a process to remove interfering quantities of chloride with silver perchlorate (Armstrong, 1936).

Zhu et al. (2005) investigated the use of cyanine dye as a reagent. The cyanine dye was reacted with tert-butyldimethylsilane, abbreviated as TBS, to form silanated dye (Zhu et al., 2005). Fluoride ions selectively attacked silanated dye to reform cyanine dye (Zhu et al., 2005). Fluoride has a specific affinity for the TBS functional group on silanated dye, therefore interference is limited (Zhu et al., 2005).

The spectrophotometric determination of fluoride in solution discussed by Shu-Chuan et al. (1956) was selected as a method of analysis due to the fact that there is no interference from the presence of chloride ions. The method is based on the bleaching effect of fluoride on coloured complexes. Yoe (1932) suggested that ferron be used in the determination of ferric iron and studied this method in great detail. This reaction was then adapted by Fahey (1939) for the determination of fluoride colorimetrically (Shu-Chuan et al., 1956). Ferron and ferric iron were used because their colour was very stable and it was not influenced by fluctuations in room temperature (Shu-Chuan et al., 1956). For the spectrophotometric determination of fluoride, Shu-Chuan et al (1956) investigated the reaction of ferron and ferric chloride. The reaction of ferron with ferric chloride produced a stable colour. The absorbency was measured at a wavelength of 620 nm. Sodium chloride was used by the authors to establish the effect of the chloride ion on the determination of the fluoride ion. There was

found to be insignificant interference from the chloride ions. Table 2-14 reports in chronological order, the spectrophotometric methods and the relevant reagents, applicable to a fluoride concentration analysis.

Table 2-12. Titration methods in literature for fluoride analysis

Authors	Method	Reagents	Accuracy	Interference from Cl^-
Willard and Winter (1933)	Titration: Volumetric	Thorium nitrate Zirconium - alizarin indicator	-	-
Armstrong (1936)	Titration: Distillation	Thorium nitrate Sodium perchlorate Silver perchlorate Buffer	-	None
Nichols and Olsen (1943)	Titration: Visual Electrometric	Cerous nitrate Sodium peroxide Nitric acid Ammonium nitrate	± 1%	-
Bond and Murray (1952)	Titration: Direct	Thorium nitrate Sodium alizarin sulphonate indicator	± 0.02 ml thorium nitrate (± 0.8 µg fluorine)	None

Table 2-13. Ion selective electrode for fluoride analysis

Brand	Reference	Auxiliary Equipment	Accuracy	Sensitivity	Reproducibility	Interference from Cl^-
OMEGA FIE	Omega (1993)	pH/mV meter reference electrode TISAB 1 (buffer) TISAB 2 (buffer)	-	-	± 2%	None
PASCO FIE	PASCO Scientific (1997)	ISE amplifier fill solution computer interface TISAB 1,2,3 (buffer)	-	-	± 2%	None
TELEDYNE FIE	Teledyne Analytical Instruments (2006)	pH electrodes	± 0.1%	± 0.05%	-	None

Table 2-14. Spectrophotometric methods in literature for fluoride analysis

Authors	Method	Reagents	Interference from Cl^-
Armstrong (1933)	Spectrophotometric	Ferric chloride acetyl acetone	-
Smith and Dutcher (1934)	Colorimetric	Zirconium quinalizarin Sodium hydroxide	None
Shu-Chuan (1956)	Spectrophotometric	Ferron Ferric iron HCl	None
Zhu et. al. (2005)	Spectrophotometric	Cyanine dye TBS buffer solution chloroform	-

CHAPTER 3

THEORY

3.1. Model of reaction chemistry

The reaction scheme that was used for the kinetic parameter identification was based on the proposed α-dehydrohalogenation mechanism (Figure 2-6 in Section 2.5.1.) of Hine and Porter (1957). A simplified model for the reactions is presented. The reaction between R-22 and sodium methoxide produces a difluoromethylene intermediate. The intermediate reacts further with methanol to form difluorodimethyl ether. The intermediate also simultaneously reacts with sodium methoxide and methanol to form trimethyl orthoformate. The simplified version of both reaction steps is described further on. For the reaction step that produces difluorodimethyl ether:

$$CHClF_2 + CH_3ONa \longrightarrow CF_2 + CH_3OH + NaCl \quad (3\text{-}1)$$

$$CF_2 + CH_3OH \longrightarrow CH_3OCHF_2 \quad (3\text{-}2)$$

These reactions can be combined such that the difluoromethylene intermediates and methanol molecules cancel to give:

$$CHClF_2 + CH_3ONa \longrightarrow CH_3OCHF_2 + NaCl \quad (3\text{-}3)$$

For the reaction step promoting trimethyl orthoformate production:

$$CHClF_2 + CH_3ONa \longrightarrow CF_2 + CH_3OH + NaCl \quad (3\text{-}4)$$

$$CF_2 + 2CH_3ONa + CH_3OH \longrightarrow (CH_3O)_3CH + 2NaF \quad (3\text{-}5)$$

These reactions can be combined such that the difluoromethylene intermediates and methanol molecules cancel to give:

$$CHClF_2 + 3CH_3ONa \longrightarrow (CH_3O)_3CH + 2NaF + NaCl \quad (3\text{-}6)$$

The final two reactions that describe the reaction between R-22 and sodium methoxide are presented in Table 3-1 together with their respective estimated enthalpies of reaction. The latter were calculated to gauge the heat effects and aid in proper design of the experimental reactor. The calculations are presented in Appendix A. Both reactions were found to be exothermic.

Table 3-1. Final derived reactions with the respective heats of reaction

Reaction no.	Reaction	ΔH_r / kJ·mol^{-1}
1	$CHClF_2 + CH_3ONa \rightarrow CH_3OCHF_2 + NaCl$	-119.58
2	$CHClF_2 + 3CH_3ONa \rightarrow (CH_3O)_3\,CH + 2NaF + NaCl$	-1183.64

3.2. Kinetic modeling

The rates of reaction for the reactions presented in Table 3-1 were regarded as:

$$r_1 = k_1 C_{R-22} C_{NaOH}^2 \tag{3-7}$$

$$r_2 = k_2 C_{R-22} C_{NaOH} \tag{3-8}$$

Reaction 1 in Table 3-1 was determined experimentally by Kato and Nishiumi (2003) to be second order with respect to sodium hydroxide in methanol and first order with respect to R-22. The second reaction in Table 3-1 has not been considered in any kinetic study prior to the current investigation and is assumed to be first order with respect to both R-22 and sodium hydroxide in methanol.

The net rates of change for each component due to reactions 1 and 2 in Table 3-1 are:

$$R_{R-22} = -k_1 C_{R-22} C_{NaOH}^2 - k_2 C_{R-22} C_{NaOH} \tag{3-9}$$

$$R_{NaOH} = -k_1 C_{R-22} C_{NaOH}^2 - 3k_2 C_{R-22} C_{NaOH} \tag{3-10}$$

$$R_{NaCl} = k_1 C_{R-22} C_{NaOH}^2 + k_2 C_{R-22} C_{NaOH} \quad (3\text{-}11)$$

$$R_{NaF} = 2k_2 C_{R-22} C_{NaOH} \quad (3\text{-}12)$$

Using conventional means, it is difficult to determine the instantaneous concentration of difluorodimethyl ether and trimethyl orthoformate in the reactor; and hence the net rate of change for these components. An alternative method was proposed in which the concentration of the salts in the reactor is measured. The measured concentration of these particular products was used to determine the kinetic parameters.

The dependent relationship between the reaction rate constant, k, and temperature, T, is described by the Arrhenius equation, developed by Svante Arrhenius in 1889.

$$k = Ae^{-E_a/RT} \quad (3\text{-}13)$$

where A is the pre-exponential factor and E_a is the activation energy. The activation energy represents the minimum energy required for a reaction to occur. Kinetic data were available in literature for reaction 1 only at 303 K (Nishiumi and Kato, 2003).

3.3. Reactor model

3.3.1. Material balances

Gas-liquid reactions require material balances to be expressed for both the gas and liquid phase. In this investigation several simplifying assumptions were made. The process was assumed to occur under isothermal conditions. The reactions were regarded as irreversible as indicated by Hine and Porter (1957). The reactor in this work was operated with a batch liquid phase and gas continuously sparged and well dispersed within this liquid by means of mechanical agitation. Nauman (1987) derived general material balances for the gas and liquid phase. The derived balances (for each phase) are described by Equations 3-14 and 3-15 for the gas phase and liquid phase, respectively. The balances were modified with the inclusion of the enhancement factor E_A. It is known that the solubility of R-22 in the liquid mixture is low (Takenouchi et al., 2001; Kato and Nishiumi, 2003).

This would imply that there is negligible resistance to mass transfer on the gas-side of the gas-liquid interface. Hence, the overall mass transfer coefficient can be replaced by the liquid side mass transfer coefficient. Figure 3-1 shows a schematic representation of the reactor system.

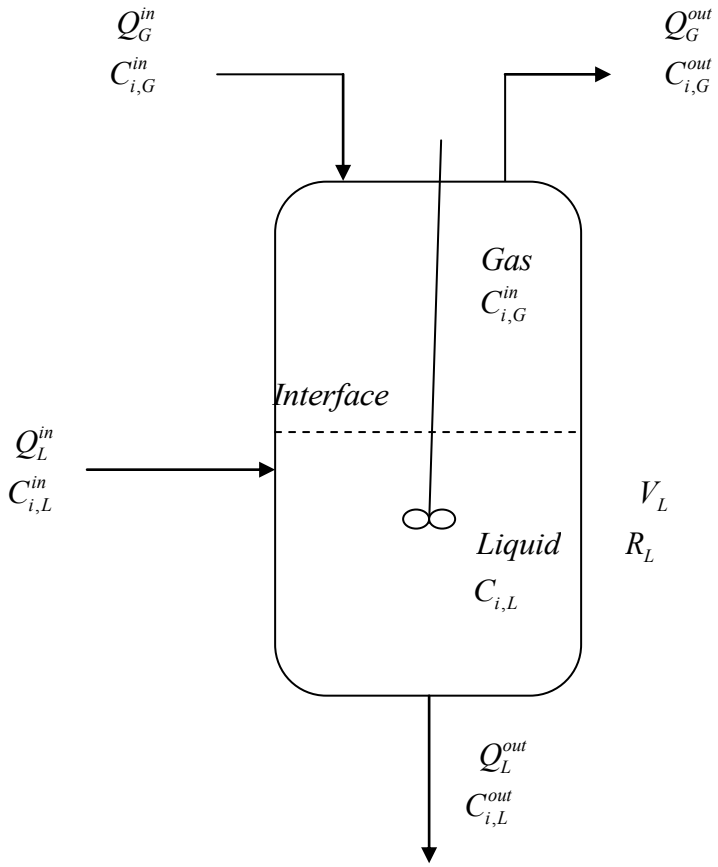

Figure 3-1. Schematic representation of the gas-liquid reactor

$$\frac{d(V_G C_{i,G})}{dt} = Q_G^{in} C_{i,G}^{in} - E_A k_L a V \left(\frac{C_{i,G}^{out}}{H^{cc}} - C_{i,L} \right) + V_G R_G - Q_G^{out} C_{i,G}^{out} \tag{3-14}$$

$$\frac{d\left(V_L C_{i,L}\right)}{dt} = Q_L^{in} C_{i,L}^{in} + E_A k_L a V \left(\frac{C_{i,G}^{out}}{H^{cc}} - C_{i,L} \right) + V_L R_L - Q_L^{out} C_{i,L}^{out} \tag{3-15}$$

where $k_L a$ is the volumetric mass transfer coefficient and H^{cc} is the Henry's law constant defined as the ratio of solute concentration in the gas and liquid phases, respectively. R defines the net

formation rates. C_i denotes the concentration of component i and Q denotes the volumetric flow rate of fluid. V and V_G represent the total volume and gas hold-up respectively.

$$V = V_G + V_L \tag{3-16}$$

The reactor was operated under semi-batch conditions, in which the liquid was initially charged into the reactor vessel and the gas was subsequently sparged continuously. The following restrictions should apply. Since no liquid entered or exited the reactor:

$$Q_L^{in} = Q_L^{out} = 0 \tag{3-17}$$

For fed-batch operation with an initial liquid charge and continuous gas sparging, the accumulation term appearing in Equation 3-14 is usually assumed to be negligible (Nauman, 1987):

$$\frac{d\left(V_G C_{i,G}\right)}{dt} = 0 \tag{3-18}$$

Since no reaction occurs in the gas phase:

$$R_G = 0 \tag{3-19}$$

Now, simplifying Equation 3-14 and Equation 3-15 gives:

$$0 = Q_G^{in} C_{i,G}^{in} - E_A k_L a V \left(\frac{C_{i,G}^{out}}{H^{cc}} - C_{i,L} \right) - Q_G^{out} C_{i,G}^{out} \tag{3-20}$$

$$\frac{d\left(V_L C_{i,L}\right)}{dt} = E_A k_L a V \left(\frac{C_{i,G}^{out}}{H^{cc}} - C_{i,L} \right) + V_L R_L \tag{3-21}$$

The outlet gas volumetric flow rate, Q_G^{out}, was not measured experimentally. It can however be related to the outlet gas-phase concentration of the refrigerant, $C_{i,G}^{out}$ as follows.

$$Q_G^{out} = \dot{n}_{tot}^{out} \frac{RT}{P} \tag{3-22}$$

$$\dot{n}_{tot}^{out} = \dot{n}_{N_2}^{out} + C_{i,G}^{out} Q_G^{out} \tag{3-23}$$

Since,
$$\dot{n}_{N_2}^{out} = \dot{n}_{N_2}^{in} \tag{3-24}$$

$$\dot{n}_{tot}^{out} = \dot{n}_{N_2}^{in} + C_{i,G}^{out} Q_G^{out} \tag{3-25}$$

$\Rightarrow$
$$Q_G^{out} = \left[\dot{n}_{N_2}^{in} + C_{i,G}^{out} Q_G^{out} \right] \frac{RT}{P} \tag{3-26}$$

$$Q_G^{out} = \frac{\dot{n}_{N_2}^{in}}{\left[\frac{P}{RT} - C_{i,G}^{out} \right]} \tag{3-27}$$

Now, substitute the expression for Q_G^{out} (in Equation 3-27) into the simplified gas-phase balance (Equation 3-20) to obtain:

$$0 = Q_G^{in} C_{i,G}^{in} - E_A k_L a V \left(\frac{C_{i,G}^{out}}{H^{cc}} - C_{i,L} \right) - \frac{\dot{n}_{N_2}^{in}}{\left[\frac{P}{RT} - C_{i,G}^{out} \right]} C_{i,G}^{out} \tag{3-28}$$

The quadratic in Equation 3-28 is solved to find the roots for $C_{i,G}^{out}$. There are two roots to a quadratic. In order to establish which of the two roots is correct, the following conditions are first adhered to. Firstly, the refrigerant concentration should be less than the total gas concentration. Secondly, the driving force for absorption of the gas in the balance should be positive (as sketched in Figure 3-2). A combination of these two conditions implies that:

$$H^{cc} C_{i,L} < C_{i,G} < \frac{P}{RT} \tag{3-29}$$

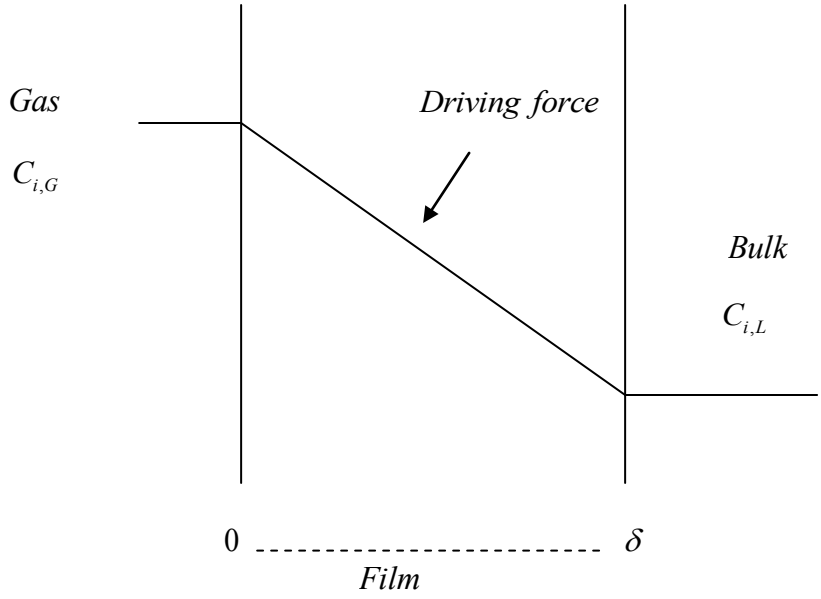

Figure 3-2. Diagram depicting the transfer of gas from the gas-phase to the bulk liquid

In solving the quadratic, the acceptable root is that root which satisfies the aforementioned conditions. Terms were grouped in order to present the quadratic in the form of:

$$x = \frac{-b \pm \sqrt{b^2 - 4ac}}{2a} \tag{3-30}$$

The following notation was used to represent the grouped terms:

$$\alpha = \frac{k_L a V}{Q_G^{in} C_{i,G}^{in}} \tag{3-31}$$

$$\beta = \frac{\dot{n}_{N_2}^{in}}{Q_G^{in} C_{i,G}^{in}} \tag{3-32}$$

$$\gamma = \frac{P}{RT} \tag{3-33}$$

Substitution of this notation into the gas-phase balance gives:

$$\gamma - C_{i,G}^{out} - \alpha\left[\frac{C_{i,G}^{out}}{H^{cc}} - C_{i,L}\right]\left[\gamma - C_{i,G}^{out}\right] - \beta C_{i,G}^{out} = 0 \tag{3-34}$$

This can be arranged to give:

$$\left(C_{i,G}^{out}\right)^2 - \left[\gamma + \frac{H^{cc}}{\alpha}\left(1+\beta\right) + H^{cc}C_{i,L}\right]C_{i,G}^{out} + \frac{\gamma H^{cc}}{\alpha}\left(1+\alpha C_{i,L}\right) = 0 \tag{3-35}$$

The roots are therefore:

$$C_{i,G}^{out} = \frac{\gamma + \frac{H^{cc}}{\alpha}\left(1+\beta\right) + H^{cc}C_{i,L} \pm \sqrt{\Delta}}{2} \tag{3-36}$$

where

$$\Delta = \left(\gamma + \frac{H^{cc}}{\alpha}\left(1+\beta\right) + H^{cc}C_{i,L}\right)^2 - 4\frac{\gamma H^{cc}}{\alpha}\left(1+\alpha C_{i,L}\right) \tag{3-37}$$

The only valid root will include $-\sqrt{\Delta}$ since the alternative would violate the condition that the refrigerant concentration is less than the total gas phase concentration. For the full description of the reactor material balances, several quantities need to be determined. These include gas solubility data in the form of the Henry's law constant, the volumetric mass transfer coefficient and the enhancement factor. Each of these will be discussed in the subsections that follow.

3.3.2. Gas Solubility

Henry's law states that the solubility of a gas in a liquid is directly proportional to the partial pressure of the gas in equilibrium with that liquid. Takenouchi et al. (2001) measured the solubility of R-22 in pure methanol within the temperature range considered in this study and correlated their results with the following equation:

$$\ln H^{px} = 81.923 - \frac{5659.544}{T} - 10.953 \ln T \tag{3-38}$$

where H^{px} is the Henry's law constant defined as the partial pressure of the solute in the gas phase divided by the mole fraction of the solute in the liquid phase and T is in Kelvin.

In order to apply the available solubility data in the material balances derived in Section 3.3.1., concentration-based Henry's law constants (H^{cc}) had to be calculated. The details of this conversion are presented in Appendix B. Table 3-2 lists the concentration-based Henry's law constants.

Table 3-2. Concentration-based Henry's law constants at the experimental temperatures

	Temperature / K		
	283.15	**293.15**	**303.15**
H^{cc}	0.020	0.026	0.033

The solubility of a gas in a liquid generally decreases when salts are added to the solution. This is commonly called the 'salting out' effect. The decrease is due to an increase in the activity coefficient of the dissolved gas in the liquid phase. A detailed description of the effect of dissolved salts on gas solubility is given by Tiepel and Gubbins (1973). The 'salting out' effect on gas solubility is described by the following form of the Sechenov equation (Fallabella et al., 2006):

$$\ln\left[\frac{H_{salt}^{cc}}{H^{cc}}\right] = K_S C_S \tag{3-39}$$

where H_{salt}^{cc} is the Henry's law constant for the solution containing a dissolved salt, H^{cc} is the Henry's law constant for the pure liquid, K_S is the Sechenov coefficient for the salt and C_S is the molar concentration of the salt. For a mixture of different salts the following extension of Equation 3-39 applies (Schumpe, 1993):

$$\ln\left[\frac{H_{salt}^{cc}}{H^{cc}}\right] = \sum_i K_i C_i \tag{3-40}$$

where K_i is the Sechenov coefficient for salt *i* and C_i is the concentration of salt *i*. The Sechenov coefficients of different salts are usually unique for a particular gas-liquid system (Battino et al., 1983; Schumpe, 1993). There is practically no data in the literature for sodium fluoride, sodium chloride and sodium methoxide in methanol with R-22 as the dissolved gas.

3.3.3. Mass transfer coefficient

The volumetric mass transfer coefficient for a specific reactor arrangement is typically determined using a dissolved oxygen probe and some form of a dynamic measurement test. In this investigation, the gassing-out method was used to measure the oxygen mass transfer coefficient. The technique involves the de-oxygenation of the solution with nitrogen and the subsequent saturation of the solution with air (Gauthier et al., 1990). Air was regarded as a safer alternate to pure oxygen as the risk of explosion was minimized. A dissolved oxygen probe was used to measure the concentration of dissolved oxygen in methanol.

Assuming the liquid is perfectly mixed, the rate of oxygen absorbed by the liquid is given by:

$$\frac{dC}{dt} = k_L a\left(C^* - C\right) \tag{3-41}$$

where $k_L a$ is the volumetric mass transfer coefficient, C^* is the oxygen saturated concentration and C is the temporal dissolved oxygen concentration in the liquid.

It was known that the dissolved oxygen probe used in this investigation had a very slow response time. Therefore the electrode dynamics had to be included in the oxygen mass transfer model. The response of the probe can be described in terms of first order dynamics:

$$\frac{dC_{probe}}{dt} = k_{probe}\left(C - C_{probe}\right) \tag{3-42}$$

where k_{probe} is the sensor lag constant and C_{probe} is the concentration of dissolved oxygen indicated by the probe. Integration of Equation 3-41 yields:

$$C(t) = C^*\left[1 - e^{-k_L a t}\right] \tag{3-43}$$

Equation 3-43 is used as a forcing term in the electrode ODE (Equation 3-42) which is integrated again to give an expression for the dissolved oxygen concentration indicated by the probe (Letzel et al., 1999):

$$C_{probe} = C^*\left(1 - \frac{1}{k_{probe} - k_L a}\left[k_{probe}e^{-k_L a t} - k_L a e^{-k_{probe} t}\right]\right) \tag{3-44}$$

If there is a finite concentration of oxygen at the beginning of the test (C_o), the integration yields:

$$C_{probe} = C^* - \frac{C^* - C_o}{k_{probe} - k_L a}\left[k_{probe}e^{-k_L a t} - k_L a e^{-k_{probe} t}\right] \tag{3-45}$$

The volumetric mass transfer coefficient $k_L a$ can then be determined through nonlinear regression.

The response time of the sensor can be determined independently using a step experiment, where the concentration of dissolved oxygen is instantaneously changed by transferring the probe from a vessel containing solvent saturated with oxygen to a vessel containing solvent saturated with nitrogen until a negligible dissolved oxygen concentration is measured. Three sets of data are obtained to test for reproducibility.

The probe dynamics is once again given by the following ODE:

$$\frac{dC_{probe}}{dt} = k_{probe}\left(C_{sat} - C_{probe}\right) \tag{3-46}$$

where C_{sat} is now the saturated concentration of dissolved oxygen in the first vessel. Integrating Equation 3-46 gives:

$$\frac{C_{probe}}{C_{sat}} = 1 - \mathrm{e}^{-k_{probe}t} \tag{3-47}$$

which can be linearized to obtain:

$$\ln\left(\frac{C_{probe}}{C_{sat}}\right) = -k_{probe}t \tag{3-48}$$

The unknown variable k_{probe} can then be easily obtained through simple linear regression of the C_{sensor} experimental data.

The general relationship between gas-liquid mass transfer coefficients and diffusion coefficients allows for the estimation of the mass transfer coefficient of R-22 from the measured oxygen data. According to the film theory of interfacial mass transfer, the total mass flux equals the diffusion flux provided that the solution is dilute. For mass transfer across spherical boundaries (e.g. gas bubbles) the result can be written in terms of the Sherwood number (Cussler, 2007):

$$Sh = \frac{k_M \delta}{D} = 2 \tag{3-49}$$

where k_M is the mass transfer coefficient, D is the diffusivity and δ is the film thickness. Thus the mass transfer coefficient is directly proportional to the diffusion coefficient. The volumetric mass transfer coefficient of R-22 can then be estimated according to (Kroschwitz, 2007):

$$\left(k_L a\right)_{R-22} = \frac{D_{R-22}}{D_{oxygen}} \left(k_L a\right)_{oxygen} \tag{3-50}$$

Since the gas has a low solubility in the liquid, the solution is expected to be dilute. The film theory was employed in order to maintain consistency with the enhancement factor calculation presented at the end of this chapter.

When investigating the reaction of R-22 with sodium hydroxide in methanol, Nishiumi et al. (2003) found that the mass transfer was inhibited by the formation of salt crystals. Separate experiments were performed to determine the mass transfer of R-22 gas in methanol containing different amounts of sodium chloride. It was consistently found that an increased amount of salt crystals decreased the measured mass transfer coefficient. It was therefore concluded that the presence of salt crystals prevented efficient mixing of the solution, which in turn reduced the rate of mass transfer. However, the actual mechanism of this process remains unknown. In order to account for this effect on mass transfer the authors introduced an empirical correction to the overall volumetric mass transfer coefficient in the following exponential form involving the cumulative superficial concentration of sodium chloride only (both dissolved and precipitated salt):

$$k_L a = k_L a^0 \exp\left(-m C'_{NaCl}\right) \tag{3-51}$$

They fitted their experimental data to a simple reaction model, ignoring the formation of sodium fluoride, and determined the value of m to be 3. The proposed mixing effect had to be revised for the current work. There appears to be some support for this theory in the literature (Li et al., 1995) where the effect of rheological properties of the fluid on mass transfer was described using a similar exponential equation.

The solubilities in methanol of the two product salts that are formed are given in Table 3-3. The solubility of sodium fluoride is much lower than the solubility of sodium chloride. It would be expected that if the mixing effect is only due to precipitated salt crystals then sodium fluoride would also contribute. Also the correction to the mass transfer coefficient should only take into account the concentration of precipitated salts. Hence, the following was applicable:

$$k_L a = k_L a^0 \exp\left\{-m\left[\left(C'_{NaCl} - C^{so\,\mathrm{lub}}_{NaCl}\right) + \left(C'_{NaF} - C^{so\,\mathrm{lub}}_{NaF}\right)\right]\right\} \tag{3-52}$$

where C'_{NaCl} and C'_{NaF} represent the cumulative superficial concentration of sodium chloride (both dissolved and precipitated salt). $C^{so\,\mathrm{lub}}_{NaCl}$ and $C^{so\,\mathrm{lub}}_{NaF}$ are the solubility limits of sodium chloride and sodium fluoride in methanol, respectively.

Table 3-3. Solubilities of the two product salts that are formed in methanol

Salt	Solubility at 298.15 K	Reference
Sodium fluoride	0.03g/100g methanol	Stenger (1996)
Sodium chloride	1.4g/100g methanol	Stenger (1996)

3.3.4. Enhancement factor

The enhancement factor accounts for the increase in mass transfer that would result from a fast reaction (Nauman, 1987):

$$k_L = \left(k_L\right)_0 E_A \tag{3-53}$$

where $\left(k_L\right)_0$ is the mass transfer coefficient in the absence of a reaction. E_A denotes the enhancement factor. Krevelen and Hoftijer (1948) proposed an approximation method to calculate the enhancement factor according to the film and penetration model (van Swaaij and Versteeg, 1992):

$$E_A = \frac{Ha\sqrt{\frac{E_{A,\infty} - E_A}{E_{A,\infty} - 1}}}{\tanh Ha\sqrt{\frac{E_{A,\infty} - E_A}{E_{A,\infty} - 1}}} \tag{3-54}$$

where $E_{A,\infty}$ is defined as:

$$E_{A,\infty} = 1 + \frac{D_B C_{CH_3ONa,L}}{\nu_{CH_3ONa} D_A C^*_{R-22,L}} \tag{3-55}$$

$C^*_{R-22,L}$ and $C_{CH_3ONa,L}$ represent the concentrations of R-22 gas and sodium methoxide in the liquid phase, respectively and ν_{CH_3ONa} is the stoichiometric coefficient of sodium methoxide. D_A denotes the diffusivity of R-22 gas in liquid methanol at 303 K. The method of Wilke and Chang (1955) predicts the diffusivity of a dissolved gas in a liquid under dilute conditions (Perry et al., 1999).

$$D_A = 1.1728 \times 10^{-16} \frac{T\left(\chi_{CH_3ONa} M_{CH_3OH}\right)^{1/2}}{\mu_{CH_3OH} \hat{V}^{0.6}_{R-22}} \tag{3-56}$$

where χ_{CH_3ONa} is the solvent association parameter, specified as 1.9 for methanol (Perry et al., 1999), μ_{CH_3OH} represents the viscosity of methanol and M_{CH_3OH} is the molecular weight of methanol. $\hat{V}_{R-22}$ is the solute molar volume at the normal boiling point, in $m^3 \cdot kmol^{-1}$ with temperature T in Kelvin.

D_B in Equation 3-55 denotes the diffusivity of sodium methoxide in liquid methanol at 303 K. Sodium methoxide behaves as an electrolyte in methanol (Hine and Porter, 1957). The appropriate correlation for the infinite-dilution diffusivity of a solitary salt in a solvent was estimated using the Nernst-Haskell equation for binary electrolyte mixtures (Seader and Henley, 2006):

$$D_B = \frac{RT}{F^2} \frac{\left|\frac{1}{n_+}\right| + \left|\frac{1}{n_-}\right|}{\frac{1}{\lambda_+^0} + \frac{1}{\lambda_-^0}} \tag{3-57}$$

where $n_\pm$ is the valence of the cation and anion respectively and $\lambda_\pm^0$ is the limiting ionic conductances in $(A \cdot cm^{-2})(V \cdot cm^{-1})(g\text{-}equiv \cdot cm^{-3})$. The mole fraction of sodium methoxide in methanol was 0.02, so the application of the infinite-dilution diffusivity correlation was justified. For limiting ionic conductances at temperatures other than 298 K, $\lambda_\pm^o$ is multiplied by the temperature correction factor, given as (Seader and Henley, 2006):

$$Temperature\ correction\ factor = \frac{T}{334 \mu_{CH_3OH}} \tag{3-58}$$

Ha written in the enhancement factor expression in Equation 3-54 is the Hatta number, expressed as:

$$Ha = \frac{\sqrt{\frac{2}{m+1} k_{m,n} C_{R-22,L}^{*m-n} C_{CH_3ONa,L}^{n} D_A}}{k_L} \tag{3-59}$$

where m and n represent the orders with respect to R-22 and sodium methoxide, respectively. k_L is the liquid-phase mass transfer coefficient and $k_{m,n}$ represents the reaction rate constant in $(m^3)^2 \cdot mol^{-2} \cdot s^{-1}$. To determine k_L in the Hatta number, the volumetric mass transfer coefficient ($k_L a$) was divided by the interfacial area a. The volumetric mass transfer coefficient, the reaction rate constant, the orders of the reactants and the concentrations of the reactants were obtained from Nishiumi and Kato (2003). The interfacial area is defined by Garcia-Ochoa and Gomez (2004) as:

$$a = \frac{6\Phi}{d_b} \tag{3-60}$$

where Φ represents the dimensionless gas-holdup and d_b is the average bubble size. Kudrewizki (1982) estimated the gas-holdup as (Garcia-Ochoa and Gomez, 2004):

$$\frac{\Phi}{1-\Phi} = \frac{0.819 V_s^{2/3} N^{2/5} d_{imp}^{4/15}}{g^{1/3}} \left(\frac{\rho_L}{\sigma}\right)^{1/15} \left(\frac{\rho_L}{\rho_L - \rho_G}\right) \left(\frac{\rho_L}{\rho_G}\right)^{-1/15} \tag{3-61}$$

Equation 3-61 assumes that the impeller speed contributes to the size of the bubble and accounts for this (Garcia-Ochoa and Gomez, 2004). V_s is the superficial gas velocity, N is the impeller speed in rps, d_{imp} is the stirrer diameter and g represents the gravitational acceleration in $m^2 \cdot s^{-1}$. σ and ρ are the surface tension and density, respectively. Calderbank (1958) proposed an equation to determine the average bubble size, d_b (Garcia-Ochoa and Gomez, 2004):

$$d_b = \frac{0.7\sigma^{0.6}}{\left(P/V_L\right)^{0.4} \rho_L^{0.2}} \left(\frac{\mu_L}{\mu_G}\right)^{0.1} \tag{3-62}$$

where P represents the power input in W and V_L is the volume of liquid in the reactor. Power input is related to the Reynolds number (Re) by means of the Power number (Pw) defined according to Couper at al. (2005) as:

$$\mathrm{Re} = \frac{N d_{imp}^2 \rho_L}{\mu_L} \tag{3-63}$$

$$Pw = \frac{Pg}{N^3 d_{imp}^5 \rho_L} \tag{3-64}$$

The plot of Power number against Reynolds number is shown in Figure 3-3 for various impeller types. Line 13 on the graph was used as it represents a paddle without baffles.

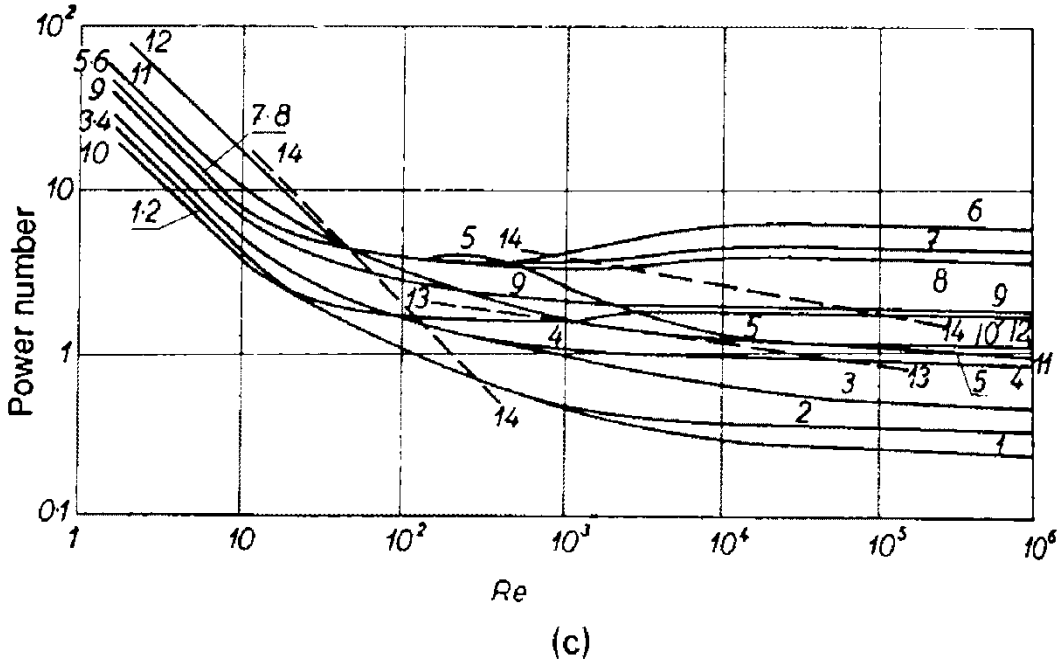

Figure 3-3. Plot of Power number against Reynolds number (Couper et al., 2005)

In order to determine the relevance of the enhancement factor in the model, a calculation was performed using the experimental conditions and data collected by Nishiumi and Kato (2003). For a first order reaction with respect to R-22 and a second order reaction with respect to sodium methoxide, the enhancement factor was calculated to be 1.007 at a reaction rate of 0.0823 $(dm^3)^2 \cdot mol^{-2} \cdot min^{-1}$ and reaction temperature of 303 K. The calculations are presented in Appendix D.

CHAPTER 4

EXPERIMENTAL

4.1. Equipment

The investigation of the gas-liquid reaction between R-22 and methanol was undertaken in two phases. In total, four different reactors were used in the study. Three reactors comprised the initial phase of study. The fourth reactor was designed specifically for the second phase of the project. The first phase involved preliminary experiments to determine the effect of temperature and sodium hydroxide concentration on the production of difluorodimethyl ether as well as to obtain suitable parameter ranges for the optimization of reaction conditions. A simple glass flask was used as the first reactor. The flask was equipped with neither a cooling coil nor a heating jacket. The design was identical to that proposed by Satoh et al. (1998). Temperature control proved to be very difficult. Reasons for this are given in the sections that follow. Other avenues were therefore explored. A semi-batch stainless steel bench-top reactor was constructed in accordance with the reactor design presented by Lee et al. (2001). A performance study on this system generated no constructive results with poor yields. Experiments were thus repeated with a small bench-top single-jacketed glass reactor. The performance factors analyzed were found to be significantly improved.

Experiments conducted in phase II consisted of an optimization study. The details of the study are presented in Section 4.4. Due to the inadequacies of the former reactors, a fourth reactor was designed and constructed for a kinetic study to be conducted. This reactor was void of the flaws present in the previous reactor systems. It was modified with improved temperature control by means of a single heating jacket and an internal cooling coil mechanism, improved mixing by the replacement of the magnetic stirrer with an overhead mechanical stirrer, and, most importantly, a sample point on the reactor head to extract a sample of liquid from within the reactor at pre-determined time intervals. A vacuum degassing rig was commissioned to terminate the reaction in each sample by removal of the reactant gas, R-22.

4.1.1. Preliminary testing on semi-batch reactor systems

Researchers from the Thermodynamic Research Unit, initially working on the project, designed a glass flask reactor unit shown in Figure 4-1. The design was obtained from Satoh et al. (1998). As this was the only equipment available at the initial stages of the project, testing of the above-mentioned apparatus was undertaken.

The initial design of the system utilized three cold traps for collecting reaction products, *viz.* the U-tube trap containing molecular sieve to trap methanol, the cold trap for trimethyl orthoformate removal, and the final cold trap to collect difluorodimethyl ether. A 1 dm^3 glass flask was submerged in a water bath at 273.15 K using ice/water slurry. The three necks on the glass flask were each used for a thermometer, a sintered gas sparger and an exit line. Solution was charged into the reactor prior to the commencement of an experiment. A magnetic stirrer bar within the reactor ensured that the solution was mixed. Due to the unnecessarily large size of the water bath, the required reactor temperature could not be maintained. The water bath was therefore replaced with a glass bowl. The compact fit of the reactor in the glass bowl allowed for faster and more efficient cooling with lower heat losses to the environment.

¼" glass tubing was used for the piping to connect each piece of equipment. Silicon tubing connected the glass tubing to allow for flexibility and minimize breakage. The inlet gas line to the reactor was a ¼" length of glass tubing with a sintered disc at the bottom end to disperse gas. Tubing lines were attached to all equipment by means of a screw cap fitting with a Teflon ring. This allowed for the height of the inlet and exit lines to be adjusted in case the situation presented itself.

The exit line from the reactor passed into the glass U-tube trap filled with molecular sieve 3A, an adsorbent used to trap alcohols such as methanol. The trap was succeeded by a second cold trap to trap trimethyl orthoformate. This trap was a glass bottle with an inlet and outlet port. The inlet line was coiled within the bottle. This increased the surface area of the tubing, thereby providing more adequate time for the vapours to pass through the trap. The former and latter traps were submerged in an ethanol bath at 268.15 K. A third trap was commissioned to collect the final product gas, difluorodimethyl ether. The trap was identical to the second cold trap, but larger in size, and submerged in a bath containing 2-propanol at 238.15 K.

Due to inadequacies in the design of this system, it was not possible to trap the final product gas without loss to the atmosphere. The apparatus (as available) was not practical as there were no valves on the glass vapour lines to isolate the difluorodimethyl ether (product) cold trap and the trimethyl orthoformate (by-product) cold trap. Removal of the traps (from their respective baths) for the contents to be weighed was therefore impossible without compromising the quality and composition of the products. The system design also failed to accommodate for a sample point from which product gas samples could be withdrawn for analysis. Modifications were undertaken to render the apparatus functional. The difluorodimethyl ether cold trap was removed and the line exiting the second cold trap was connected directly to a bubble flow meter and sampling point. The product gas flow was directed to the bubble flow meter with the option of flow to vent. The bubble flow meter measured the flow rate of product gas. Vapour samples withdrawn from the sampling point were injected into the gas chromatograph for analysis. The temperature at which the sample was taken was measured by a thermocouple fitted onto the sampling line. The ice/water slurry was used as a cooling medium to maintain a reaction temperature of 273.15 K. The reactor could not be maintained at this temperature with the existing cooling system. The ice/water slurry was not effective in counteracting the heat effects of the highly exothermic nature of the reactions.

Due to these experimental difficulties it was not possible to quantify the amount of difluorodimethyl ether that was produced by the reaction in this system.

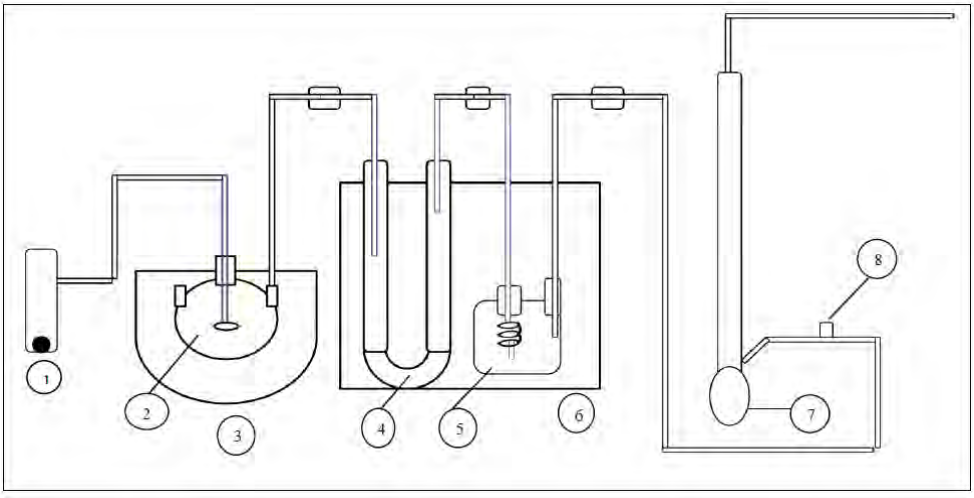

Figure 4-1. Glass flask system

1 – Rotameter, 2 – reactor with NaOH/methanol solution, 3 – ice bath at 273.15 K, 4 – cold trap 1: molecular sieve, 5 – cold trap 2, 6 – ethanol bath at 268.15 K, 7 – bubble flow meter, 8 – sample point

Since no useful results could be obtained with the previous system due to the poor design, in particular, the lack of temperature control, it was decided that system be discarded. As a result, a new reactor was commissioned.

A semi-batch stainless steel laboratory scale reactor was designed in accordance with Lee et al. (2001). The concept of the cold traps was used in this system despite the fact that Lee et al. (2001) used a batch system. A small semi-batch glass bench-top reactor was available at the School of Chemical Engineering. Note that this glass reactor is not the same reactor that was designed and used for the kinetic measurements that will be presented in Section 4.1.2. Experiments conducted on the stainless steel reactor were repeated with the glass reactor and a comparison of the results was made. The difluorodimethyl ether yields obtained in the stainless steel system were lower than those obtained in the glass reactor system.

Each of the latter two reactors was connected to the same auxiliary equipment, except for the condensers. Experimentation was initiated with the stainless steel reactor. The equipment setup is shown in Figure 4-2. The gas feed line from the R-22 cylinder bottle was connected to the R-22 rotameter using ¼" Polyflow tubing. The regulator fitted onto the cylinder bottle read 3 bar(g). The ¼" Polyflow tubing was also used for the line leading from the rotameter to the valve on the inlet of the gas sparger. The valve was used to close the inlet line during shutdown to prevent the flow of solution up the sparger as a result of backpressure. The vapour exit line leaving the reactor (Figure 4-3) was fabricated from ¼" stainless steel pipe and was fitted with a pressure gauge, a pressure relief valve and an isolation valve. The isolation valve was fitted on the vapour exit line, rendering the system capable of being used for either a batch or flow process. A stainless steel ¼" round handle Swagelok needle valve was selected for this purpose. The two ball valves in parallel on the outlet line of the reactor allowed for the choice between runnings as a batch or flow process. Valve V-104 in the process and instrumentation diagram was treated as a second outlet valve for flow experiments.

Figure 4-2. The experimental stainless steel rig excluding the cold traps

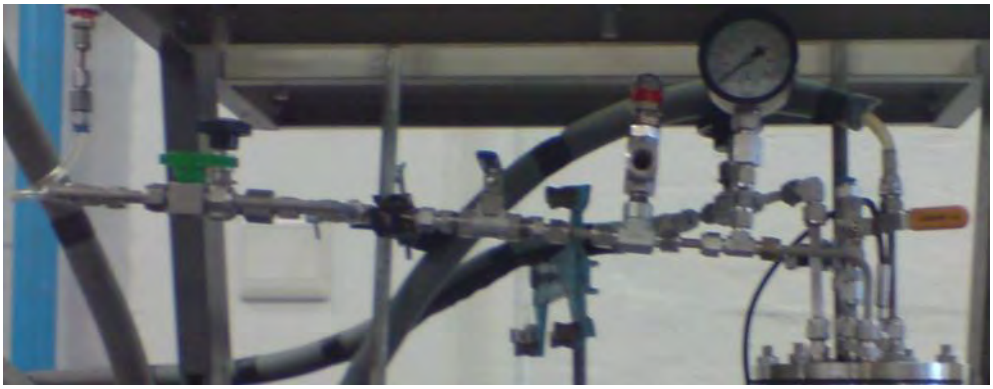

Figure 4-3. Vapour exit line leaving the reactor

A series of cold traps succeeded the condenser. The stainless steel U-tube trap contained molecular sieve 3A adsorbent to remove methanol from the product stream. A second trap cell (fabricated from stainless steel) removed any trimethyl orthoformate carried with the exit gas. Trimethyl orthoformate was present in the reactor in the liquid phase since its boiling point was greater than the reaction temperature. However, droplets of the liquid were carried out with the exit gas and were therefore removed using the second trap cell. Both the former and the latter traps were constructed from stainless steel and submerged in an ethylene glycol/water bath at 269.15 K (Figure 4-4). All Polyflow lines were attached to equipment by means of push-in fittings. The product gas, containing difluorodimethyl ether with residual methanol and trimethyl orthoformate, was collected

in a third cold trap submerged in ethanol at 235.05 K (Figure 4-5). This trap had an internal diameter of 65 mm and was fabricated from stainless steel (Figure 4-6).

Figure 4-4. Ethylene-glycol bath containing the first two traps

The o-Ring, manufactured from EPDM (P.R.) because of its resistance to R-22 and its ability to withstand a wide temperature range, was used between the flanges of the cold trap to prevent ethanol leaks into the trap. Six bolts tightly secured the flange of the vessel to the flange of the cold trap head. The valve on the sample point of the trap was initially submerged in the ethanol bath. The valve was manufactured to withstand a minimum of 263.15 K. The very low bath temperature rendered the valve useless. A length of ¼" stainless steel tubing was therefore used to raise the valve position above the bath liquid height. Valves on the inlet and exit of the cold trap allowed for the trap to be sealed off to the atmosphere after an experiment was completed. The exit line of the cold trap was also connected to an on-line sampling point and bubble flow meter.

Figure 4-5. Ethanol bath containing the difluorodimethyl ether cold trap

Figure 4-6. Difluorodimethyl ether cold trap

The reaction between R-22 and methanol was first carried out isothermally in the 0.5 dm^3, semi-batch reactor equipped with an internal cooling coil. The reactor cylinder was constructed from stainless steel with an internal diameter of 65 mm. The reactor cylinder was placed in a metal ring clamped to a retort stand to keep it in position and ensure that the reactor did not tip over. The cooling coil, fabricated with ¼" stainless steel pipe, was permanently fixed into the reactor top flange. Six holes were drilled into the flange of the cylinder and the reactor top flange. Six bolts tightly sealed the reactor top flange to the vessel body. A 3 mm thick PVDF gasket was placed between the flanges to prevent leakage of the gas (Figure 4-7). The gasket was securely kept in

place by the six bolts holding down the reactor top flange to the vessel. The band heater, screwed tight around the reactor, brought the reaction mixture up to the required temperature. The Pt 100 temperature probe measured the temperature of the solution within the reactor. The Pt 100 probe and the band heater were connected to an ACS temperature controller unit with auto tuned parameters. A rotating magnet with a motor was placed beneath the reactor. The magnetic stirrer bar was loaded into the reactor together with the feed mixture to mix the solution and prevent the settling of crystals of product salts. Gas was dispersed into the solution by means of a sparger. The sparger was simply a ¼" stainless steel tube with a metal sintered disc at the end. The gas exit line was screwed onto the reactor top flange to allow for easy removal during cleaning procedures.

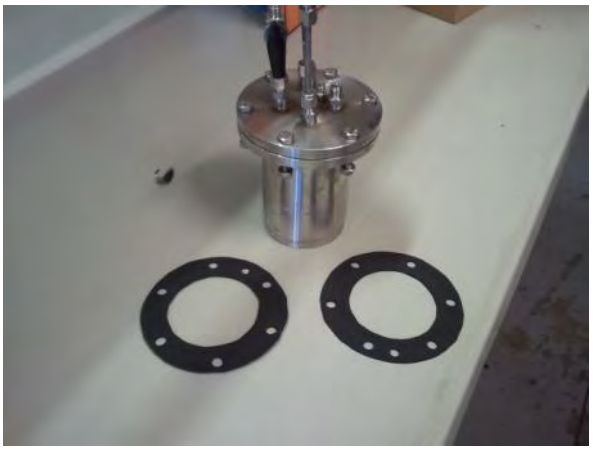

Figure 4-7. Reactor vessel with the PVDF gasket

The exit line from the reactor extended to the inlet of the vertical reflux condenser. This flow line was constructed partly from Polyflow tubing and partly from stainless steel piping. The condenser, fabricated from stainless steel had an internal diameter of 50 mm. The $^{1}/_{8}$" copper pipe was bent into a coil, the approximate length of the condenser. A hole was drilled in each flange for an inlet and exit line to be attached. A 50:50 coolant mixture of water/ethylene glycol flowed through the condenser shell at 269.15 K. Figure 4-8 shows a drawing of the stainless steel condenser without the insulation.

Figure 4-8. Vertical insulated stainless steel condenser shown without insulation

Figure 4-9. The experimental glass rig excluding the cold traps

Yields of difluorodimethyl ether obtained from experiments conducted with the stainless steel reactor were very low, averaging around 5%. It was suspected that the stainless steel could possibly be catalyzing the formation of trimethyl orthoformate. Experiments were therefore repeated on a vessel with a different material of construction. The reaction was therefore carried out in a 0.5 dm^3 semi-batch single-jacketed glass reactor with a magnetic stirrer (Figure 4-9). Water was circulated through the jacket as a form of heating/cooling medium. The reactor top flange had three necks: each for a thermometer, a condenser and a gas sparger. The gas sparger was constructed from a ¼" glass tube with a concave sintered disc. The disc shape did not provide adequate surface area for bubbling.

A double-jacketed reflux condenser, fabricated from glass, was connected to the reactor to reflux the methanol carried out with the product gas. A 50:50 mixture of water/ethylene glycol flowed through the condenser at 269.15 K. The outlet of the condenser was connected to the series of cold traps mentioned previously. The reactor was placed on a magnetic plate and a stirrer bar placed in the reactor provided sufficient mixing.

The process and instrumentation diagrams for the experimental setups using the stainless steel reactor and the single-jacketed glass reactor are shown in Figures 4-10 and 4-11, respectively.

CT-1-3	Cold trap
HX-101	Condenser
R-101	Semi-batch reactor
T-101	Gas cylinder bottle
V-101-109	Valves

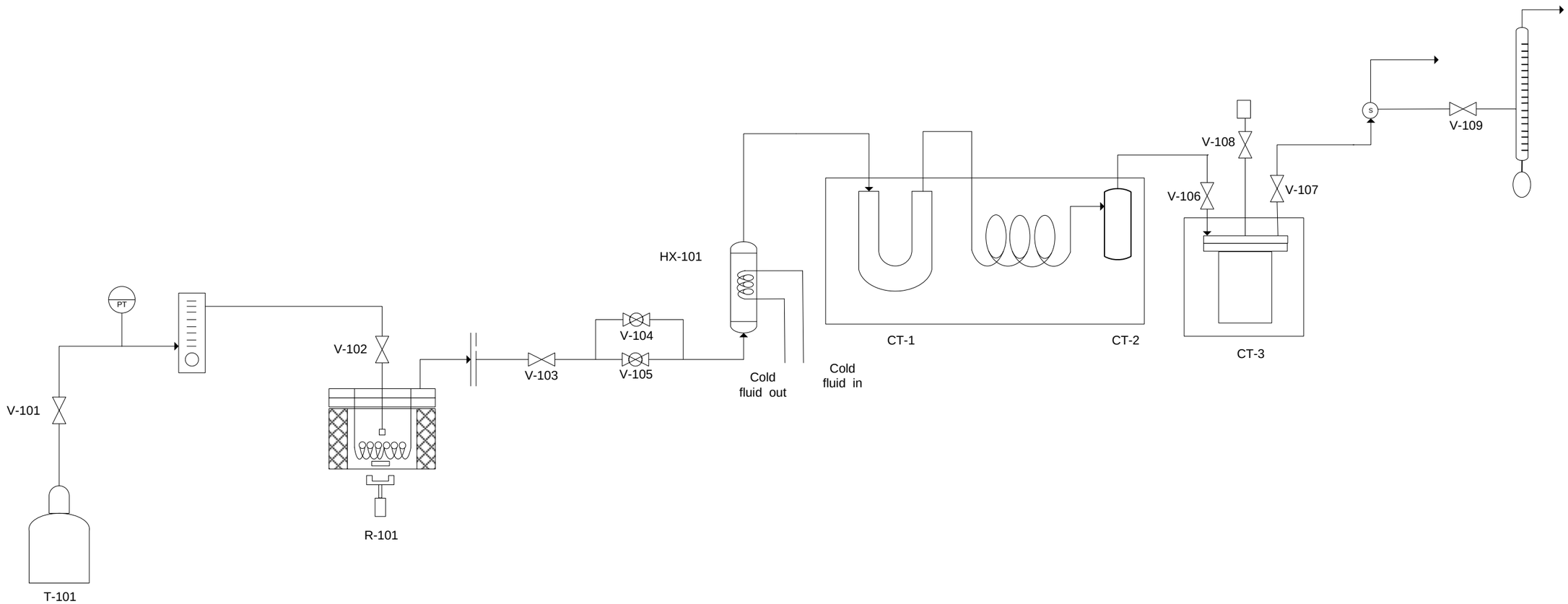

Figure 4-10. Process and Instrumentation diagram for the selective production of difluorodimethyl ether in a stainless-steel semi-batch reactor

Author: Rasmika Prithipal

Drawing no. 001

Date: 21 November 2012

CT-1-3	Cold trap
HX-101	Condenser
R-101	Semi-batch reactor
T-101	Gas cylinder bottle
V-101-109	Valves

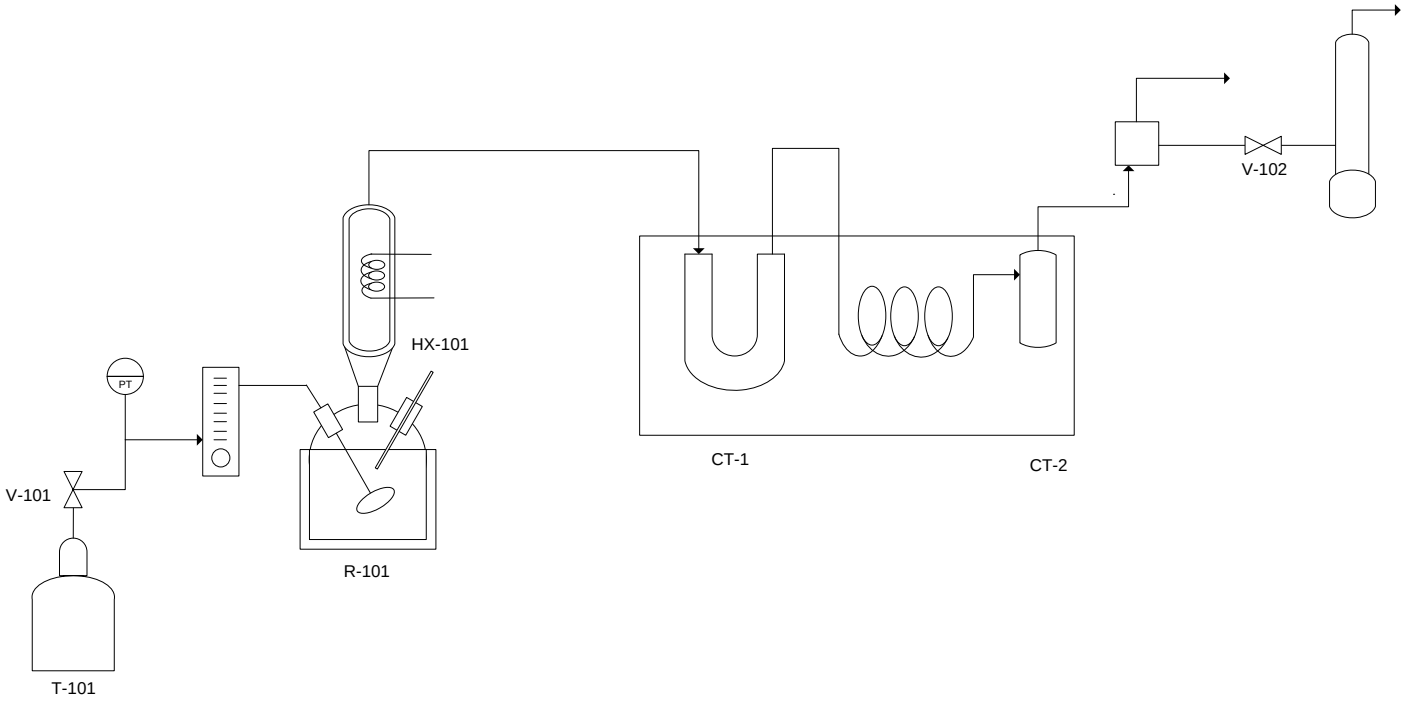

Figure 4-11. Process and Instrumentation diagram for the selective production of difluorodimethyl ether in a glass reactor

Author: Rasmika Prithipal

Drawing no. 002

Date: 21 November 2012

4.1.2. Batch Absorber for the R-22-methanol kinetic study

Based on the observations and the pitfalls of the former reactor systems, a semi-batch reactor was designed and constructed specifically to conduct a kinetic study. The design of the reactor was dependent on the heat transfer calculation undertaken to determine the area of the coil that was required to provide sufficient cooling for the exothermic reactions that occur in the reactor as well as the external convective heat transfer coefficient (Appendix A). The reaction was conducted in a 2 dm^3 isothermal, semi-batch reactor equipped with a single heating jacket and an internal cooling coil. The reactor was fabricated from glass with an internal diameter of 76 mm. Glass was selected as the material of construction since stainless steel exhibited possible catalytic tendencies toward the by-product.

4.1.2.1. Setting the feed gas composition

Different partial pressures of R-22 were obtained by diluting the pure refrigerant with nitrogen gas. This was accomplished by feeding R-22 gas and nitrogen gas through different and parallel rotameters and combining the gases at the mixing point. A series of 2-way ball valves (Swagelok, 316, AFS) was used to close off flow to the rotameters, should the operator opt to. 3-way switching ball valves (Swagelok, 316 SS, PTFE) were installed in order to alternate between the directionality of flow to vent or to reactor, and the directionality of product flow to vent or bubble flow meter. R-22 and nitrogen were combined at the mixing point located before the 3-way valves. All the valves were mounted on a panel shown in Figure 4-12. Pressure regulating assemblies, consisting of a pressure regulator and a needle valve, were connected to each gas cylinder. Flow rates of each gas were measured with rotameters calibrated for the respective gas (Section 4.2.2). Combinations of nitrogen gas and R-22 gas flow rates were selected such that the total feed flow rate of gases equaled 2 $dm^3 \cdot min^{-1}$. The partial pressure of R-22 was calculated according to the following equation using a total volumetric flow rate of 2 $dm^3 \cdot min^{-1}$:

$$P_{R-22} = \frac{V_{R-22}}{V_{TOT}} P_{TOT} \tag{4-1}$$

Figure 4-12. The valve panel: front view and back view

4.1.2.2. Reactor vessel

The reactor apparatus is shown in Figure 4-13. The reactor vessel consisted of a long cylindrical unit surrounded by a glass jacket. A drainage valve at the bottom of the reactor allowed for ease of cleaning. Water was pumped through the jacket at reaction temperature. The reactor unit was mounted on a tripod stand, thereby supplying the operator access to the drainage valve. Support was supplemented by situating the reactor within a confinement structure. A thick slab of board was screwed onto one side of a wire mesh cage. The reactor was placed within a square hole cut into the structure.

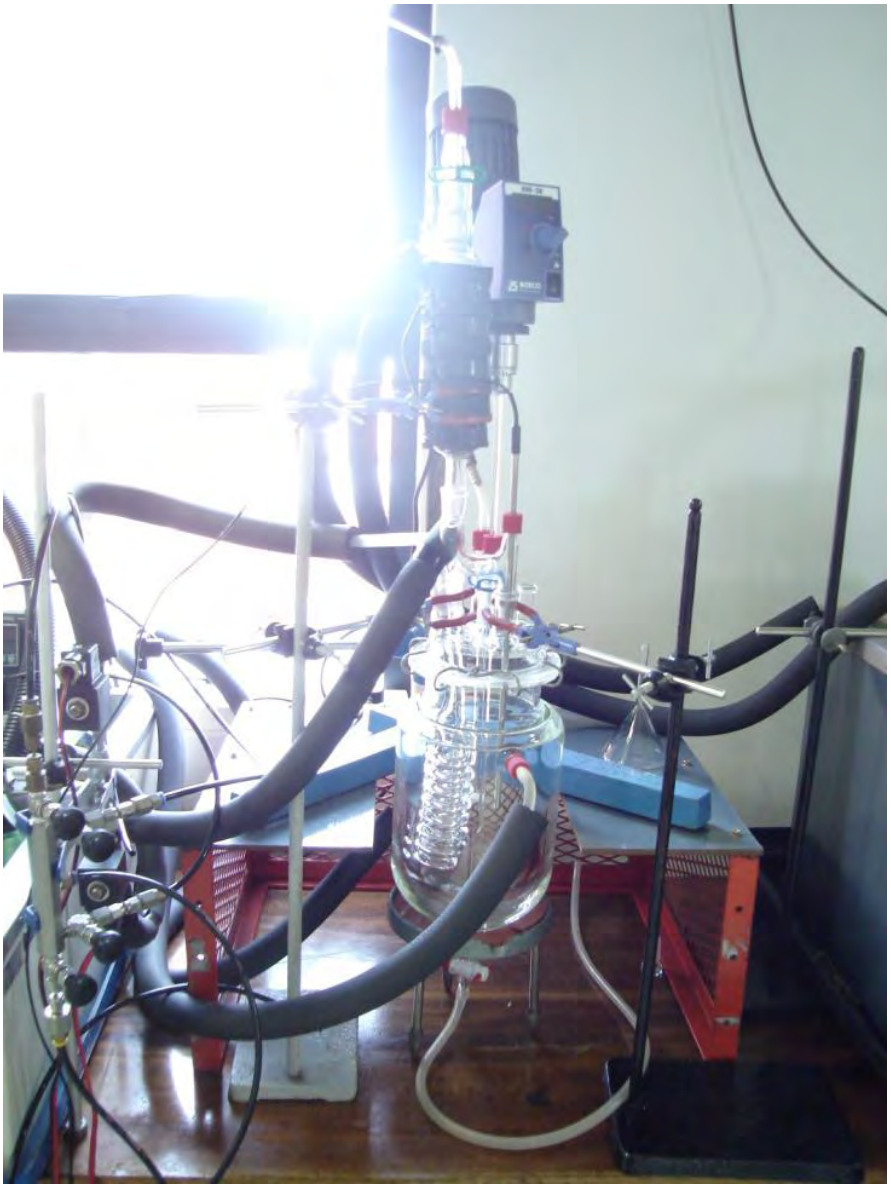

Figure 4-13. Reactor apparatus

The reactor top flange was manufactured with four necks, although the original design specified five necks. By attaching a forked neck to a single neck on the reactor top flange, both the temperature probe and the reflux condenser were accommodated for. The three other necks were utilized for the gas sparger, a liquid sample point and an overhead stirrer. The cooling coil, fabricated from ¼" glass tubing, was permanently attached through the reactor top flange for ease of assembly. The purpose of the cooling coil was to maintain the reactor temperature because of the highly exothermic nature of the reaction. The double-jacketed reflux condenser was manufactured from glass. The double jacket provided a greater surface area for increased cooling. The condenser

refluxed methanol carried out with the product gas. Loss of methanol would alter the conditions within the reactor because methanol is the sole source of the methoxide anion, CH_3O^- (Hine and Porter, 1957). The flanges were greased with silicone gel to maintain an airtight vessel. A metal clamp sealed the flanges of the reactor and the reactor top tight.

An overhead mechanical stirrer was used to provide more efficient mixing of the reactor contents. The stirrer comprised a glass rod attached to an overhead stirrer motor, with a Teflon paddle of length 50 mm. To achieve the appropriate height above the reactor, the stirrer motor was mounted onto a thick metal rod supported by angled leg stands. The gas sparger was a glass rod with a sintered disc at the lower end.

4.1.2.3. Reactor temperature control system

Both reactions considered in this work are exothermic resulting in a combined reactor heat duty of 545 W, as determined by the summaric product of the reaction rate and the heat of reaction for each reaction, respectively. The details of this calculation are explained in Appendix A. Continuous cooling was therefore required to maintain the correct reaction temperature. The glass reactor was equipped with an internal glass cooling coil for this purpose. A portion of the study required experiments to be carried out at above ambient temperatures. The glass reactor was therefore also equipped with a heating jacket. Input from a 200 mm long Pt 100 temperature detector was passed to an RKC microprocessor based digital temperature controller with a supply voltage of 100-240 V AC. The Pt 100 had a probe diameter of 8 mm and was attached to a 3 m 3-core Teflon insulated cable. The two outputs of the temperature controller were equipped with two control actions: heating and cooling. Output 1 and Output 2 provided a heating and cooling action respectively. Both outputs were contact relays. The PID parameters were tuned for ideal temperature control (Section 4.2.). Two solenoid valves were placed on the cooling line (as demonstrated in Figure 4-14) such that flow would be alternated between the cooling coil and the bypass line returning to the source. ½" normally closed stainless steel solenoid valves were used with pressure limitations ranging between 0-9 bar. During actual experiments, the heating and cooling media passing through the jacket and coil, respectively, were used in conjunction to maintain the set point temperature. The heating medium passed continuously through the jacket. When cooling was required the solenoid valve on the cooling line leading to the coil was opened allowing cooling of the reaction mixture.

When the cooling cycle was over, the solenoid valve on the bypass line was opened. Hot water was used as the heating medium. Ethanol was used as the cooling medium.

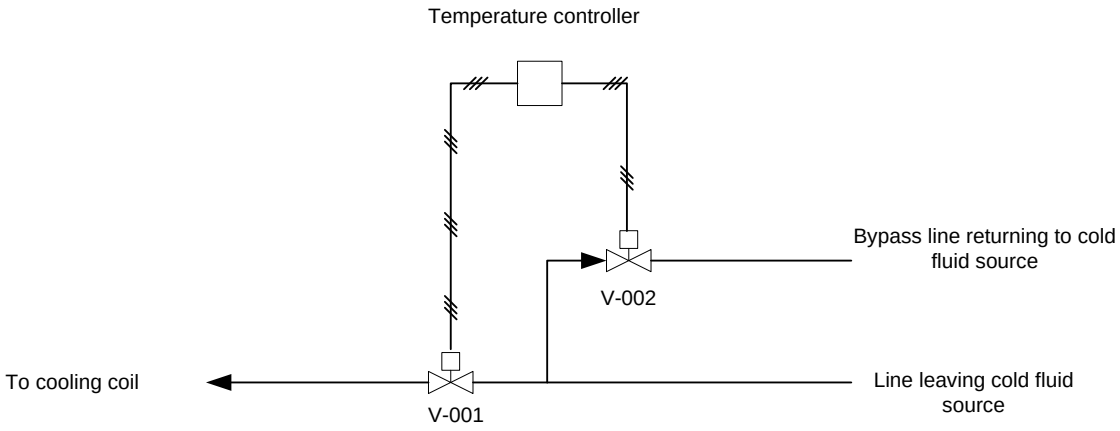

Figure 4-14. Schematic of temperature control system

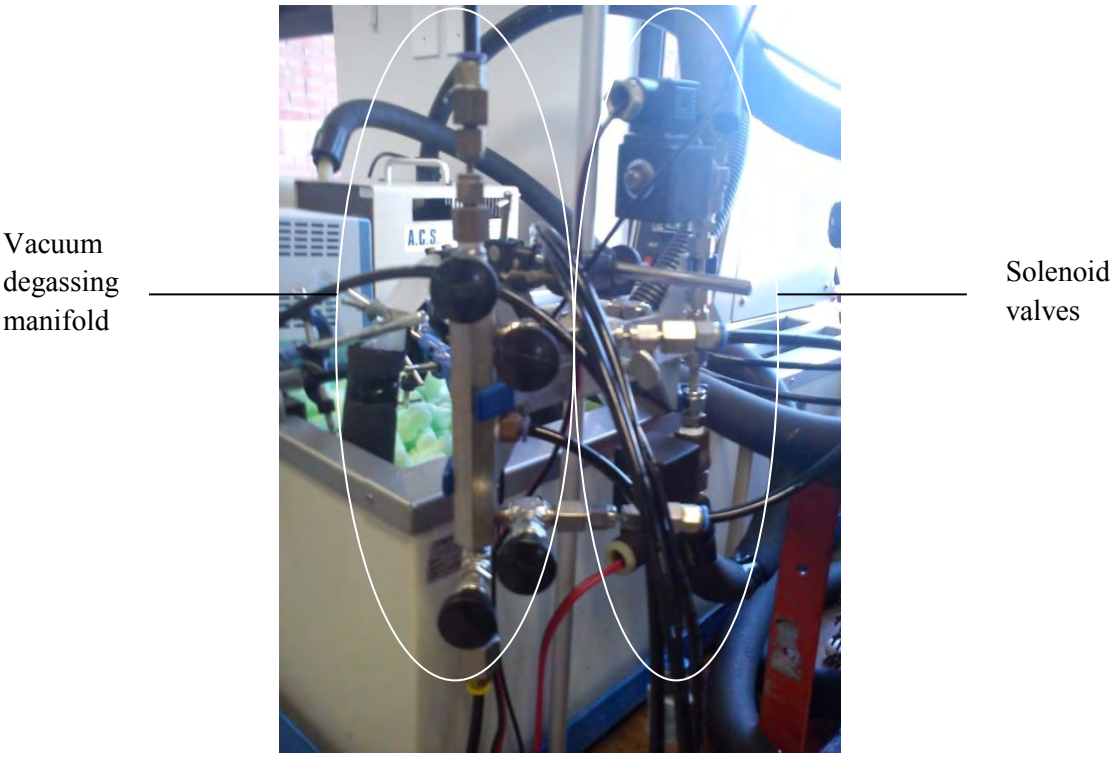

Figure 4-15. Solenoid valves and vacuum degassing manifold

4.1.2.4. Vacuum degassing rig

Vacuum degassing is a process that preceded the analysis of samples withdrawn from the reactor vessel. The reactions occurring in the reactor vessel do not cease once the withdrawn samples are decanted into the volumetric flasks for storage (prior to analysis). To stop the reactions, the reactant gas (R-22) was removed from the samples by means of vacuum degassing. The degassing rig was constructed in the ethanol bath that fed cold fluid to the cooling coils (Figure 4-16). A metal rod was secured across the width of the bath. Four clamps were attached to the rod using boss heads. A Polyflow tubing line connected the vacuum pump to the central connection point on the manifold in Figure 4-15. The manifold had four other connection points: at the top, bottom, top right and bottom right. All five connection points on the manifold had push-in fittings at the ends. Four ¼" round handle Swagelok needle valves were attached to the manifold at the connection points. In this way, each connection point could be opened or closed independent of the other points. The Polyflow lines leaving the push-in fittings were fitted into rubber bungs on the opposite end. An annular space was created in the rubber bung for this purpose. The rubber bungs were sized to fit the necks of the 50 cm^3 volumetric flasks used to store the samples.

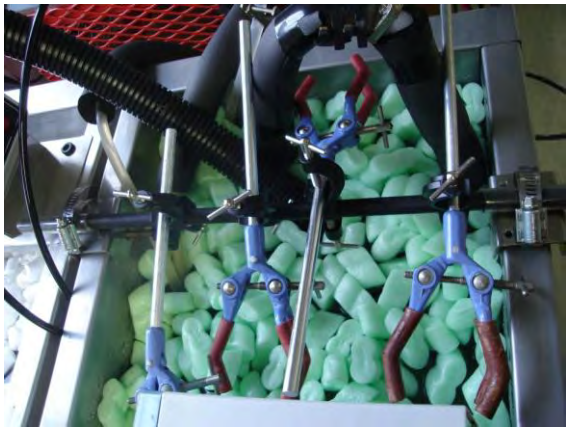

Figure 4-16. Ethanol bath used for the degassing process

Figure 4-17 shows the process and instrumentation diagram for the experimental setup using the batch absorber.

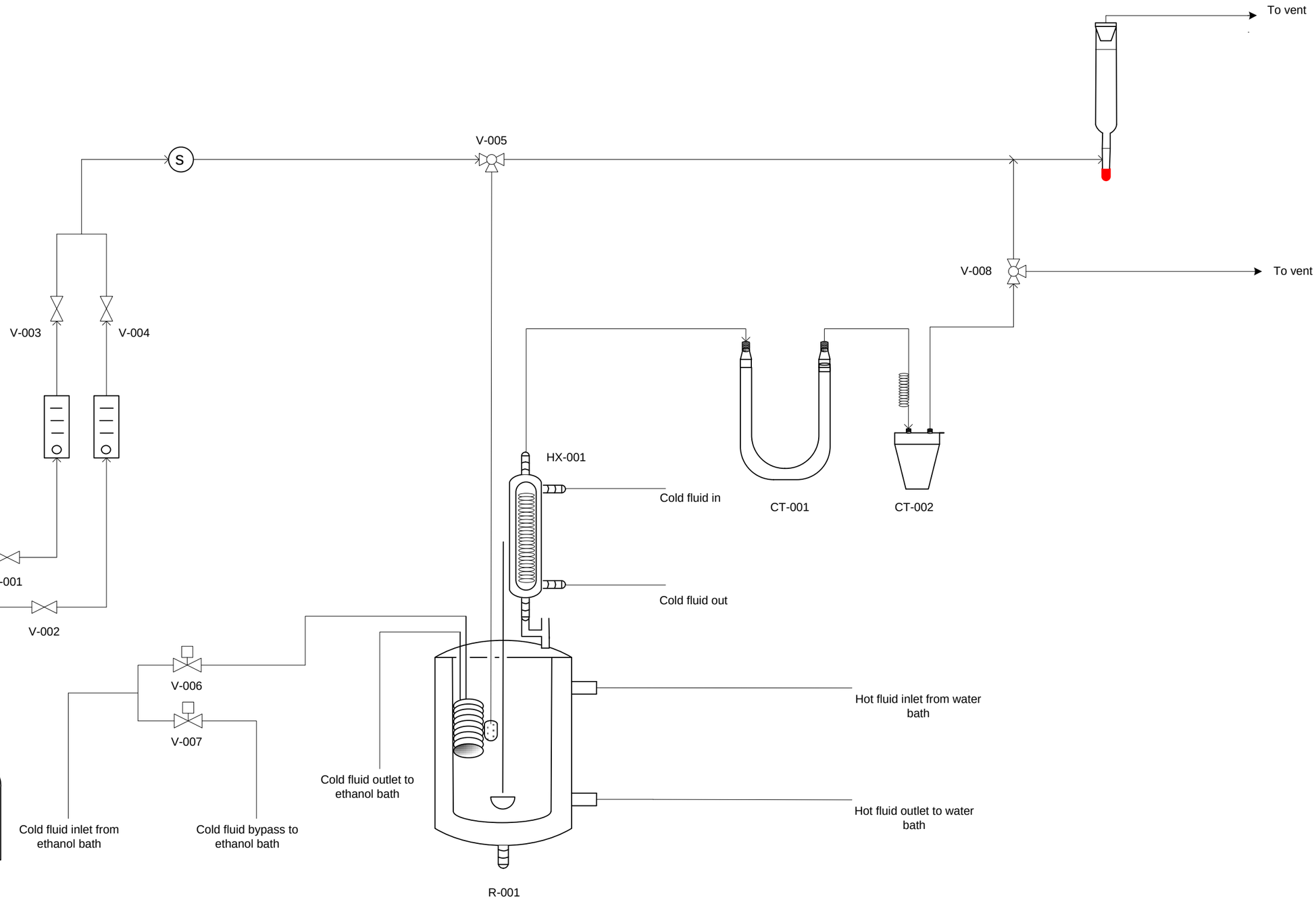

CT-001-002	Cold traps
R-001	Semi-batch reactor
T-001	Cylinder bottles
V-001-004	Two-way valves
V-005, V-008	Three-way valves
V-006, V-007	Solenoid valves

Figure 4-17. Process and instrumentation diagram of the kinetic study for the selective production of difluorodimethyl ether from R-22 in a jacketed glass reactor

Author: Rasmika Prithipal

Drawing no. 003

Date: 21 November 2012

4.1.3. Apparatus for the measurement of $(k_La)_{oxygen}$

4.1.3.1. Setup for $(k_La)_{oxygen}$ tests

Despite the availability of numerous correlations in literature to estimate the overall mass transfer coefficient of a gas in a liquid, none afforded a reliable estimation for the system in this project due to the specific reactor dimensions and operating conditions associated with this system. Overall mass transfer coefficients were measured for oxygen (Appendix F). These values were then used to calculate the overall mass transfer coefficients for the refrigerant gas, R-22, according to the well-known mass transfer relationships as described in Section 3.3.3.

All $(k_La)_{oxygen}$ experiments were conducted in a vessel, that operated as a batch absorber with no reaction, at the identical conditions to the kinetic experiments. A Hamilton Visiferm Dissolved Oxygen (DO) ARC probe was used to measure the concentration of dissolved oxygen in methanol. The probe was inserted into the reactor through a hole on the top flange (Figure 4-18). A clamp loosely held the probe in place. The probe was connected to the computer interface via a USB-RS485 Modbus converter. The previous R-22 lines were disconnected and replaced with air-lines.

Figure 4-18. Hamilton Visiferm DO ARC probe in reactor

4.1.3.2. Rig for the determination of the sensor lag

The accuracy of the measured overall mass transfer coefficient is limited by the response time of the sensor. A fast sensor response is favourable. The response time of the sensor can be neglected if the sensor lag constant (k_{probe}) is much smaller than the inverse of the overall mass transfer coefficient $\left(\frac{1}{k_L a}\right)$ (Gauthier et al., 1990). A step experiment was used to determine the sensor response time (Appendix F). The experiment involved the instantaneous change in dissolved oxygen concentration by the transfer of the probe from a vessel containing solvent saturated with oxygen (in this study air was used as the source of oxygen) to a vessel containing solvent saturated with pure nitrogen, until a negligible dissolved oxygen concentration was measured. Two 1 dm^3 beakers were each placed on a magnetic stirrer plate. A gas sparger was partially submerged in each beaker, held in place by a clamp attached to the retort stand. The gas sparger in the beaker on the left in Figure 4-19 was connected to the oxygen cylinder with Polyflow tubing. The gas sparger in the beaker on the right of Figure 4-19 was connected to the nitrogen cylinder. A clamp was attached to each retort stand to secure the Hamilton Visiferm DO ARC probe.

Figure 4-19. Rig for sensor lag measurements

4.2. Materials and Procedures

R-22 gas and nitrogen gas with purities of >98% and 99.9999%, respectively, were purchased from Afrox. Methanol and sodium hydroxide were required to prepare the liquid reactant. Analytical grade (AR) methanol with a purity of 99.5%, sodium hydroxide pellets, 95% pure ethanol, 99% pure ethylene glycol and 2-propanol were obtained from Merck. Merck also supplied all chemicals pertaining to the spectrophotometric analysis of samples. Although spectrophotometric grade reagents are commonly used for such analyses, the cost is too great. AR grade reagents are commonly used for analytical purposes. The majority of the reagents used were available only in AR grade, with the exception of ferric chloride. As a result, all chemicals purchased from Merck were of AR grade. Mercury (II) thiocyanate, iron (iii) perchlorate hydrate, sodium chloride and 60% perchloric acid were purchased for the chloride analysis. Ferron, ferric chloride hexahydrate and sodium fluoride were purchased for the intended fluoride method. A chemical data table is given in Appendix E.

As with any analytical method, preparation involving the use of water requires access to distilled water. 250 dm^3 of distilled water was prepared in the laboratory for this project.

4.2.1. Feed Preparation

A 5 dm^3 glass beaker was filled to the required volume (1.5 dm^3) with methanol. A calculated total mass of sodium hydroxide was charged into the beaker in small quantities. The sodium hydroxide reacted with the methanol to give sodium methoxide. A molar excess of methanol was used. There are two advantages to this method: the heat generated from the reaction between sodium hydroxide and methanol will dissipate and all the sodium hydroxide pellets will dissolve in time for the next charge. The beaker was placed on a magnetic stirrer plate and a magnetic stirrer bar was used to mix the contents of the beaker. Once all the sodium hydroxide pellets were dissolved in the methanol, the solution was emptied and stored in a glass bottle with a plastic air tight cap. Prior to the beginning of an experiment, the solution was charged into the reactor via the sample point.

4.2.2. Calibration

The calibration of measuring instruments is vital to obtain accurate measurements of experimental data. Repeated calibrations provide information on the reliability of equipment as well as the reproducibility of data.

4.2.2.1. Rotameter Calibrations

Rotameter calibrations for the volumetric flow rate were undertaken first to determine the partial pressures of R-22, according to Equation 4-1, that were required for the experimental design. The nitrogen and R-22 rotameters were each calibrated at standard conditions. At each float position on a rotameter, the time taken for a bubble to reach the 200 cm^3 mark on the bubble flow meter was recorded. The procedure was repeated three times to show repeatability. A plot of the volumetric flow rate of gas against float position revealed a linear response for both rotameters. Figure 4-20 and Figure 4-21 show the calibration curves for the R-22 rotameter and nitrogen rotameter, respectively. The average relative uncertainties were 1.24 % and 1.45 % for the R-22 rotameter and nitrogen rotameter, respectively.

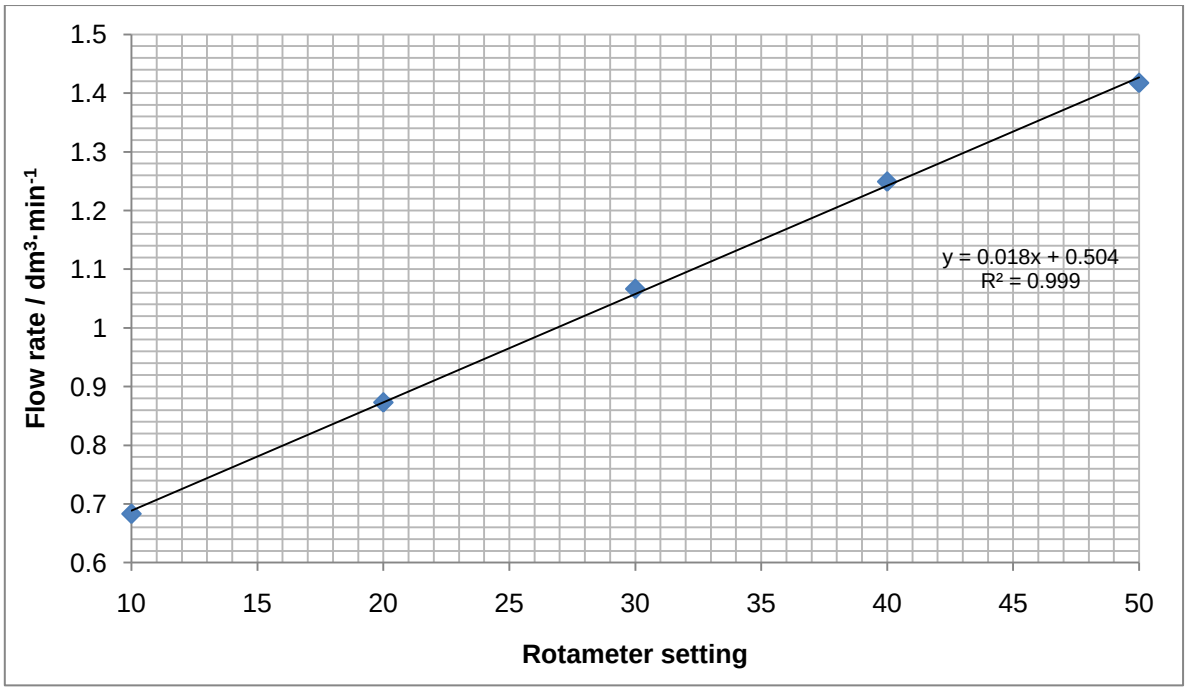

Figure 4-20. Calibration chart for the R-22 rotameter

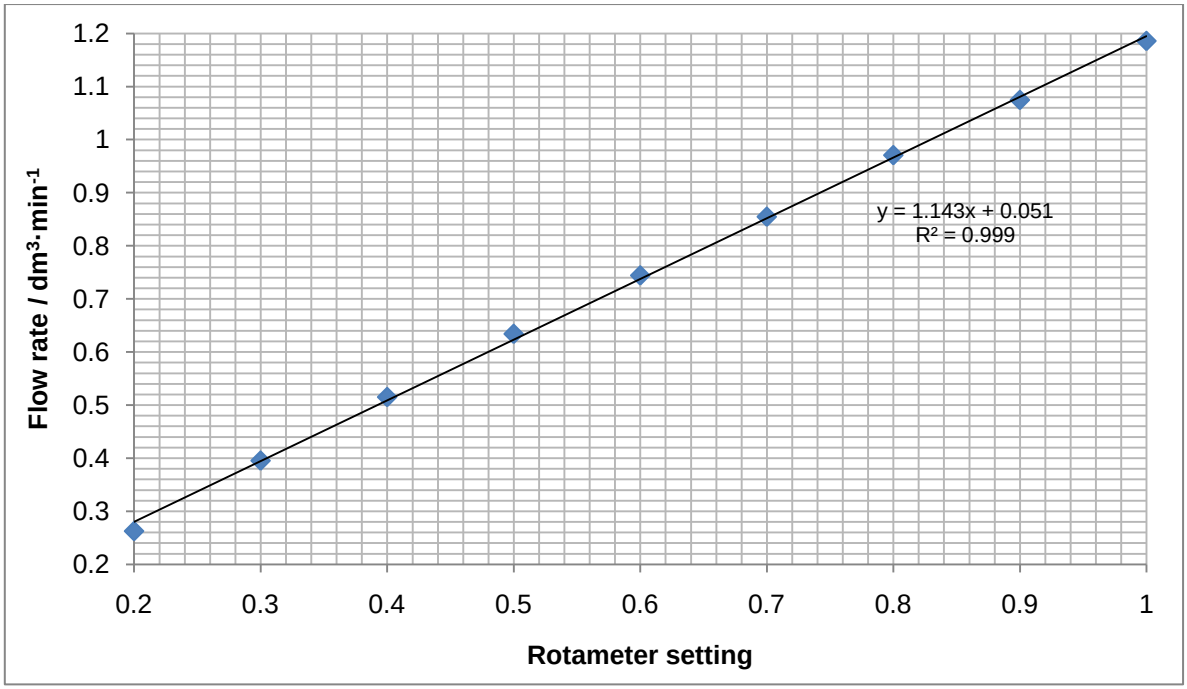

Figure 4-21. Calibration chart for the N_2 rotameter

4.2.2.2. Temperature sensor calibration

A Pt 100 temperature detector was used in the apparatus for the kinetic study. The probe must be calibrated to ensure an accurate, stable performance of the measuring device. The thermal calibration was achieved using a WIKA CTH 6500 display with a Pt 100 standard probe and a CTB 9100 thermo stated oil bath (Figure 4-22). The standard probe was connected to the display unit and was immersed in the oil bath together with the Pt 100 probe.

Figure 4-22. WIKA CTH 6500 display with thermo stated oil bath

The temperature of the oil was elevated to a desired set point and the system was allowed to reach thermal equilibrium. The temperatures of the standard probe and the Pt 100 probe were recorded. The procedure was performed three times for repeatability. The calibration chart in Figure 4-23 was generated, with absolute uncertainties plotted in Figure 4-24. The maximum absolute measurement error for the temperature range of interest was 0.35 K.

A fixed heat load was inserted into the reactor to determine the effectiveness of the heating/cooling mechanism. A 238 Ω, 200 V cartridge heater simulated the reaction heat in methanol. The system was found to be capable of handling a much larger heat load than the estimated reaction heat (as specified in section 4.1.2.3) and was able to effectively maintain the set-point temperature. The controller PID parameters were tuned for ideal temperature control using the auto tuning feature of the instrument. The optimized parameter values are listed in Table 4-1. Using these parameters the temperature in the reactor vessel with a fixed heat load was maintained to within 1.2 K of the set point temperature which was deemed to be acceptable.

Table 4-1. PID tuning parameters

Gain	20
Derivative time / s	50
Integral time / s	200

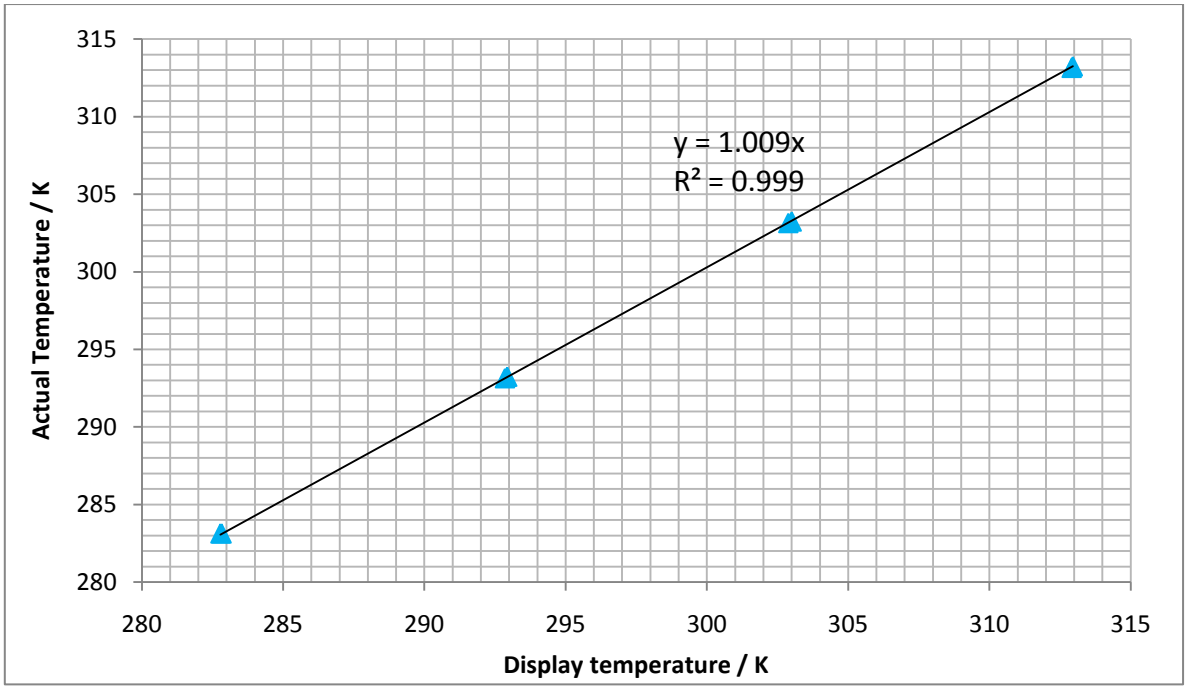

Figure 4-23. Calibration of the temperature sensor

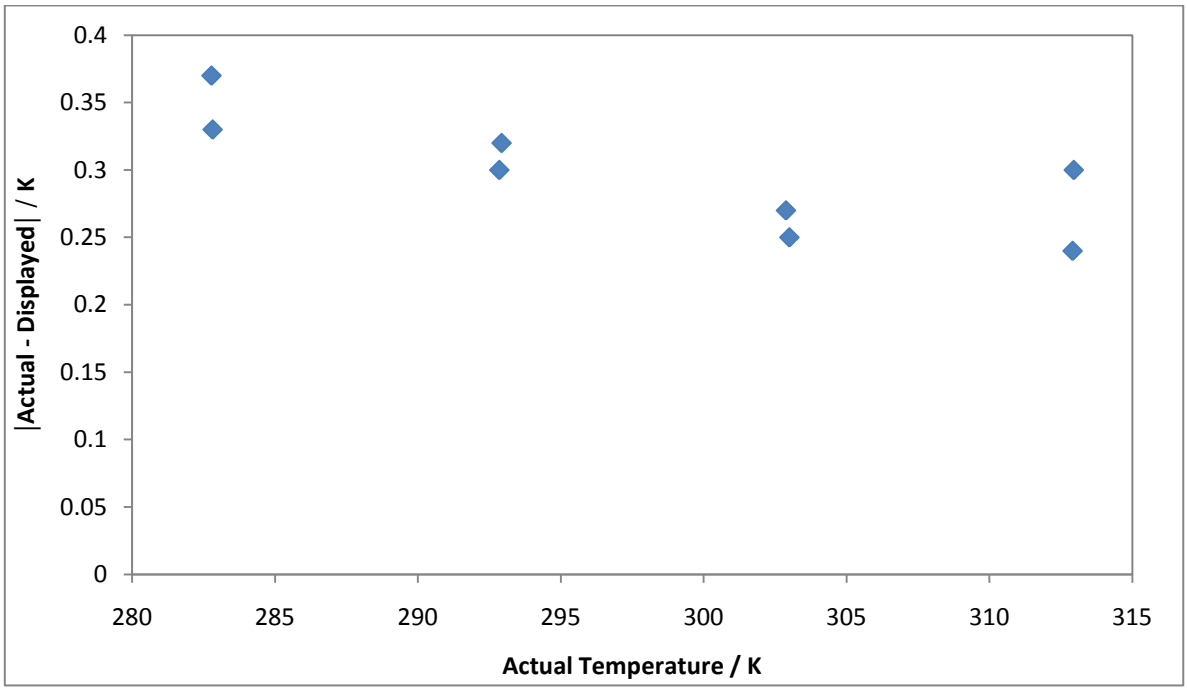

Figure 4-24. Temperature uncertainty plot

4.2.2.3. GC Calibration

Vapour samples obtained from preliminary experiments were analyzed on a Shimadzu GC 2014 gas chromatograph. The instrument was equipped with a flame ionization detector and a Poropak Q column. Nitrogen was used as the carrier gas. The operating conditions of the instrument are presented in Table 4-2.

Table 4-2. Operating conditions of the Shimadzu GC 2014

Column: Poropak Q		**Detector:** FID
Method	**column oven**	313 K
	hold time	1 min
	rate	313 K·min^{-1}
	column oven	423 K
	hold time	40 min

The components that were present in the product gas included methanol, difluorodimethyl ether, trimethyl orthoformate and R-22. For a few of the experimental runs a small quantity of ethanol was also present. This was probably introduced into the system from the ethanol bath in which the cold trap was submerged. Since pure samples of difluorodimethyl ether and trimethyl orthoformate were not available for gas chromatograph detector calibration, the simple area ratio method was used to determine the mole fraction of the individual species. The area of each component peak *i* obtained on the chromatograph is divided by the summation of all the area peaks (representative of the whole sample). The mole fraction of component *i* is given by:

$$x_i = \frac{A_i}{\sum_i A_i} \tag{4-2}$$

The latter assumes that the detector response factors are equal for all components in the mixture and should be used as a first approximation. Samples of R-22 gas, methanol and ethanol were injected into the G.C. and the retention times were noted. Pure trimethyl orthoformate formed during a preliminary experiment (confirmed by analysis through the G.C.M.S.) was also injected into the G.C. in order to find the retention time of the component. Since, the retention times of R-22 gas,

methanol, ethanol and trimethyl orthoformate were now known, the outstanding peak would be difluorodimethyl ether (as per the reaction mechanism). A typical chromatogram is shown in Figure 4-25.

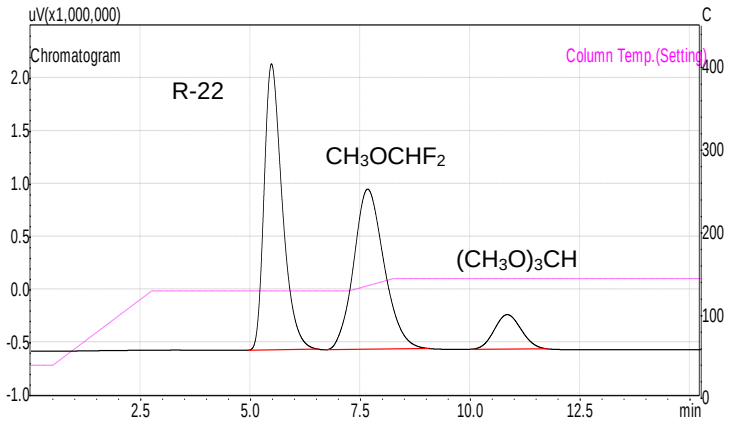

Figure 4-25. A typical chromatogram showing the component peaks

For the instrument used in this investigation detector response factors for light hydrocarbons have been found to be within a consistent range (i.e. relative response factors very close to 1). However, completely fluorinated species have been found to have detector response factors differing by several orders of magnitude. The partially fluorinated species considered here are likely to have different responses as well but not to the same degree as perfluorinated compounds. The G.C. method was used only for the preliminary experiments, where a qualitative comparison of performance between a glass and metal reactor was made. The bulk of the experimental results and model identification were therefore not affected by these variations in detector response.

4.2.3. Experimental Procedure

4.2.3.1. Procedure for preliminary experiments

Prior to conducting an experiment, the liquid reactant was prepared according to the method outlined in Section 4.2.1. The procedures undertaken for runs conducted with the stainless steel reactor and the jacketed glass reactor are similar as these two pieces of equipment were connected to the same auxiliary equipment. For the stainless steel unit the following procedure applied. Reference is made to Figure 4-10.

First the circulator in the ethylene glycol bath (feeding the cooling coil and condenser shell) was set to 269.15 K. Thereafter liquid reactant feed was charged into the reactor followed by the placement of the magnetic stirrer bar in the reactor. The gasket was then aligned properly on the reactor vessel flange. The vessel was lifted into the ring holder after which the reactor top flange was aligned into position and tightly bolted with six bolts. The exit line of the reactor was then attached to the reactor top flange. An allen key was used to tighten the band heater around the vessel. The motorized magnet was raised until it was positioned just below the reactor, without touching the underneath of the reactor. At this point the equipment was ready for the experiment to begin.

The R-22 inlet valve on the reactor, valve V-103 was turned to the close position. The pump, temperature controller and thermocouple power were switched on. The controller was set to the reaction temperature. Once this temperature was attained, the ethylene glycol flow was diverted from the bypass stream. Next, the inlet and exit valves on the difluorodimethyl ether trap (valves V-106 and V-107) were turned to the open position, followed by the valve on the R-22 inlet line (V-102) and the isolation valve (valve V-103). The R-22 cylinder valve (valve V-101) was finally opened and the appropriate flow rate was set on the rotameter. Simultaneously, the timer was started. At five minute intervals, the direction of product flow was switched to the bubble flow meter. Samples were withdrawn on-line with a gas-tight syringe and injected into the gas chromatograph for analysis. Flow was redirected to the vent after withdrawal of each sample via valve V-109.

The first step in the shutdown procedure involved closing the R-22 cylinder valve (valve V-101). Thereafter the inlet valve to the reactor (V-102), the isolation valve (valve V-103) and the difluorodimethyl ether trap valves (valves V-106 and V-107) were closed. The rotameter was purged and the thermocouple, temperature controller and pump were turned off. Flow of ethylene-glycol was redirected to the bypass line. Finally, the circulator in the ethylene glycol bath was set back to 283.15 K.

The procedure for the single jacketed glass reactor was similar to that described above. The reactor was charged with the liquid reactant followed by the placement of the magnetic stirrer bar. The vessel flange was well greased before placing the reactor top flange onto the reactor vessel. The metal clamp was tightened around the flanges with a flathead screwdriver. The double-jacketed reflux condenser was then lowered onto the reactor neck and securely clamped. The pump was switched on and once the reaction temperature was attained, ethylene-glycol flow was diverted to

the condenser. The exit and inlet valves on the difluorodimethyl ether trap were turned to the open position. The procedure hereon was identical to that mentioned previously.

The shutdown procedure follows that previously presented with exception of the steps involving the reactor inlet valve, isolation valve and thermocouple.

4.2.3.2. Procedure for the R-22-methanol kinetic study

Once again, the liquid reactant was prepared prior to initiation of the experiment. The controller and heat pump in the hot water bath were switched on approximately an hour before commencement of the experiment. The reactor temperature was then set on the controller. The jacket was allowed to attain the desired temperature. The reactor was thereafter filled with the liquid reactant. The overhead stirrer was switched on. The reactor temperature controller and the power supply to the solenoid valves were turned on. The flow from the cold bath containing ethanol was directed to the solenoid valves. Coolant flow was also directed to the reflux condenser. Valve V-005 was directed from the vent to the reactor. Once the reaction mixture had attained the desired temperature, valves V-001 and V-002 were opened, followed by valves V-003 and V-004. The rotameters were set to the desired flow rates. The flow was directed from bubble flow meter to the reactor with the simultaneous start of the timer. Samples were withdrawn at 2.5, 5, 10 and 15 minute intervals. Each withdrawn sample was emptied into a 50 cm^3 volumetric flask and sealed with the rubber bung. Quantitatively only the non-volatile salts were of interest. The flask was then submerged in the ethanol bath and clamped. The vacuum pump was turned on and the manifold valve for the relevant line was opened sufficiently.

The shutdown procedure involved the re-direction of feed flow to the vent and closure of valves V-001 and V-002. The rotameters were individually purged to remove any residual gas in the lines. The flow to the solenoid valves and the flow to the condenser were re-directed to the respective bypass lines. The power supply and controller were then switched off. The overhead stirrer was turned off. The drainage valve was opened and the reactor contents were emptied into a waste container. The reactor was then rinsed twice with water and allowed to dry.

4.2.3.3. Procedure for the dissolved oxygen sensor lag measurements

Each of the two 1 dm^3 beakers was filled with the same volume of methanol. A stirrer bar was placed in each beaker. The air cylinder was opened slowly and air was sparged into the methanol in the first beaker. Nitrogen gas was sparged into the methanol in the second beaker. Whilst both solutions reached saturation, the power cable for the probe was connected to a power source and the USB was plugged into the computer. The configurator interface was opened and the trace file was selected. Once the methanol in each beaker was saturated with oxygen and nitrogen, respectively, and the GO button was selected on the interface, the probe was inserted into the air beaker until a constant dissolved oxygen concentration was measured. Thereafter, the probe was swiftly shifted into the nitrogen beaker. The measurements were repeated three times. The sensor time constant was obtained through linear regression of the sensor lag experimental data according to Equation 3-48. The results are presented in Table 4-3.

Table 4-3. Sensor lag measurements

Experiment no.	k_{probe} / min^{-1}
1	2.410
2	2.415
3	2.429
Average	*2.418*

4.2.3.4. Procedure for $(k_La)_{oxygen}$ measurements

The startup procedure was identical to that described in Section 4.2.3.2. The reactor vessel was filled with methanol and the probe was inserted at the sample point. The power source was switched on and the USB was connected to the computer. The GO button was selected on the interface to begin measurement recordings of dissolved oxygen concentration every 15 seconds. Nitrogen was sparged into the reactor at 2 $dm^3 \cdot min^{-1}$ to strip the methanol of oxygen. Once a negligible oxygen concentration was measured, air was sparged into the reactor at 2 $dm^3 \cdot min^{-1}$. The measurements were stopped after an hour had elapsed; when constant measurements were obtained implying that the methanol was saturated with oxygen. At each temperature three runs were performed. The mass transfer coefficient was obtained through nonlinear regression of the concentration data according to Equation 3-45. The average results are presented in Table 4-4, together with the estimated values of the volumetric mass transfer coefficients for R-22 obtained from Equation 3-50.

Table 4-4. Overall mass transfer coefficients measured for oxygen and R-22

	Temperature / K		
	283.15	**293.15**	**303.15**
$(k_L a)_{oxygen}$ / **min^{-1}**	0.445	0.487	0.551
$(k_L a)_{R-22}$ / **min^{-1}**	0.786	0.860	0.973

4.3. Analytical

Spectrophotometry involves the absorption of radiant energy, be it UV, visible or infrared, by a chemical substance at a specific wavelength. A number of different methods of analysis were described in the literature review. The critical components of the spectrophotometer are the monochromator and detector. Figure 4-26 illustrates the components as discussed in detail by Fritz and Schenk, 1979).

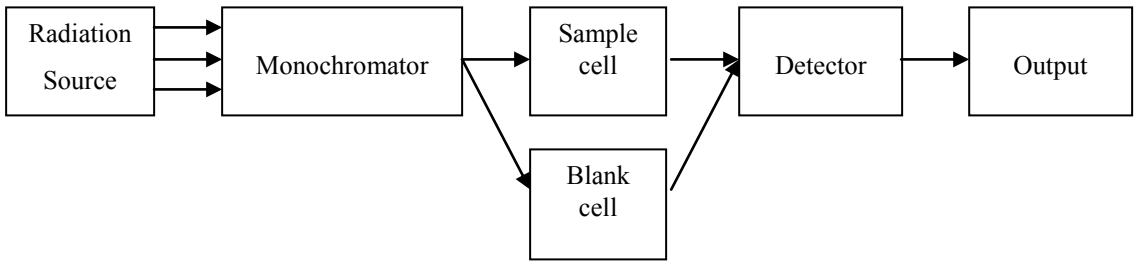

Figure 4-26. The critical components of a spectrophotometer (Fritz and Schenk, 1979)

A glass cell (10 mm path length) containing a sample is inserted into the spectrophotometer. The monochromator selects the narrow wavelength band at which radiant light will pass through the sample. A fraction of the radiant power directed on the cell is absorbed by the chemical substance. The remainder of the radiant power is transmitted (Fritz and Schenk, 1979). P_o represents the radiant power of the incident beam (as it enters the sample) and P represents the radiant power of the transmitted beam (as it exits the sample). Although the absolute values of P and P_o cannot be measured directly, the ratio can be measured using a photoelectric detector (Fritz and Schenk, 1979). The spectrophotometer measures two quantities: absorbance and transmittance. Equation 4-3 defines transmittance as:

$$T = \frac{P}{P_0} \tag{4-3}$$

Absorbance is expressed as the inverse logarithmic of transmittance as defined below:

$$\begin{aligned} A &= -\log \frac{P}{P_0} \\ &= -\log T \\ &= -\log \frac{\%T}{100} \end{aligned} \tag{4-4}$$

There is a linear relationship between absorbance and concentration. The spectrophotometric method for the analysis of sodium chloride chosen was based on the displacement of thiocyanate from mercuric thiocyanate by chloride ion (Zall et al., 1956). The spectrophotometric method for the analysis of sodium fluoride chosen was based on the bleaching effect of fluoride on coloured complexes (Shu-Chuan et al., 1956). These methods are discussed in greater detail in the literature review. Tests using the method proposed by Zall et al. (1956) showed reagent colour changes when added to the solution; however, once the sample was diluted to 50 cm^3 as proposed, the colour became almost undetectable. The method was modified by removing the dilution procedure. The spectrophotometric analysis of sodium chloride was thereafter satisfactory. The tests conducted for the method by Shu-Chuan (1956) failed as no colour change was observed when the reagents were added to the samples containing fluoride ions. This implied that the reagents did not react with the fluoride ions, thereby rendering the method invalid. The spectrophotometric analysis for fluoride ions therefore had to be abandoned.

The concentration of sodium fluoride was not measured directly. As a means of determining the total concentration of all salts present in each sample withdrawn from the reactor (this would include sodium fluoride, sodium chloride and unreacted sodium methoxide), the sample was dried and the salt crystals were weighed after evaporation of the volatiles (as per Section 5.2). The concentration of sodium fluoride and sodium methoxide could then be inferred by substituting the concentration of sodium chloride determined through spectrophotometry.

4.3.1. Preparation of reagents

In the spectrophotometric determination of chloride ions, a set of reagents that produce a reaction specific to the chloride ion are: mercuric thiocyanate, ferric perchlorate and 60% perchloric acid. The reaction was reviewed extensively in chapter two. Distilled water was utilized in all the procedures.

A 0.07% saturated aqueous solution of mercuric thiocyanate was prepared by dissolving 0.7 g of the reagent in 1 dm^3 of distilled water. The solution was stored in a 1 dm^3 volumetric flask. According to the reagent method by Zall et al. (1956), a ferric perchlorate solution is prepared by dissolving ferric perchlorate in 4 N perchloric acid. Therefore, to prepare the solution, the 4 N perchloric acid was first prepared as follows. A small volume of distilled water was transferred into a 100 cm^3 volumetric flask. 56 cm^3 of 60% perchloric acid was pipetted into the volumetric flask; the solution was made up to volume (100 cm^3) with distilled water and then mixed well. Acid was added to water as it constitutes safer laboratory practice. Once the 4 N perchloric acid solution was prepared, 6 g of ferric perchlorate was dissolved into the solution.

4.3.2. Preparation of standard solutions for the calibration of the spectrophotometer

Sodium chloride was dried for 3 hours in an oven at 378 K. After drying, 1 g of the salt was weighed out and emptied into a 1 dm^3 volumetric flask. Distilled water was added and the contents were swirled. The solution was made up to volume and mixed thoroughly. Such a solution was labeled the master solution with a concentration of 1000 p.p.m. A series of standards with known concentrations ranging between 1 p.p.m. and 5 p.p.m. was prepared from the master solution.

The following method describes only a single concentration but was representative of each standard; with the exception of the volume of master solution pipetted for each standard. For a standard concentration of 1 p.p.m., 1 cm^3 of the master solution was pipetted into a 1 dm^3 volumetric flask, made up to volume with distilled water and mixed well. The procedure was repeated using 2, 3, 4 and 5 cm^3 of the master solution to prepare 2, 3, 4 and 5 p.p.m of standard solutions, respectively.

4.3.3. Calibration of spectrophotometer

A series of standards with known concentrations of sodium chloride was prepared and their respective absorbance measured after the colour developed. The procedure was repeated a further three times for reproducibility. The plot of absorbance against concentration is represented graphically in Figure 4-27. The use of a reagent blank was not recommended in the paper from which the method was obtained. Instead a water blank was recommended by the authors. Because the reagents themselves have a strong absorbance, the calibration plot for zero salt concentration does not pass through the origin but rather intercepts at the reagent absorbance (Zall et al., 1956).

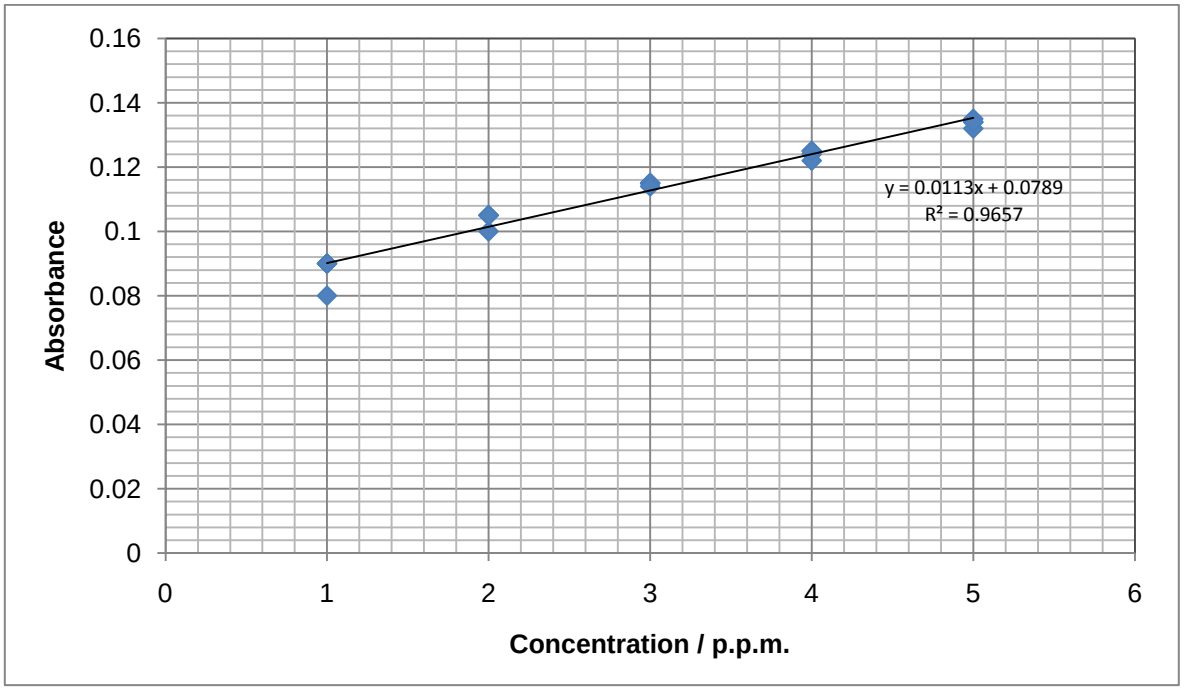

Figure 4-27. Calibration of standards for the spectrophotometric analysis of chlorides

4.3.4. Pre-preparation of samples for spectrophotometric analysis

Liquid samples withdrawn from the reactor with a 2 cm^3 pipette were degassed under vacuum as a pre-preparation to analysis to remove the refrigerant gas (R-22 gas) and stop the reaction. This was important since the sample had to represent the conditions inside the reactor at the time that it was removed. Thereafter, each unknown sample was treated according to the procedure that follows. A heating mantle was set up on low heat. The 50 cm^3 volumetric flask containing the sample was

rinsed with excess distilled water and the contents were emptied into a glass flask. It was assumed that all of the sodium methoxide present in the sample was hydrolyzed to sodium hydroxide during this step according to the reaction:

$$CH_3O^- + H_2O \rightarrow OH^- + CH_3OH \quad (4\text{-}5)$$

The glass flask was placed in the heating mantle to be heated for a day until all the water and methanol evaporated. After all the liquid had evaporated, the dry sample was dried further in the oven at 378.15 K for 2 hours to remove any excess moisture. The sample was cooled and the total mass of the flask, including the dried contents, was weighed on a Mettler Toledo balance accurate to ±0.001 g.

4.3.5. Preparation of samples for spectrophotometric analysis

Once the pre-preparation was concluded, distilled water was used to dilute the dry contents of the flask. The sample contents were poured into a 1 dm^3 volumetric flask. This step was repeated thrice to ensure that the entire sample was diluted, as well as to prevent loss of sample. The contents of the 1 dm^3 volumetric flask was made up to volume and mixed well. This resulted in a dilution factor of 500. 10 cm^3 of the diluted solution was pipetted into the 100 cm^3 volumetric flask, made up to volume and mixed well. This resulted in a dilution factor of 10. A further 10 cm^3 was pipetted from the 100 cm^3 volumetric flask into a 50 cm^3 volumetric flask, ready for analysis.

4.3.6. Procedure for analysis

The procedure for analysis began with the 50 cm^3 volumetric flask ready for analysis. Reagents were then added to the diluted sample. 5 cm^3 of 60% perchloric acid, 1 cm^3 of mercuric thiocyanate and 2 cm^3 of ferric perchlorate were each successively pipetted into the sample resulting in the development of colour. The sample was gently mixed and allowed to rest for 10 minutes before analysis.

For the analysis, the cuvette was first filled with distilled water using a Pastille pipette. The cuvette was inserted into the spectrophotometer and the blank control on the machine set the absorbance to

zero. The cuvette was removed, rinsed and dried. The unknown sample was then filled into the cuvette using a Pastille pipette. The cuvette was, once again, inserted into the spectrophotometer. The reading on the scale was noted. The sample was removed, the cuvettes were rinsed and dried and the procedure repeated for all the samples in the experiment.

4.4. Experimental Design

4.4.1. Preliminary tests using the OVAT approach

The OVAT (one-variable-at-a-time) method of experimental design is carried out in such a manner that one variable of interest is changed and all other variables remain constant for the duration of the experiment. Such an experiment is termed a 'controlled experiment' (Baumol and Blinder, 2011). The OVAT approach was used to investigate the influence of each variable independently. Reactor temperature and base concentration (sodium hydroxide in methanol) were selected as the variables of interest for the preliminary study. Identical experiments were conducted on both the reactors used in the preliminary investigations. The influence of base concentration on the performance factors was investigated at 0.586, 2 and 3.414 $mol \cdot dm^{-3}$ for a reactor temperature of 298.15 K. Similarly, the influence of reactor temperature was investigated at 276.94, 298.15 and 313.15 K for a base concentration of 2 $mol \cdot dm^{-3}$.

The independent performance factors evaluated were the conversion of R-22 and selectivity of difluorodimethyl ether (fluoroether). Conversion of R-22 was defined as the ratio of the number of moles of R-22 reacted to the number of moles of R-22 feed into the system.

$$X = 100 \frac{(moles\ R-22\ in) - (moles\ R-22\ out)}{moles\ R-22\ in} \tag{4-6}$$

Selectivity was defined as the ratio of the number of moles of fluoroether produced to the number of moles of R-22 that reacted, expressed as a percentage.

$$S = 100 \frac{moles\ fluoroether\ produced}{(moles\ R-22\ in) - (moles\ R-22\ out)} \tag{4-7}$$

Yield was defined as the ratio of the number of moles of fluoroether produced to the number of moles of R-22 gas fed into the system, expressed as a percentage.

$$Y = \frac{XS}{100} = 100 \frac{moles\ fluoroether\ produced}{moles\ R-22\ in} \tag{4-8}$$

4.4.2. Experimental design for the kinetic study

The Box-Behnken design is a three factor, three level factorial design that fits a second order polynomial of the form (Box and Behnken, 1960):

$$Y = b_0 + \sum_{i=1}^{3} b_i x_i + \sum_{i=1}^{3} b_{ii} x_i^2 + \sum_{i<j} b_{ij} x_i x_j \tag{4-9}$$

where Y is the response variable representing sodium chloride concentration and x_1, x_2 and x_3 are independent variables representing base concentration, reactor temperature and R-22 partial pressure, respectively. The coefficients of the polynomial (b_0, b_i, b_{ij}), termed interaction parameters, are estimated by the method of least squares.

The design is advantageous over the central composite design (CCD). Besides the situation where $\left(2^k\right)^{1/4} = 1$ (k represents the number of factors), CCDs demand five levels per variable (Vining and Kowalski, 2010). For three variables, a total of 15 runs are required for the Box-Behnken design, as compared to a central composite design, which requires 20 experiments.

The Box-Behnken design exhibits rotatibility. The designs are spherical as all the design points are located on a sphere of radius $\sqrt{2}$ (Vining and Kowalski, 2010). This is useful when avoiding potentially extreme process conditions, represented by cube corners. The Box-Behnken design is drawn in Figure 4-28.

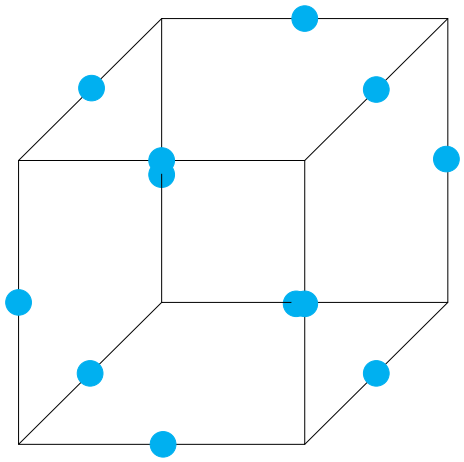

Figure 4-28. Box-Behnken design with design points of radius $\sqrt{2}$ from the centre of the cube

The coded variables for the Box-Behnken design are drawn in Table 4-5 and shown graphically in Figure 4-29. Reactor temperature was varied from 283 to 303 K, with inlet R-22 partial pressures between 40.5 and 60.8 kPa (absolute) and base concentrations between 1.5 and 2.5 mol·dm^{-3}.

Table 4-5. Coded variables for the Box-Behnken design

Experiment No.	Concentration / mol·dm^{-3}	Temperature / K	P_{R22} / kPa	*Coded Variables* x_1	x_2	x_3
1	1.5	293	40.5	-	0	-
2	2	283	40.5	0	-	-
3	2.5	293	40.5	+	0	-
4	2	303	40.5	0	+	-
5	2.5	303	50.7	+	+	0
6	2	303	60.8	0	+	+
7	1.5	303	50.7	-	+	0
8	2.5	293	60.8	+	0	+
9	2	283	60.8	0	-	+
10	2.5	283	50.7	+	-	0
11	1.5	283	50.7	-	-	0
12	1.5	293	60.8	-	0	+

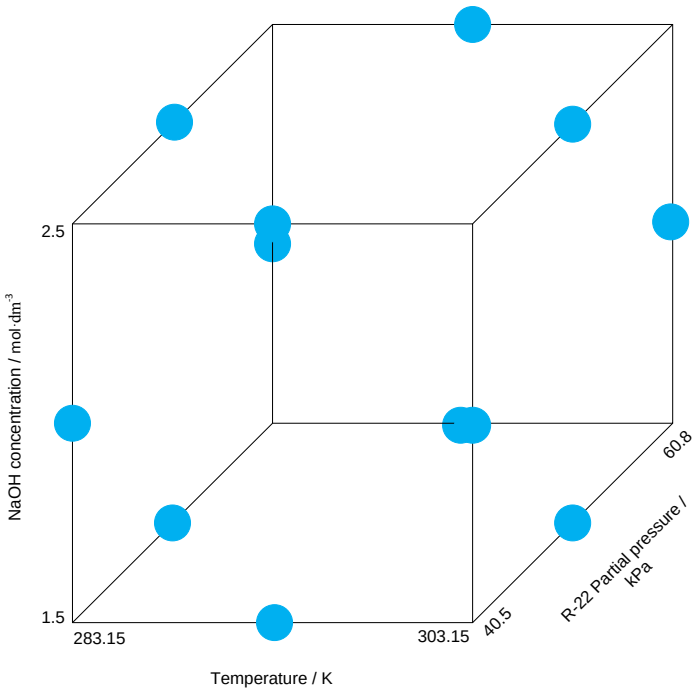

Figure 4-29. Box-Behnken design at the experimental conditions

CHAPTER 5

RESULTS AND DISCUSSION

5.1. Preliminary experiments

Identical experiments were conducted with the semi-batch stainless steel reactor and the semi-batch jacketed glass reactor. Experimental tests with the stainless steel reactor were carried out before using the jacketed glass reactor. Using the OVAT approach, three base concentrations were investigated *viz.* 0.586, 2 and 3.414 mol·dm^{-3} at a constant reactor temperature of 298.15 K. This was succeeded by the variation of three reactor temperatures *viz.* 276.94, 298.15 and 313.15 K at a constant base concentration of 2 mol·dm^{-3}. Sodium hydroxide, a strong base, was used for the hydrogen atom abstraction because of the lower required operating temperatures. Sample calculations are presented in Appendix C. The chromatograms are shown in Appendix G.

Poor difluorodimethyl ether yields were obtained from experiments conducted in the stainless steel reactor. The reactions were characterized by a large amount of salt precipitate in the reactor. It was believed that the salt precipitate had caused the reaction rate to drop because it inhibited good mixing of sodium hydroxide with methanol. A maximum difluorodimethyl ether yield of 39.62 % was observed in the jacketed glass reactor, at 298.15 K and 2 mol·dm^{-3} with an R-22 conversion of 83%. Gas chromatographic analysis of the filtered liquid from the reactor confirmed the presence of trimethyl orthoformate.

Figure 5-1 and Figure 5-4 show the comparisons between the difluorodimethyl ether yields obtained in the reactors at constant temperature and constant concentration, respectively. Figure 5-1 shows that the difluorodimethyl ether yields obtained with the jacketed glass reactor increased with base concentration. At constant temperature, the difluorodimethyl ether yields obtained with the stainless steel system appeared to remain constant after 2 mol·dm^{-3}. Figures 5-2 and 5-3 show the conversion of R-22 and the selectivity of difluorodimethyl ether at 298.15 K. Despite the increase in R-22 conversion noted after 2 mol·dm^{-3}, the selectivity toward difluorodimethyl ether decreased. This implied that the selectivity towards the by-product, trimethyl orthoformate, was favoured. However, for the case of the jacketed glass reactor, conversions of R-22 between 80 and 90% were noted, with a continuous rise in difluorodimethyl ether yield.

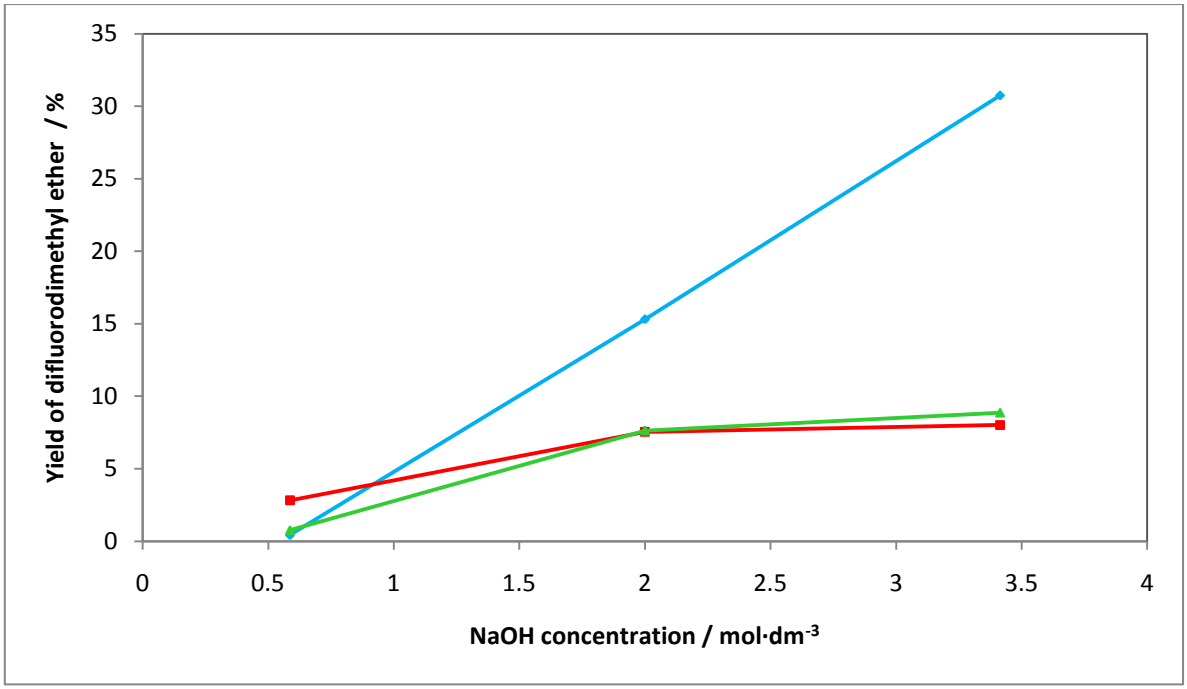

Figure 5-1. The effect of initial base concentration on the yield of difluorodimethyl ether at 298.15 K. Reactor system used: ◆, glass; ■, stainless steel; ▲, stainless steel with water

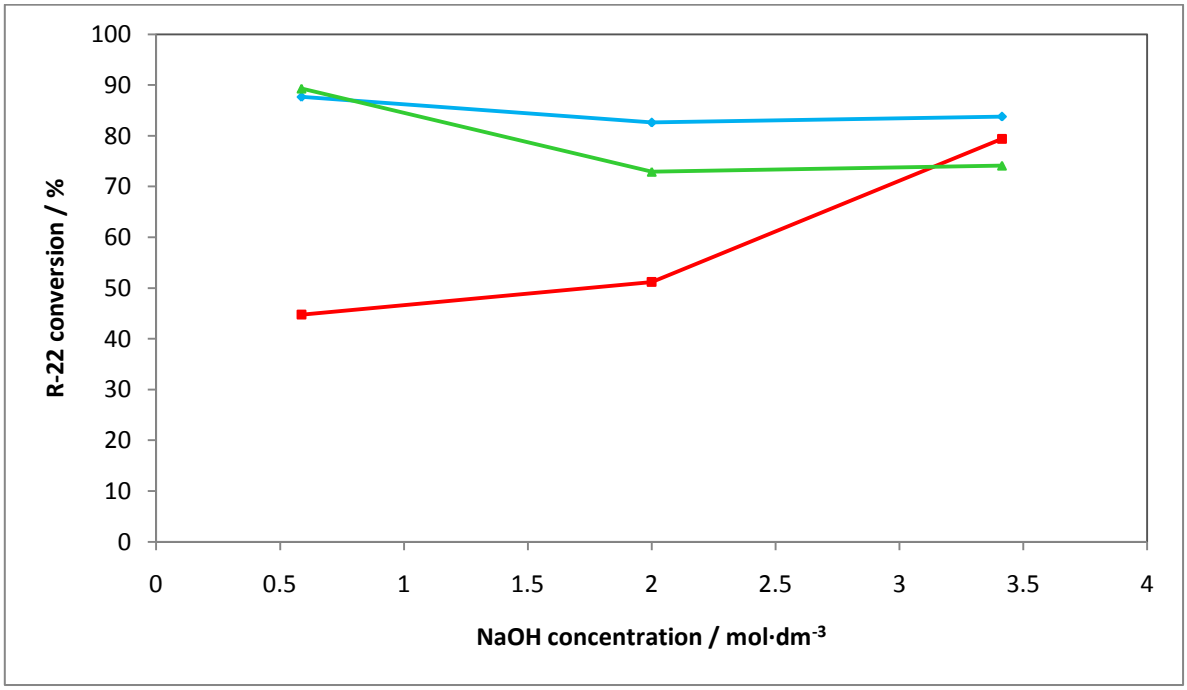

. **Figure 5-2. The effect of initial base concentration on the conversion of R-22 at 298.15 K. Reactor system used: ◆, glass; ■, stainless steel; ▲, stainless steel with water**

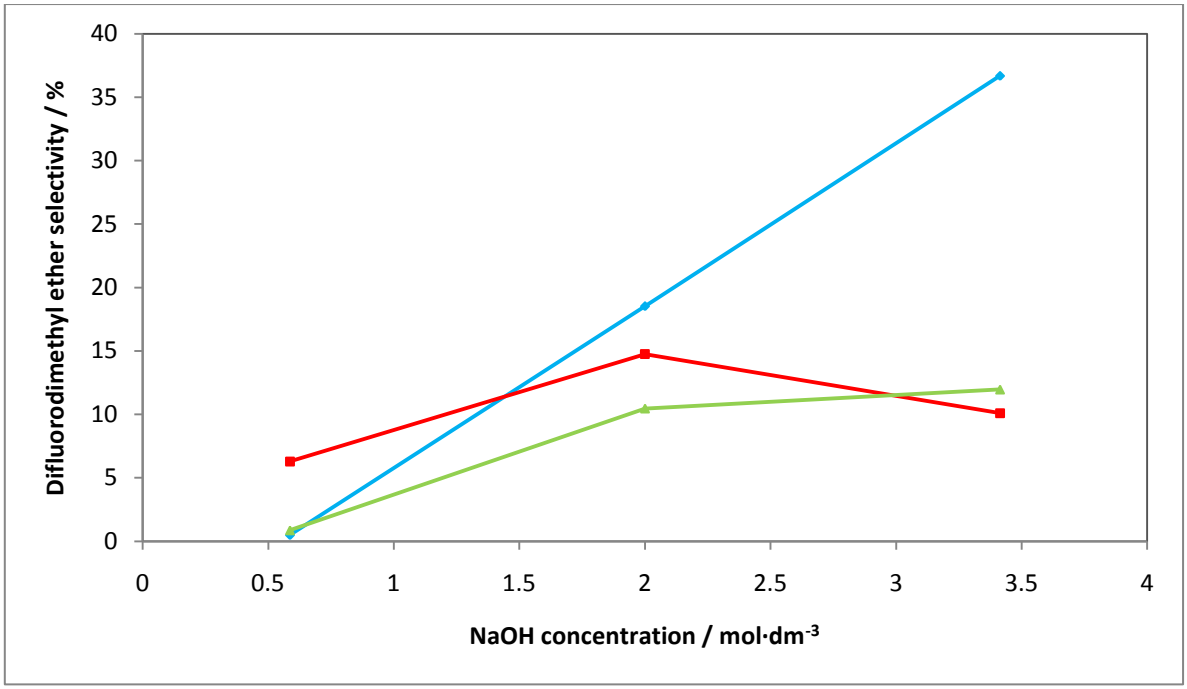

Figure 5-3. The effect of initial base concentration on the selectivity of difluorodimethyl ether at 298.15 K. Reactor system used: ◆, glass; ■, stainless steel; ▲, stainless steel with water

Figure 5-4 shows that a very small and practically constant yield of difluorodimethyl ether was obtained in the stainless steel reactor below 298.15 K. An exponential increase in the yield of difluorodimethyl ether was observed for the glass reactor system. Figure 5-5 and Figure 5-6 show the conversion of R-22 and the selectivity of difluorodimethyl ether at 2 mol·dm^{-3}. The selectivity towards difluorodimethyl ether was substantially greater with the glass reactor system in comparison to the stainless steel reactor system. This comparison suggested that an excessive amount of trimethyl orthoformate was formed in the stainless steel reactor. Trimethyl orthoformate is an unwanted by-product of the reaction between R-22 and methanol. It was suspected that the stainless steel behaved as a catalyst in the production of the by-product. A sample of reactor liquid injected into the G.C.M.S. confirmed the presence of trimethyl orthoformate. The parent peak of trimethyl orthoformate was the same as that reported by Satoh et al. (1998) i.e. (m/z 105(M^+)). The G.C.M.S operating conditions and column information is presented in Table 5-1.

Table 5-1. Shimadzu QP 2010 G.C.M.S operating conditions

Column	Restek RTX 5MS Capillary Column
Column dimensions	30 m x 0.25 mm I.D.
Injector temperature	473 K
Column temperature	313 K
Ion source	523 K
Interface temperature	523 K

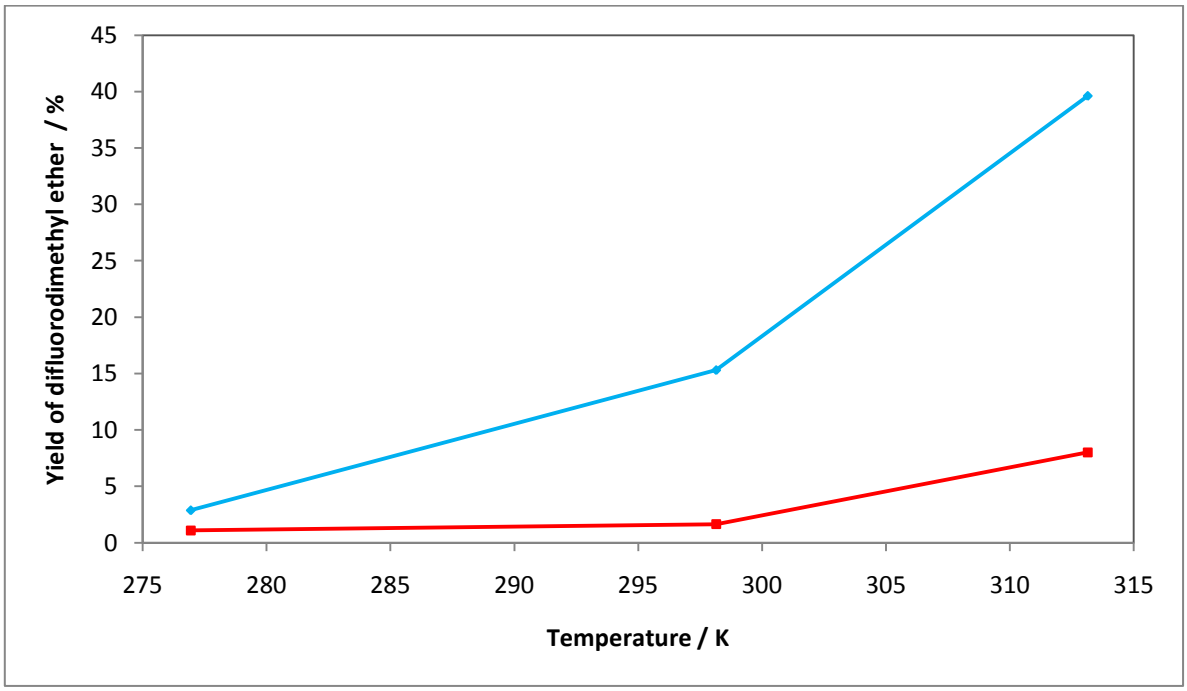

Figure 5-4. Effect of temperature on the yield of difluorodimethyl ether at 2 mol·dm^{-3}. Reactor system used: ◆, glass; ■, stainless steel

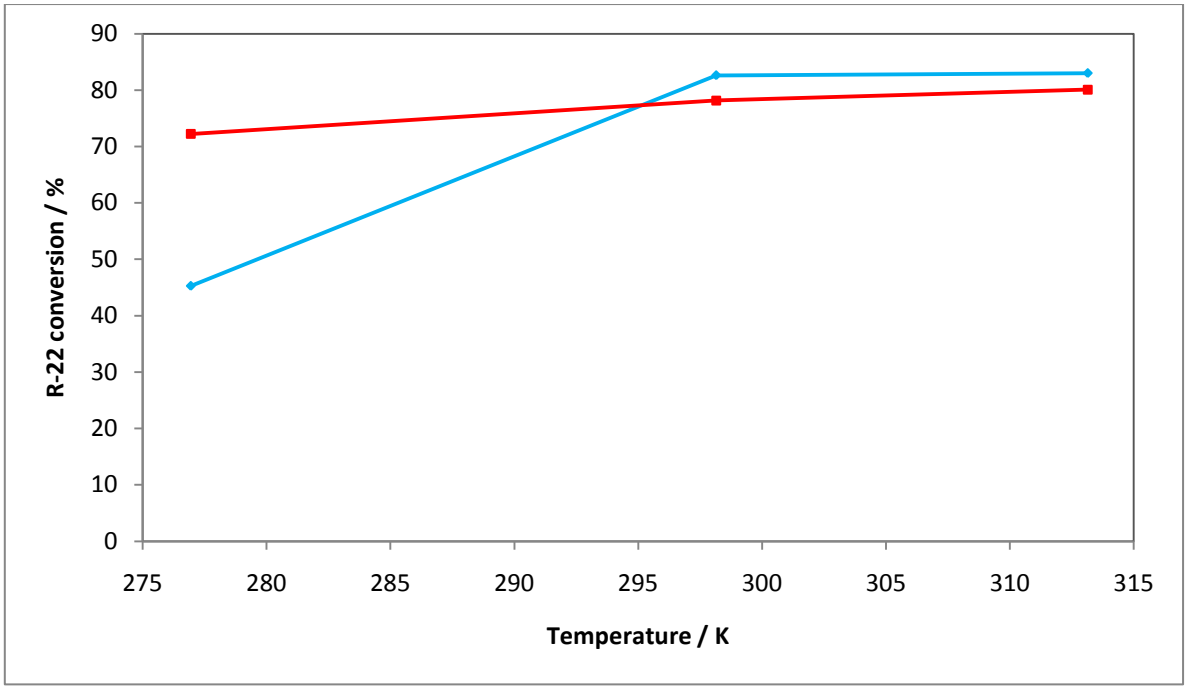

Figure 5-5. The effect of temperature on the conversion of R-22 at 2 mol·dm^{-3}.

Reactor system used: ◆, glass; ■, stainless steel

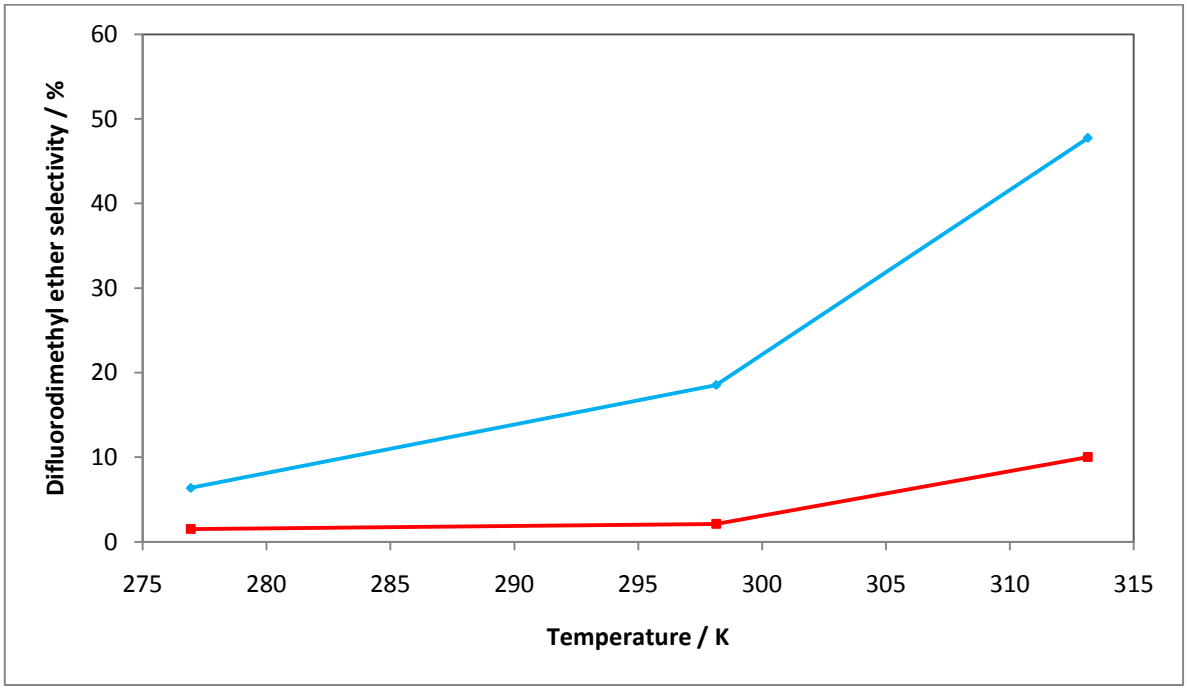

Figure 5-6. Effect of temperature on the selectivity of difluorodimethyl ether at 2 mol·dm^{-3}.

Reactor system used: ◆, glass; ■, stainless steel

Following the mechanism proposed by Hine and Porter (1957), the formation of trimethyl orthoformate results from the reaction of the difluorocarbene intermediate with the methoxide anion formed by the equilibrium reaction between OH^- and CH_3OH which is given by:

$$OH^- + CH_3OH \rightleftharpoons H_2O + CH_3O^- \tag{5-1}$$

To investigate the effect of water on the process rate, three additional experiments were carried out at a temperature of 298.15 K, using different concentrations of sodium hydroxide in methanol mixed with 50 cm^3 of distilled water. It was believed that the addition of water to the initial reaction mixture would shift the equilibrium of the reaction given in Equation 5-1 to the left and thus suppress the formation of trimethyl orthoformate. This was not verified experimentally. In fact, for the experimental run performed at a concentration of 0.5 $mol \cdot dm^{-3}$, the residual liquid in the reactor consisted of almost pure trimethyl orthoformate with very little difluorodimethyl ether formed. Results of the three experiments are tabulated in Table 5-2.

Table 5-2. Performance factors for experiments undertaken with water in the stainless steel reactor at 298.15 K

	Concentration of sodium methoxide / mol·dm^{-3}		
	0.586	**2**	**3.414**
Yield of difluorodimethyl ether / %	0.77	7.63	8.87
Conversion of R-22 / %	89.3	72.90	74.11
Selectivity of difluorodimethyl ether / %	0.87	10.47	11.96

A comparison of these experiments with the experiments in the same reactor excluding the addition of water is shown graphically in the bar plots below. Figure 5-7 shows that at 2 $mol \cdot dm^{-3}$, a negligible difference in yield of difluorodimethyl ether was noted between the two runs. The use of water to aid the reaction did not improve the yield at 0.586 $mol \cdot dm^{-3}$ and 2 $mol \cdot dm^{-3}$. Figure 5-8 shows that the conversion of R-22 increased with the use of water resulting in a decrease in selectivity rather than the expected increase.

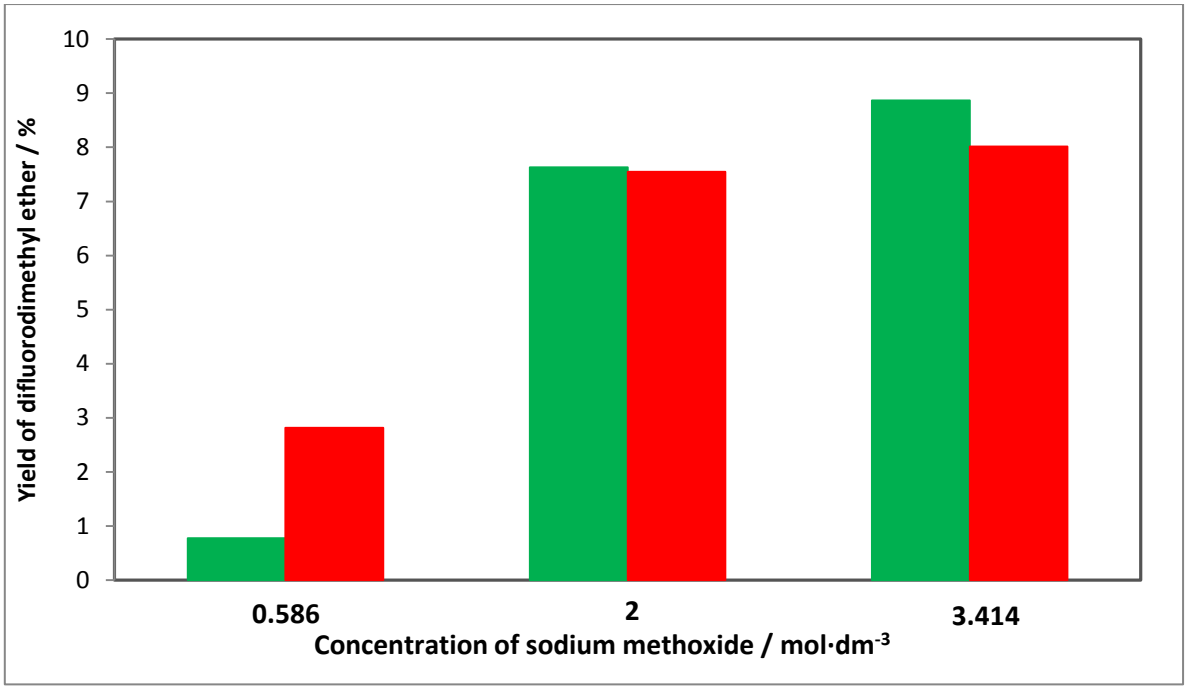

Figure 5-7: A comparison of difluorodimethyl ether yield for experiments performed with water, ■, and without water, ■, at 298.15 K in the stainless steel reactor

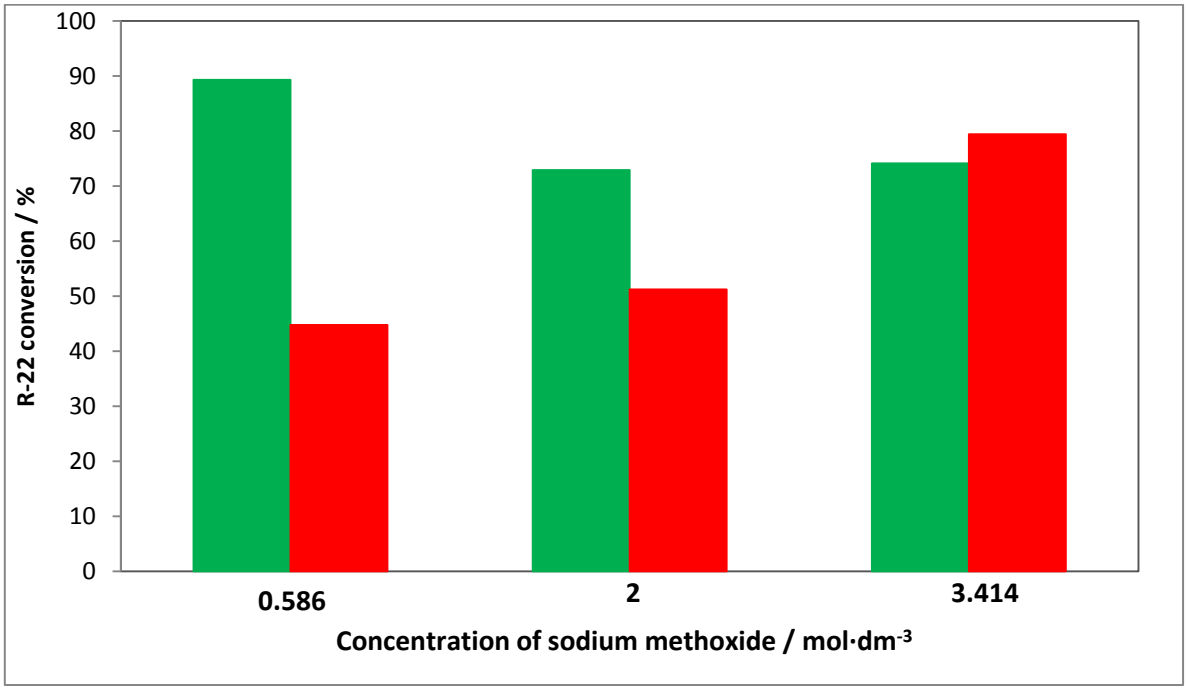

Figure 5-8: A comparison of R-22 conversion for experiments performed with water, ■, and without water, ■, at 298.15 K in the stainless steel reactor

5.2. Raw experimental data

The results of experiments conducted for the kinetic data generation according to the Box-Behnken design is presented in Table 5-3.

Table 5-3. Results of the Box-Behnken experimental design for kinetic data generation

Exp. No.	Experimental conditions			R-22 flow rate / $dm^3.min^{-1}$	N_2 flow rate / $dm^3.min^{-1}$	Time / min	NaCl conc.* / $mol \cdot dm^{-3}$	Total salt mass / g
	Temp. / K	Base conc. / $mol \cdot dm^{-3}$	R-22 partial pressure / kPa					
1a	283.15	2.0	40	0.8	1.2	5	0.163	0.161
1a	283.15	2.0	40	0.8	1.2	10	0.210	0.193
1a	283.15	2.0	40	0.8	1.2	15	0.249	0.164
1a	283.15	2.0	40	0.8	1.2	20	0.287	0.155
1b	283.15	2.0	40	0.8	1.2	5	0.155	0.164
1b	283.15	2.0	40	0.8	1.2	10	0.202	0.168
1b	283.15	2.0	40	0.8	1.2	15	0.264	0.164
1b	283.15	2.0	40	0.8	1.2	20	0.303	0.160
2a	283.15	2.0	60	1.2	0.8	2.5	0.171	0.164
2a	283.15	2.0	60	1.2	0.8	5	0.171	0.195
2a	283.15	2.0	60	1.2	0.8	10	0.210	0.169
2a	283.15	2.0	60	1.2	0.8	15	0.287	0.168
2b	283.15	2.0	60	1.2	0.8	2.5	0.132	0.166
2b	283.15	2.0	60	1.2	0.8	5	0.155	0.190
2b	283.15	2.0	60	1.2	0.8	10	0.233	0.175
2b	283.15	2.0	60	1.2	0.8	15	0.295	0.170
3a	283.15	2.5	50	1.0	1.0	2.5	0.186	0.213
3a	283.15	2.5	50	1.0	1.0	5	0.202	0.245
3a	283.15	2.5	50	1.0	1.0	10	0.210	0.227
3a	283.15	2.5	50	1.0	1.0	15	0.186	0.241
3a	283.15	2.5	50	1.0	1.0	20	0.249	0.225
3b	283.15	2.5	50	1.0	1.0	2.5	0.202	0.210
3b	283.15	2.5	50	1.0	1.0	5	0.210	0.237
3b	283.15	2.5	50	1.0	1.0	10	0.225	0.225
3b	283.15	2.5	50	1.0	1.0	15	0.241	0.220
3b	283.15	2.5	50	1.0	1.0	20	0.287	0.225
4a	283.15	1.5	50	1.0	1.0	5	0.186	0.149
4a	283.15	1.5	50	1.0	1.0	10	0.210	0.172
4a	283.15	1.5	50	1.0	1.0	15	0.186	0.151
4a	283.15	1.5	50	1.0	1.0	20	0.264	0.134
4b	283.15	1.5	50	1.0	1.0	5	0.179	0.155
4b	283.15	1.5	50	1.0	1.0	10	0.202	0.165
4b	283.15	1.5	50	1.0	1.0	15	0.225	0.155
4b	283.15	1.5	50	1.0	1.0	20	0.272	0.157
5a	293.15	1.5	40	0.8	1.2	5	0.155	0.175
5a	293.15	1.5	40	0.8	1.2	10	0.171	0.173
5a	293.15	1.5	40	0.8	1.2	15	0.186	0.163
5a	293.15	1.5	40	0.8	1.2	20	0.264	0.180

Table 5-3. ***(continued)***

Exp. No.	Experimental conditions: Temp. / K	Base conc. / mol·dm^{-3}	R-22 partial pressure / kPa	R-22 flow rate / dm^3.min^{-1}	N_2 flow rate / dm^3.min^{-1}	Time / min	NaCl conc.* / mol·dm^{-3}	Total salt mass / g
5b	293.15	1.5	40	0.8	1.2	5	0.132	0.177
5b	293.15	1.5	40	0.8	1.2	10	0.186	0.175
5b	293.15	1.5	40	0.8	1.2	15	0.210	0.173
5b	293.15	1.5	40	0.8	1.2	20	0.287	0.177
6a	293.15	2.5	40	0.8	1.2	2.5	0.264	0.178
6a	293.15	2.5	40	0.8	1.2	5	0.280	0.206
6a	293.15	2.5	40	0.8	1.2	10	0.319	0.183
6a	293.15	2.5	40	0.8	1.2	15	0.342	0.188
6a	293.15	2.5	40	0.8	1.2	20	0.326	0.178
6b	293.15	2.5	40	0.8	1.2	2.5	0.233	0.182
6b	293.15	2.5	40	0.8	1.2	5	0.264	0.188
6b	293.15	2.5	40	0.8	1.2	10	0.326	0.185
6b	293.15	2.5	40	0.8	1.2	15	0.365	0.188
6b	293.15	2.5	40	0.8	1.2	20	0.342	0.182
7a	293.15	2.5	60	1.2	0.8	2.5	0.186	0.198
7a	293.15	2.5	60	1.2	0.8	5	0.264	0.256
7a	293.15	2.5	60	1.2	0.8	10	0.311	0.189
7a	293.15	2.5	60	1.2	0.8	15	0.342	0.222
7a	293.15	2.5	60	1.2	0.8	20	0.342	0.198
7b	293.15	2.5	60	1.2	0.8	2.5	0.194	0.193
7b	293.15	2.5	60	1.2	0.8	5	0.280	0.249
7b	293.15	2.5	60	1.2	0.8	10	0.319	0.185
7b	293.15	2.5	60	1.2	0.8	15	0.334	0.230
7b	293.15	2.5	60	1.2	0.8	20	0.357	0.199
8a	293.15	1.5	60	1.2	0.8	5	0.210	0.139
8a	293.15	1.5	60	1.2	0.8	10	0.264	0.140
8a	293.15	1.5	60	1.2	0.8	15	0.326	0.127
8a	293.15	1.5	60	1.2	0.8	20	0.334	0.144
8b	293.15	1.5	60	1.2	0.8	5	0.202	0.142
8b	293.15	1.5	60	1.2	0.8	10	0.272	0.145
8b	293.15	1.5	60	1.2	0.8	15	0.342	0.136
8b	293.15	1.5	60	1.2	0.8	20	0.357	0.142
9a	303.15	2.0	40	0.8	1.2	5	0.202	0.147
9a	303.15	2.0	40	0.8	1.2	10	0.287	0.161
9a	303.15	2.0	40	0.8	1.2	15	0.334	0.148
9a	303.15	2.0	40	0.8	1.2	20	0.311	0.148
9b	303.15	2.0	40	0.8	1.2	5	0.210	0.149
9b	303.15	2.0	40	0.8	1.2	10	0.280	0.155
9b	303.15	2.0	40	0.8	1.2	15	0.326	0.152
9b	303.15	2.0	40	0.8	1.2	20	0.319	0.151
10a	303.15	2.5	50	1.0	1.0	2.5	0.287	0.210
10a	303.15	2.5	50	1.0	1.0	5	0.342	0.252

Table 5-3. ***(continued)***

Exp. No.	Experimental conditions: Temp. / K	Base conc. / mol·dm^{-3}	R-22 partial pressure / kPa	R-22 flow rate / dm^3.min^{-1}	N_2 flow rate / dm^3.min^{-1}	Time / min	NaCl conc.* / mol·dm^{-3}	Total salt mass / g
10a	303.15	2.5	50	1.0	1.0	10	0.435	0.225
10a	303.15	2.5	50	1.0	1.0	15	0.528	0.201
10a	303.15	2.5	50	1.0	1.0	20	0.544	0.229
10b	303.15	2.5	50	1.0	1.0	2.5	0.280	0.212
10b	303.15	2.5	50	1.0	1.0	5	0.334	0.242
10b	303.15	2.5	50	1.0	1.0	10	0.443	0.224
10b	303.15	2.5	50	1.0	1.0	15	0.521	0.205
10b	303.15	2.5	50	1.0	1.0	20	0.552	0.232
11a	303.15	2.0	60	1.2	0.8	2.5	0.186	0.177
11a	303.15	2.0	60	1.2	0.8	5	0.186	0.229
11a	303.15	2.0	60	1.2	0.8	10	0.249	0.204
11a	303.15	2.0	60	1.2	0.8	15	0.326	0.166
11a	303.15	2.0	60	1.2	0.8	20	0.389	0.199
11b	303.15	2.0	60	1.2	0.8	2.5	0.163	0.175
11b	303.15	2.0	60	1.2	0.8	5	0.171	0.230
11b	303.15	2.0	60	1.2	0.8	10	0.287	0.206
11b	303.15	2.0	60	1.2	0.8	15	0.334	0.169
11b	303.15	2.0	60	1.2	0.8	20	0.365	0.201
12a	303.15	1.5	50	1.0	1.0	2.5	0.264	0.086
12a	303.15	1.5	50	1.0	1.0	5	0.264	0.133
12a	303.15	1.5	50	1.0	1.0	10	0.326	0.093
12a	303.15	1.5	50	1.0	1.0	15	0.319	0.105
12b	303.15	1.5	50	1.0	1.0	2.5	0.210	0.085
12b	303.15	1.5	50	1.0	1.0	5	0.287	0.137
12b	303.15	1.5	50	1.0	1.0	10	0.342	0.095
12b	303.15	1.5	50	1.0	1.0	15	0.342	0.108

* Cumulative superficial concentration (dissolved and precipitated salt)

In the process of obtaining the experimental data, the reaction was allowed to proceed for 20 minutes, during which the salt was observed to be well dispersed in the liquid upon agitation. When longer reaction times were used, the large quantity of salt precipitating out of solution began to accumulate at the bottom of the vessel. Sampling was originally performed at 5 minute intervals. However, it was decided that the interval at the beginning of the reaction be narrowed since this was the time interval at which the rate was the highest. Sampling was thus performed 2.5 minutes after the admission of R-22 into the reactor. The cheaper all-glass construction of the impeller and shaft restricted the maximum speed at which the mixture could be agitated. Nevertheless, the system was observed to be well-mixed at the operating speed used in this work. The sintered glass sparger was not constructed to specification. It did, however; provide adequately small bubbles and satisfactory dispersion. To check the consistency of measurements, samples were drawn from two different locations in the reactor. Therefore, during one run, 10 samples had to be processed. Considering the

elaborate post-run sample preparation required for spectrophotometric analysis, it was decided not to extend the number of data points per experiment.

In most of the experiments the measured concentration of sodium chloride in the reactor increased rapidly at the beginning of the reaction and thereafter appeared to reach a stable value. Note that the sodium chloride concentration presented in Table 5-3 represents the cumulative superficial concentration in the reactor which included dissolved and precipitated sodium chloride.

5.3. Nonlinear data regression

The experimental data were fitted to the model developed in Section 3.3.1., incorporating the gas and liquid phase material balances, the 'salting-out' effect of dissolved salts and the mixing effect of precipitated salts on mass transfer. The kinetic parameters for reactions 1 and 2, the Sechenov 'salting-out' coefficients of the dissolved salts and the mixing parameter m were identified through a least squares minimization procedure.

The objective of the parameter estimation was to minimize the error between data predicted by the model and data measured experimentally. The kinetic parameters in the model were estimated using an optimization routine coupled with the integration of the set of ordinary differential equations representing the reactor balances developed in Section 3.3.1. The objective function as defined in Buzzi-Ferraris and Manenti (2009) is:

$$S(\mathbf{b}) = \sum_{i=1}^{n_E} \left[\omega_i \left(y_i - g\left(x_i, \mathbf{b}\right) \right) \right]^2 \tag{5-2}$$

where $\omega_i = \frac{1}{\sigma_i}$, σ_i^2 are the variance of each measured data point, y_i represents the measured data, g represents the values predicted by the model, $\mathbf{b}$ is a vector of kinetic parameter estimates and x_i the independent variables. (Buzzi-Ferraris and Manenti, 2009). The objective function was comprised of two parts. The first part involved the difference between the predicted NaCl concentration and the measured NaCl concentration. The second part compared the measured total salt mass with the total salt mass predicted by the model. This total salt mass included all dissolved

salts and all precipitated salts according to the solubility limits presented in Section 3.3.3. The total salt mass predicted by the model was:

$$M_{salt\,tot\,pred} = V_{sample}\left[C_{NaCl,pred}MM_{NaCl} + C_{NaF,pred}MM_{NaF} + C_{CH_3ONa,pred}MM_{NaOH}\right] \quad (5\text{-}3)$$

where $C_{NaCl,pred}$, $C_{NaF,pred}$ and $C_{CH_3ONa,pred}$ are the predicted molar concentrations of the two product salts and sodium methoxide. MM_{NaCl}, MM_{NaF} and MM_{NaOH} represent the molar masses of sodium chloride, sodium fluoride and sodium hydroxide, respectively. V_{sample} is the volume of sample withdrawn from the reactor. Note that the model does not distinguish precipitated salts from dissolved ones and the predicted values are superficial total concentrations of salts in both forms. Since the sample withdrawn from the reactor was mixed with an excess amount of water, all of the sodium methoxide was expected to be completely hydrolyzed to sodium hydroxide in one-to-one stoichiometric ratio before the sample was dried and weighed. Therefore in the calculation of the total salt mass predicted by the model, the molar mass of sodium hydroxide was used.

5.4. Total salt concentration controversy

Experimentally the total salt mass was found to be practically time independent within experimental error. Unfortunately, the proposed model was not able to reproduce this behavior satisfactorily. In order to understand the problem let us consider the two reactions leading to the salts formation:

$$CHClF_2 + CH_3ONa \rightarrow CH_3OCHF_2 + NaCl \quad (5\text{-}4)$$

$$CHClF_2 + 3CH_3ONa \rightarrow (CH_3O)_3\,CH + 2NaF + NaCl \quad (5\text{-}5)$$

Combing the salt terms and the sodium methoxide term of both the reactions above gives us:

$$CH_3ONa \quad \text{produces} \quad \tfrac{1}{2}NaF + \tfrac{1}{2}NaCl \quad (5\text{-}6)$$

If we assume complete conversion of sodium methoxide, then molar masses of the respective components could be multiplied by the corresponding stoichiometric coefficients in Equation 5-6 to

determine the change in the total salt mass per 1 mole of sodium methoxide. Since the mass of salt in the sample was determined after hydrolysis of sodium methoxide to sodium hydroxide, the molar mass of sodium hydroxide is used again. From the calculation we find that 40 g of sodium methoxide is consumed to produce 50.25 g of salt. Note that this is only applicable for complete conversion of the methoxide. The actual incremental change in the total salt mass would be smaller. Although every attempt was made to ensure that the salt was completely dispersed in the liquid within the reactor, it is possible that larger salt crystals could have accumulated in a portion of the reactor from where sampling could not be carried out. This could be the reason why the total measured salt mass did not increase as the reaction progressed, as it should theoretically have done.

5.5. Parameters of the Arrhenius equation

For the two reactions the rate constant expression described by the Arrhenius equation consists of two parameters: E_a and A, i.e. the activation energy and the frequency factor, respectively. The overall objective was to identify these parameters as well as the Sechenov coefficient and mixing parameter. An initial identification of these parameters, with all the data, is difficult, because it is not possible to obtain good initial estimates. The frequency factor A is a constant, which is generally much larger than E_a. The activation energy E_a is present in the exponential term.

Due to the large difference in the order of magnitude between E_a and A, fitting of these parameters to all the data will result in a strong, non-linear correlation between the two fitted values i.e. the value of one regressed parameter is strongly dependent on the value of the other (Wojciechowski and Rice, 2003). If a poor initial estimate is chosen that does not lie near the solution, the convergence may lie at a local minimum rather than a global minimum. A scaling method was used to diminish the strong non-linear correlation between E_a and A. The method involved *temperature centering* around a midpoint experimental design temperature T_o (Wojciechowski and Rice, 2003). The modified Arrhenius equation is:

$$k = A' \exp\left[-\frac{E}{R}\left(\frac{1}{T}-\frac{1}{T_0}\right)\right] \tag{5-7}$$

where,

$$A' = A\exp\left(-\frac{E}{RT_0}\right) \tag{5-8}$$

The reaction temperature of 293.15 K was selected as T_0 in the fitting. The usual procedure in obtaining good initial parameter estimates for the total fit is to undertake the isothermal fitting of data in order to obtain rate constants at individual temperatures and then generate Arrhenius plots from which the initial estimates of E_a and A can be determined. Hence the isothermal fitting of the experimental data to the model developed in chapter three was carried out for the three experimental temperatures.

All computations were performed on MATLAB® (version R2007b). With an initial guess for the parameters (rate constants, k_1 and k_2; Sechenov coefficient, K_{salt} and mixing parameter, m), the set of ordinary differential equations describing the gas and liquid phase material balances developed in chapter three was integrated using the function *ode15s*. *ode15s* is an implicit subroutine in Matlab®. *lsqnonlin* was used to determine the least-squares weighted fit by comparing the residuals in the objective function and minimizing the sum of squares error. The code is presented in Appendix H.

5.6. Salting-out coefficients of the Sechenov equation

During a preliminary fitting of the experimental data, individual Sechenov coefficients for the three salts (sodium chloride, sodium fluoride and sodium methoxide) were considered. The Sechenov coefficient for sodium methoxide was found to be very small and the contribution of sodium methoxide to the right hand side of the Sechenov equation (Equation 3-40 in Section 3.3.2.) was subsequently ignored. Theoretically, the contribution of sodium methoxide to the right hand side of the Sechenov equation should not be large, if the presence of dissolved salts is meant to increase the Henry's constant and decrease the gas solubility in line with the experimental results. This can be explained with the following hypothetical example. Referring to Figure 5-9, at the beginning of the reaction, sodium fluoride and sodium chloride are formed whilst sodium methoxide is consumed, thus the concentrations of the former two increase and the concentration of the latter decreases. At time t_1 the concentration of dissolved sodium fluoride reaches the solubility limit and the concentration-time plot for that salt becomes horizontal. At time t_2 the same situation occurs for

sodium chloride. This is a critical moment since after time t_2, the dissolved concentration of sodium methoxide continues to decrease. If the contribution of sodium methoxide to the right hand side of the Sechenov equation is large then the Henry's constant begins to decrease again, leading to better R-22 gas solubility than at the time that sodium chloride reached the solubility limit (t_2). Assuming that the flattening of the experimental concentration-time data is partially due to the salting-out effect, then the Henry's constant should continue to increase until there is not enough R-22 in the liquid to support the reactions. Using this logic, the Sechenov coefficient for sodium methoxide should be small.

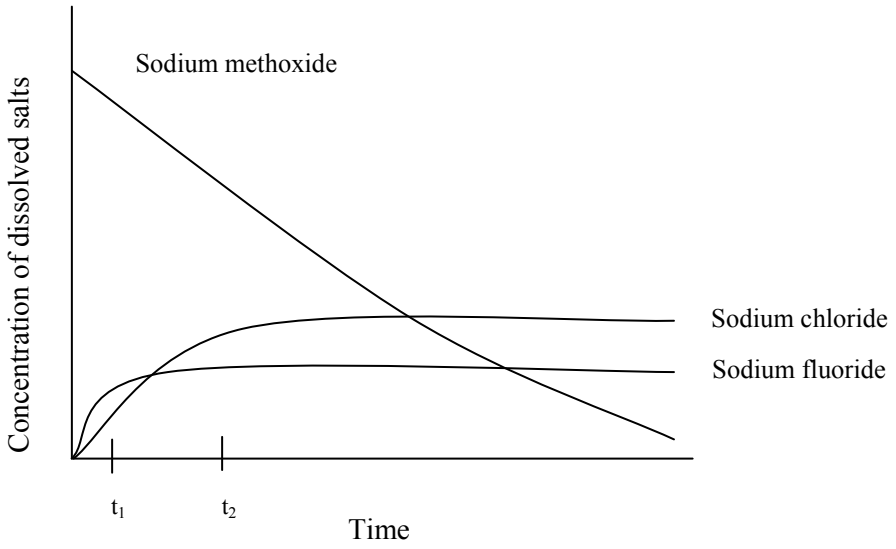

Figure 5-9. Hypothetical plot of the concentration path of the individual salts in the reactor

The solubility of sodium fluoride in the reaction mixture is very low (refer to Table 3-3). However, the contribution of sodium fluoride to the Sechenov equation could not be completely ignored. To keep the number of fitting parameters to a minimum, the Sechenov coefficient for sodium chloride and sodium fluoride were assumed to be equal. The latter appeared to be a reasonable assumption since the ionic strength for the two salts should be the same, and the Sechenov equation is occasionally expressed in terms of ionic strength (Schumpe, 1993). Note, however, that the combined Sechenov coefficient, K_{salt}, used in this investigation is a concentration based value.

5.7. Results of isothermal data fitting

For the isothermal fits the unknown parameters in the identification were the rate constants, k_1 and k_2; a single Sechenov coefficient, K_{salt}; and the mixing parameter, m. At each temperature used for the isothermal fitting (283, 293 and 303 K) parity plots for sodium chloride concentration and total salt mass were drawn to illustrate the fit of the modeled data to experimental data. Figures 5-10, 5-11 and 5-12 show the parity plots.

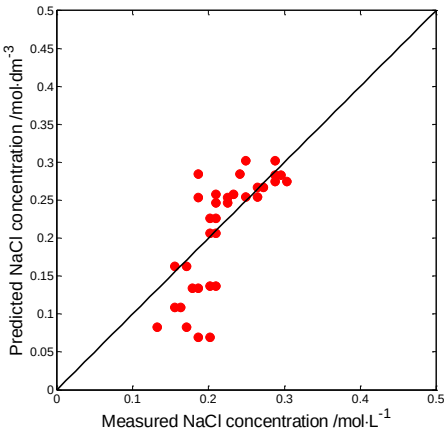

Figure 5-10a. Parity plot for sodium chloride concentration at 283 K

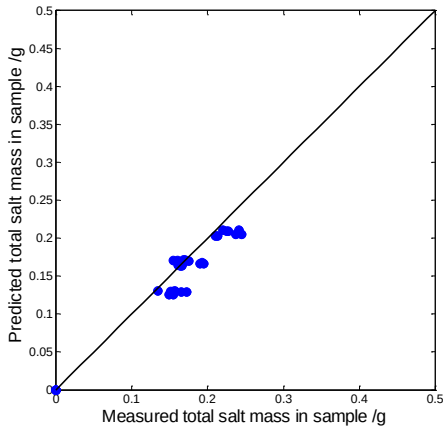

Figure 5-10b. Parity plot for total salt mass at 283 K

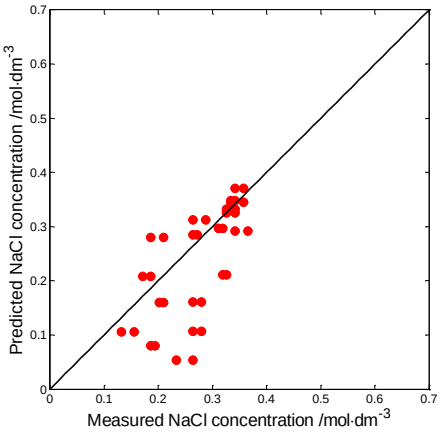

Figure 5-11a. Parity plot for sodium chloride concentration at 293 K

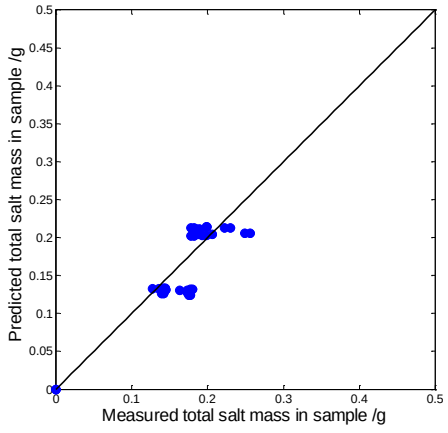

Figure 5-11b. Parity plot for total salt mass at 293 K

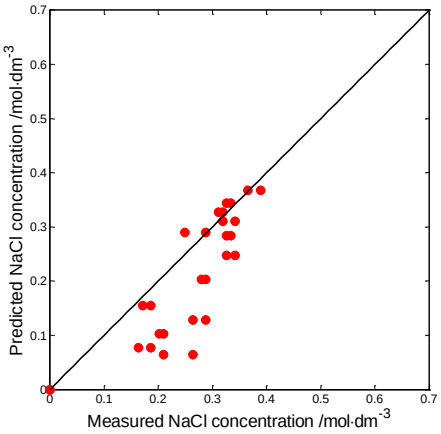

Figure 5-12a. Parity plot for sodium chloride concentration at 303 K

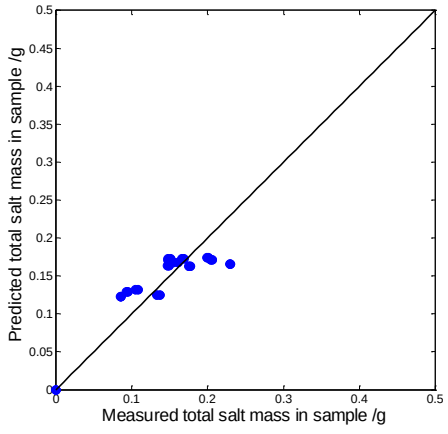

Figure 5-12b. Parity plot for total salt mass at 303 K

Concentration-time plots of the measured and predicted NaCl concentration were generated for all the experimental runs (Figure 5-13 to 5-23). The measured and predicted total salt mass in the sample as a function of time is presented in Figures 5-24 to 5-34 for all the experiments.

For all the temperatures the plots reveal an initially swift rate followed by a gradual decrease to the extent that the NaCl concentration becomes more or less constant. The flattening of each of these concentration-time profiles is firstly due to the reduction in the driving force for mass transfer (i.e. gas solubility) brought about as a result of the 'salting-out' effect and secondly due to the inhibitory effect of precipitated salts on mixing which results in a reduction in the mass transfer coefficient. The gas-chromatographic analysis of the exit gas from preliminary experiments showed that R-22 was never completely consumed, i.e. the reaction never reached completion.

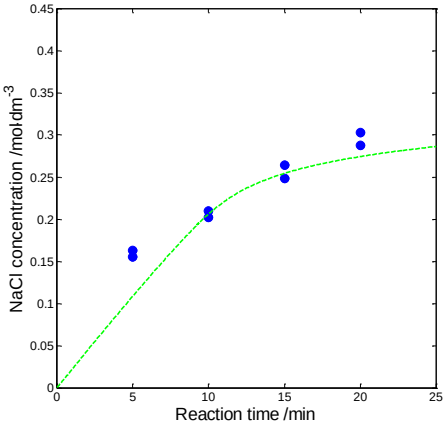

Figure 5-13. Concentration of NaCl produced vs. time, at 283.15 K with an initial NaOH concentration of 2 mol·dm^{-3} and an R-22 partial pressure of 40 kPa (•, experimental; ---, model)

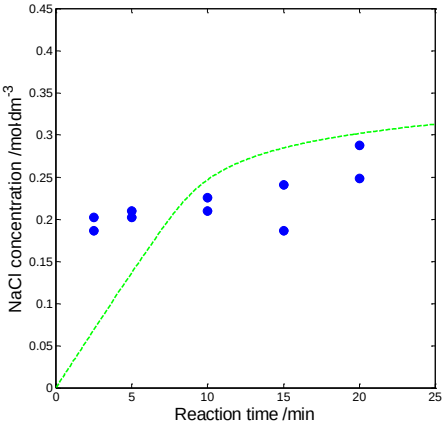

Figure 5-15. Concentration of NaCl produced vs. time, at 283.15 K with an initial NaOH concentration of 2.5 mol·dm^{-3} and an R-22 partial pressure of 50 kPa (•, experimental; ---, model)

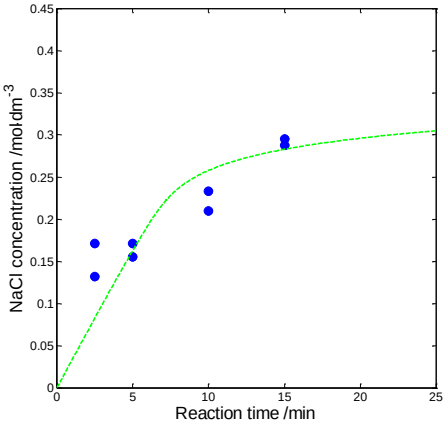

Figure 5-14. Concentration of NaCl produced vs. time, at 283.15 K with an initial NaOH concentration of 2 mol·dm^{-3} and an R-22 partial pressure of 60 kPa (•, experimental; ---, model)

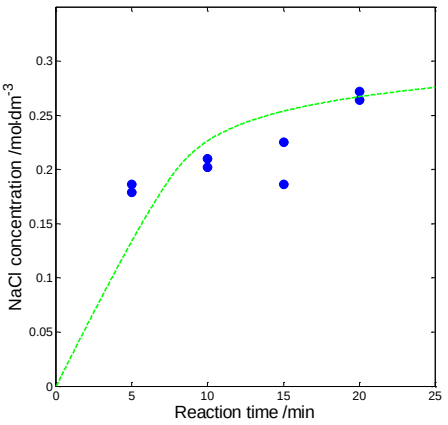

Figure 5-16. Concentration of NaCl produced vs. time, at 283.15 K with an initial NaOH concentration of 1.5 mol·dm^{-3} and an R-22 partial pressure of 50 kPa (•, experimental; ---, model)

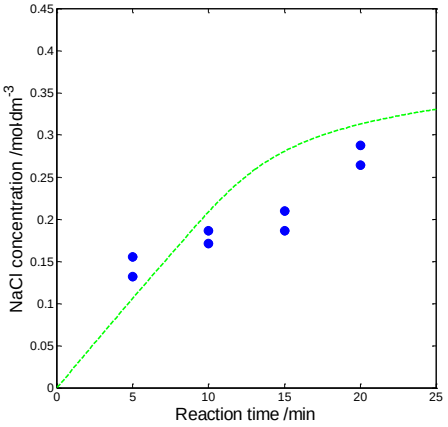

Figure 5-17. Concentration of NaCl produced vs. time, at 293.15 K with an initial NaOH concentration of 1.5 mol·dm^{-3} and an R-22 partial pressure of 40 kPa (•, experimental; ---, model)

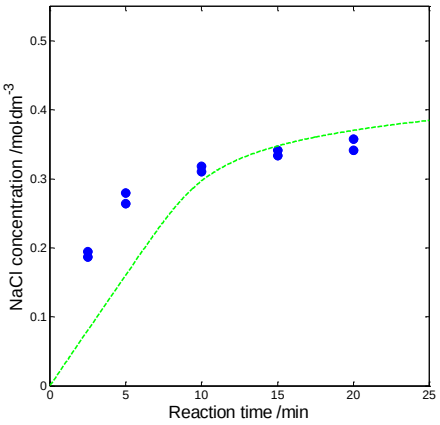

Figure 5-19. Concentration of NaCl produced vs. time, at 293.15 K with an initial NaOH concentration of 2.5 mol·dm^{-3} and an R-22 partial pressure of 60 kPa (•, experimental; ---, model)

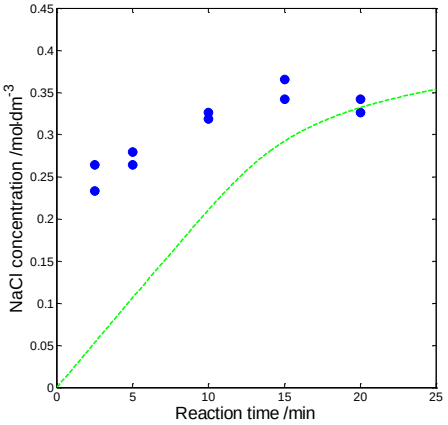

Figure 5-18. Concentration of NaCl produced vs. time, at 293.15 K with an initial NaOH concentration of 2.5 mol·dm^{-3} and an R-22 partial pressure of 40 kPa (•, experimental; ---, model)

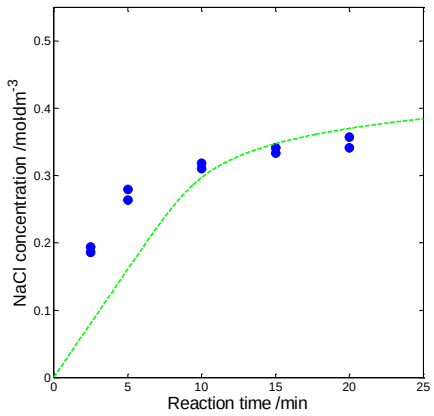

Figure 5-20. Concentration of NaCl produced vs. time, at 293.15 K with an initial NaOH concentration of 1.5 mol·dm^{-3} and an R-22 partial pressure of 60 kPa (•, experimental; ---, model)

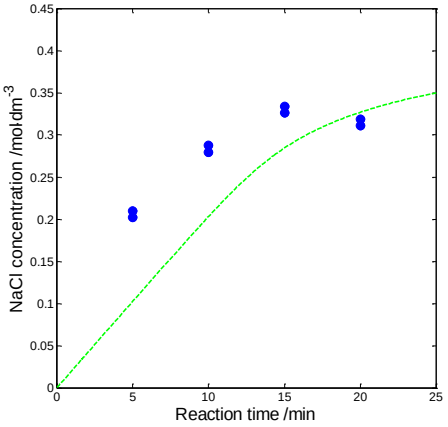

Figure 5-21. Concentration of NaCl produced vs. time, at 303.15 K with an initial NaOH concentration of 2 mol·dm^{-3} and an R-22 partial pressure of 40 kPa (•, experimental; ---, model)

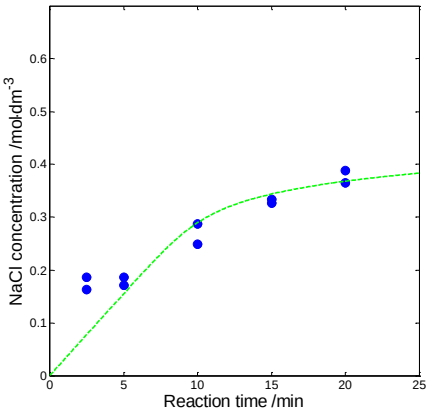

Figure 5-23. Concentration of NaCl produced vs. time, at 303.15 K with an initial NaOH concentration of 1.5 mol·dm^{-3} and an R-22 partial pressure of 50 kPa (•, experimental; ---, model)

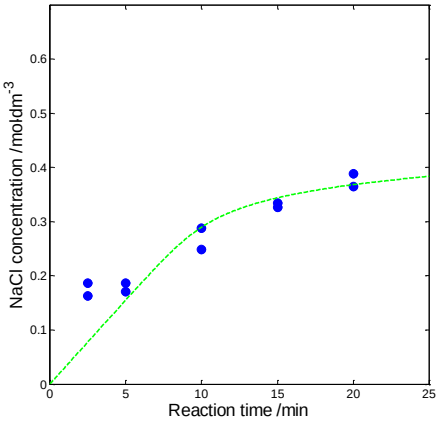

Figure 5-22. Concentration of NaCl produced vs. time, at 303.15 K with an initial NaOH concentration of 2 mol·dm^{-3} and an R-22 partial pressure of 60 kPa (•, experimental; ---, model)

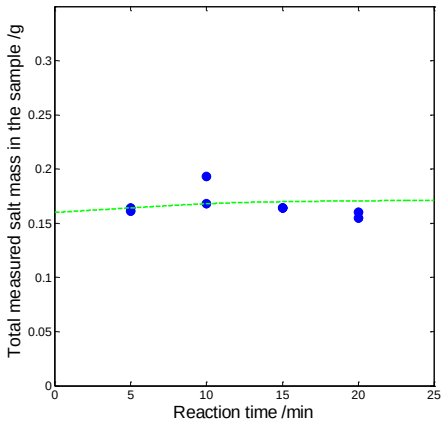

Figure 5-24. Total salt mass vs. time at 283.15 K with an initial NaOH concentration of 2 mol·dm^{-3} and an R-22 partial pressure of 40 kPa (•, experimental; ---, model)

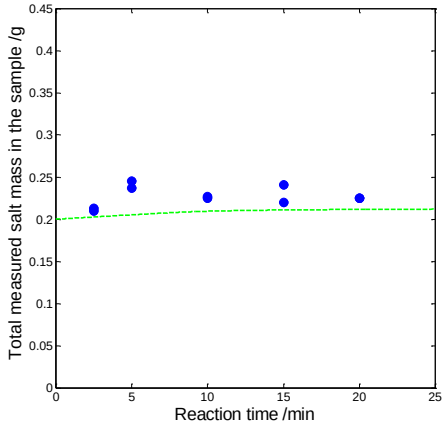

Figure 5-26. Total salt mass vs. time at 283.15 K with an initial NaOH concentration of 2.5 mol·dm^{-3} and an R-22 partial pressure of 50 kPa (•, experimental; ---, model)

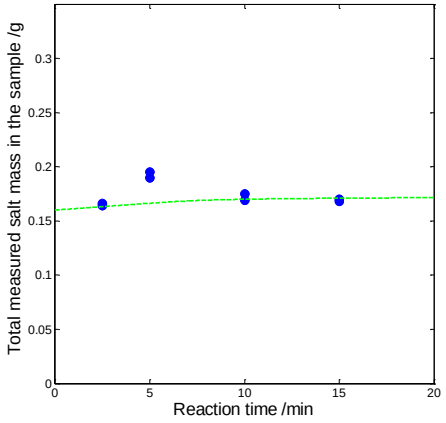

Figure 5-25. Total salt mass vs. time at 283.15 K with an initial NaOH concentration of 2 mol·dm^{-3} and an R-22 partial pressure of 60 kPa (•, experimental; ---, model)

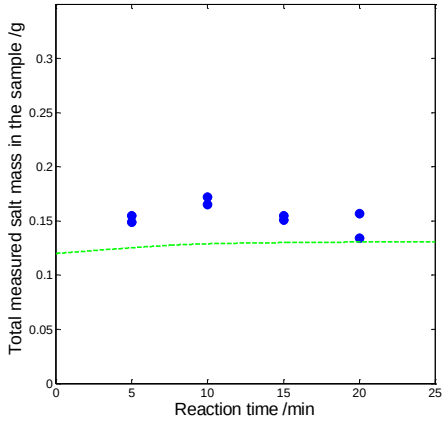

Figure 5-27. Total salt mass vs. time at 283.15 K with an initial NaOH concentration of 1.5 mol·dm^{-3} and an R-22 partial pressure of 50 kPa (•, experimental; ---, model)

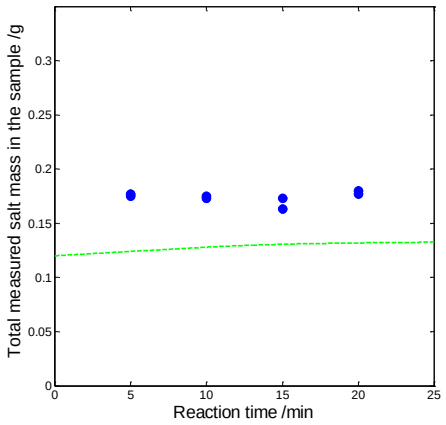

Figure 5-28. Total salt mass vs. time at 293.15 K with an initial NaOH concentration of 1.5 mol·dm^{-3} and an R-22 partial pressure of 40 kPa (•, experimental; ---, model)

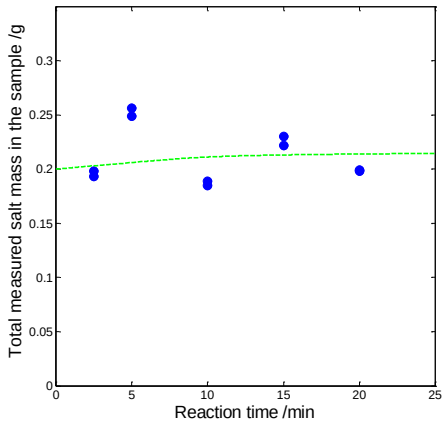

Figure 5-30. Total salt mass vs. time at 293.15 K with an initial NaOH concentration of 2.5 mol·dm^{-3} and an R-22 partial pressure of 60 kPa (•, experimental; ---, model)

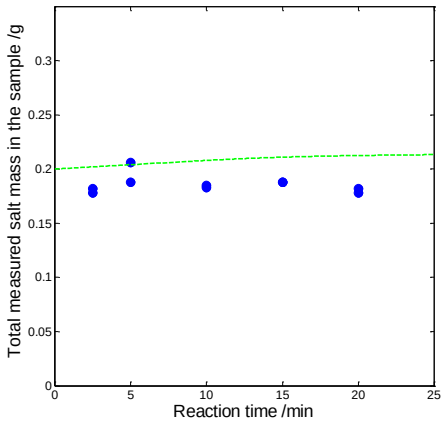

Figure 5-29. Total salt mass vs. time at 293.15 K with an initial NaOH concentration of 2.5 mol·dm^{-3} and an R-22 partial pressure of 40 kPa (•, experimental; ---, model)

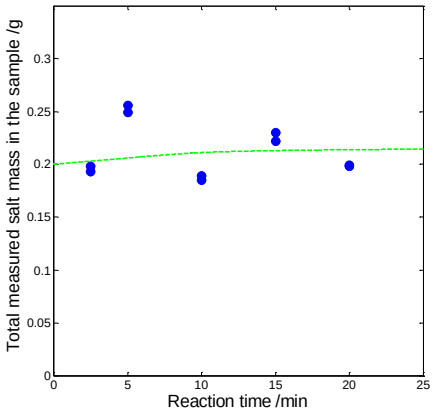

Figure 5-31. Total salt mass vs. time at 293.15 K with an initial NaOH concentration of 1.5 mol·dm^{-3} and an R-22 partial pressure of 60 kPa (•, experimental; ---, model)

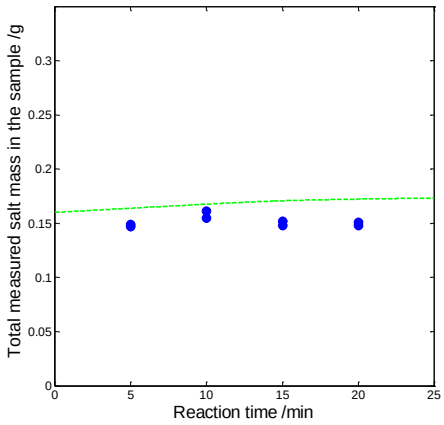

Figure 5-32. Total salt mass vs. time at 303.15 K with an initial NaOH concentration of 2 mol·dm^{-3} and an R-22 partial pressure of 40 kPa (•, experimental; ---, model)

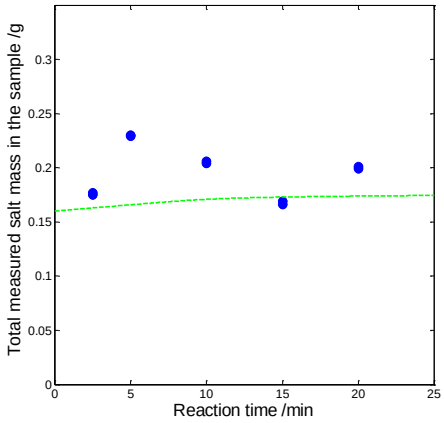

Figure 5-33. Total salt mass vs. time at 303.15 K with an initial NaOH concentration of 2 mol·dm^{-3} and an R-22 partial pressure of 60 kPa (•, experimental; ---, model)

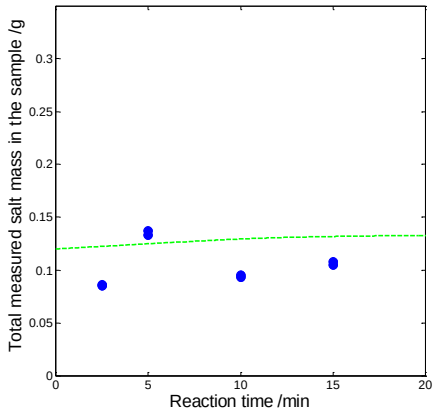

Figure 5-34. Total salt mass vs. time at 303.15 K with an initial NaOH concentration of 1.5 mol·dm^{-3} and an R-22 partial pressure of 50 kPa (•, experimental; ---, model)

The rate constants for reactions 1 and 2 as well as the Sechenov coefficient and mixing parameter obtained from the fitting procedure for all three temperatures is presented in Table 5-4.

Table 5-4. Parameters obtained from the isothermal fitting procedure

Temperature / *K*	$k_1 \left(\left(\frac{dm^3}{mol} \right)^2 / min \right)$	$k_2 \left(\frac{dm^3}{mol} / min \right)$	K_{salt}	m
283.15	16.93	10.24	0.871	23.70
293.15	109.59	21.47	0.911	22.49
303.15	203.01	38.85	0.622	20.76

The Arrhenius plots are shown in Figure 5-35. The plots indicate a linear trend of the rate constants with inverse absolute temperature. The Arrhenius parameters estimated from these plots are listed in Table 5-5.

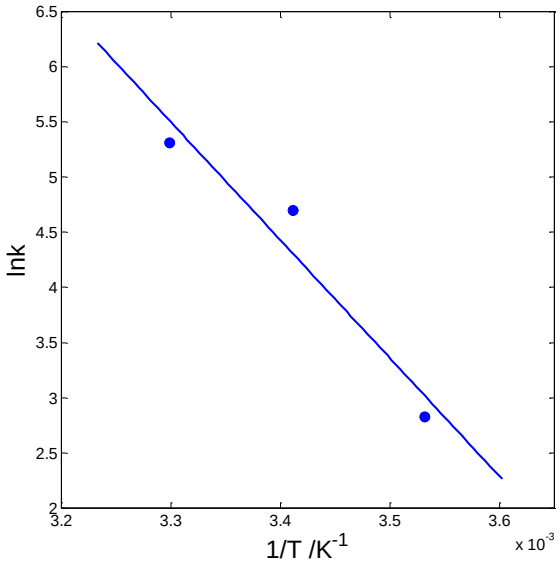

Figure 5-35a. Arrhenius plot for reaction 1

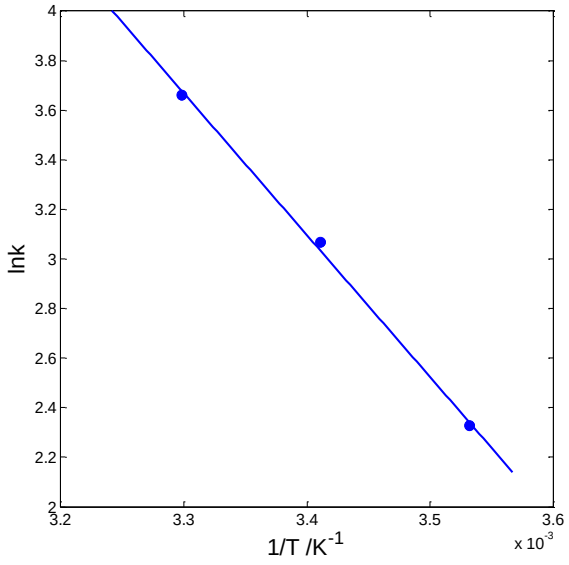

Figure 5-35b. Arrhenius plot for reaction 2

Table 5-5. Arrhenius parameters for reaction 1 and reaction 2 (isothermal fitting)

	E_a / $kJ \cdot mol^{-1}$	A
Reaction 1	89.114	5.627×10^{17}
Reaction 2	47.620	6.347×10^{9}

These parameters were used as initial parameter estimates in the scaling method to determine the final Arrhenius parameters for the total fit. 293.15 K was selected as the centering temperature. Average values of the salt Sechenov coefficient and mixing parameter were used for the total data fitting. Table 5-6 lists the pre-exponential factor and activation energy generated from the total parameter fitting, together with the final fitted values of the Sechenov coefficient and mixing parameter. The final activation energies generated for each reaction were observed to be of the same order of magnitude and physically meaningful.

Table 5-6. Arrhenius parameters for reaction 1 and reaction 2 (total fitting) using K_{salt} = 0.712 and m = 22.43

	E_a / $kJ \cdot mol^{-1}$	A
Reaction 1	89.123	5.194×10^{17}
Reaction 2	45.828	2.982×10^{9}

Unfortunately, there is no reliable kinetic data given in the literature regarding this particular system that could be compared to the data generated in this work. Based on the identified activation energies it would appear that higher reaction temperatures would favour reaction 1 and would therefore result in improved selectivity towards difluorodimethyl ether. This is in line with the preliminary experimental results presented in Figure 5-6. If the reaction is carried out at atmospheric pressure then the maximum permissible reaction temperature would be governed by the boiling point of the alcohol solution.

Parity plots for sodium chloride concentration and total salt mass were generated for the total fit and are illustrated in Figure 5-36.

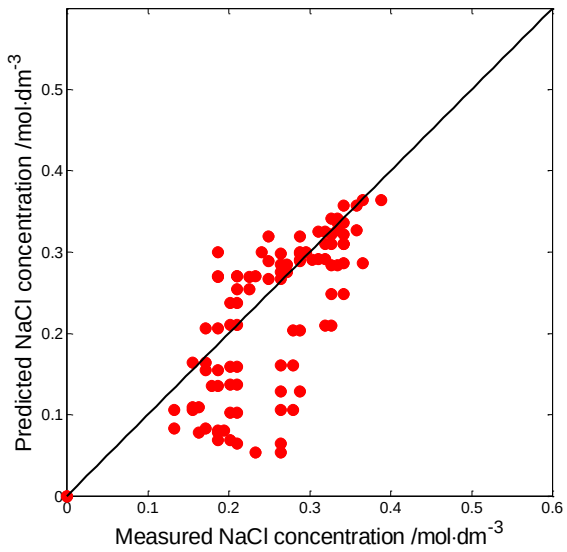

Figure 5-36a. Parity plot of sodium chloride concentration for total fitting

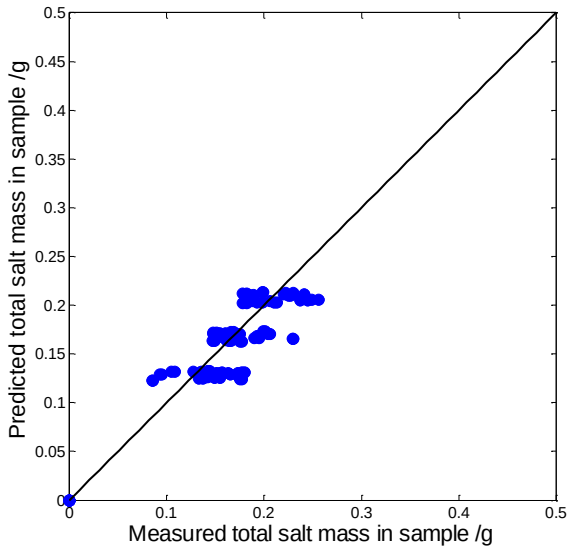

Figure 5-36b. Parity plot of total salt mass for total fitting

Figures 5-37 to 5-47 show the concentration-time plots of the measured and predicted NaCl concentration generated for all the experimental points in the total fitting.

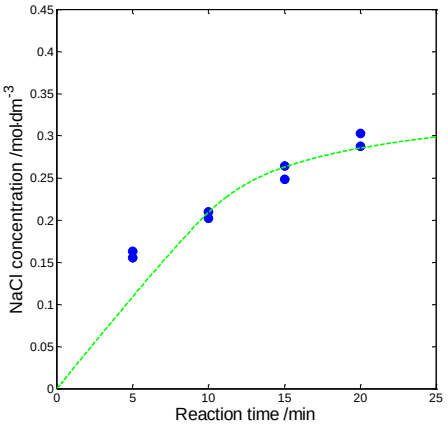

Figure 5-37. Concentration of NaCl produced vs. time for total fitting, at 283.15 K with an initial NaOH concentration of 2 mol·dm^{-3} and an R-22 partial pressure of 40 kPa (•, experimental; ---, model)

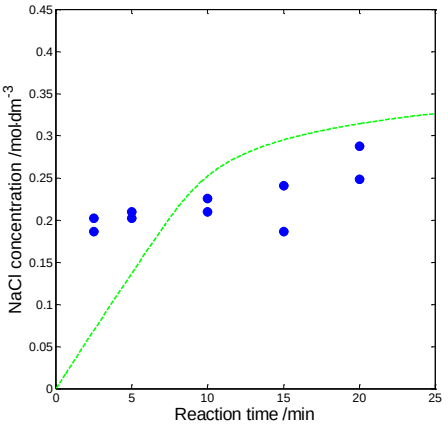

Figure 5-39. Concentration of NaCl produced vs. time for total fitting, at 283.15 K with an initial NaOH concentration of 2.5 mol·dm^{-3} and an R-22 partial pressure of 50 kPa (•, experimental; ---, model)

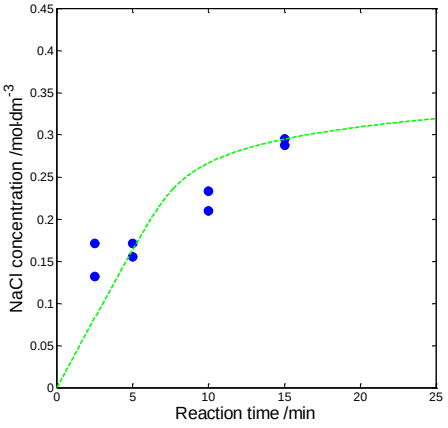

Figure 5-38. Concentration of NaCl produced vs. time for total fitting, at 283.15 K with an initial NaOH concentration of 2 mol·dm^{-3} and an R-22 partial pressure of 60 kPa (•, experimental; ---, model)

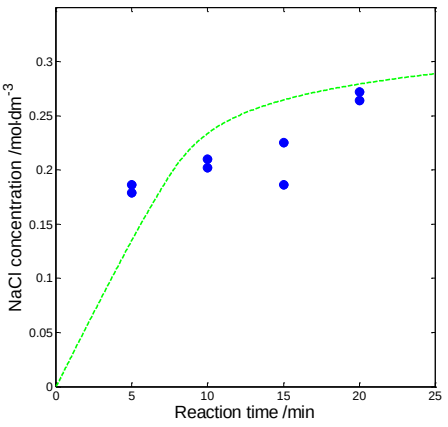

Figure 5-40. Concentration of NaCl produced vs. time for total fitting, at 283.15 K with an initial NaOH concentration of 1.5 mol·dm^{-3} and an R-22 partial pressure of 50 kPa (•, experimental; ---, model)

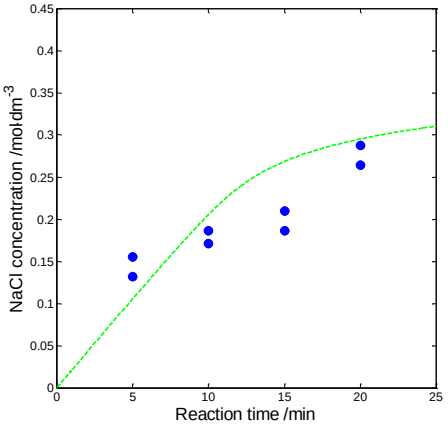

Figure 5-41. Concentration of NaCl produced vs. time for total fitting, at 293.15 K with an initial NaOH concentration of 1.5 mol·dm^{-3} and an R-22 partial pressure of 40 kPa (•, experimental; ---, model)

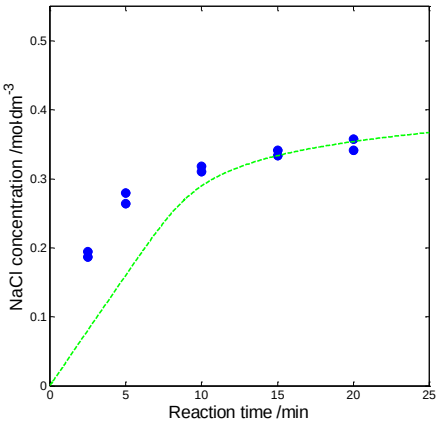

Figure 5-43. Concentration of NaCl produced vs. time for total fitting, at 293.15 K with an initial NaOH concentration of 2.5 mol·dm^{-3} and an R-22 partial pressure of 60 kPa (•, experimental; ---, model)

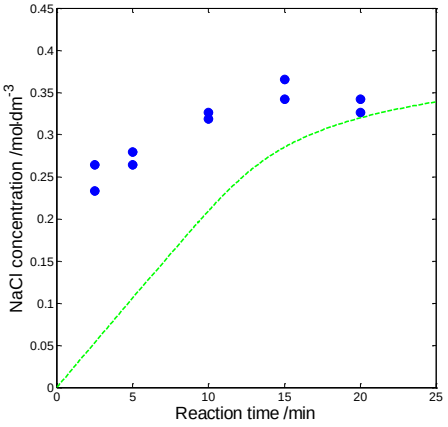

Figure 5-42. Concentration of NaCl produced vs. time for total fitting, at 293.15 K with an initial NaOH concentration of 2.5 mol·dm^{-3} and an R-22 partial pressure of 40 kPa (•, experimental; ---, model)

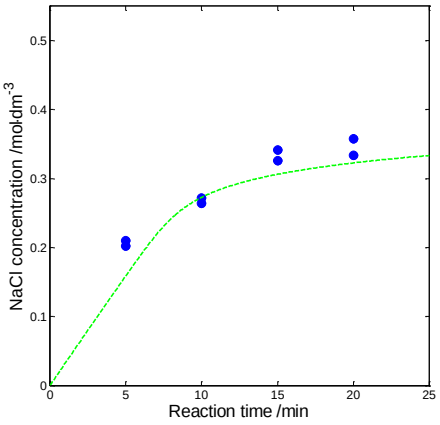

Figure 5-44. Concentration of NaCl produced vs. time for total fitting, at 293.15 K with an initial NaOH concentration of 1.5 mol·dm^{-3} and an R-22 partial pressure of 60 kPa (•, experimental; ---, model)

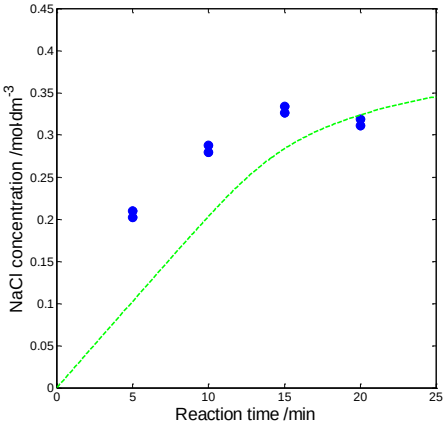

Figure 5-45. Concentration of NaCl produced vs. time for total fitting, at 303.15 K with an initial NaOH concentration of 2 mol·dm^{-3} and an R-22 partial pressure of 40 kPa (•, experimental; ---, model)

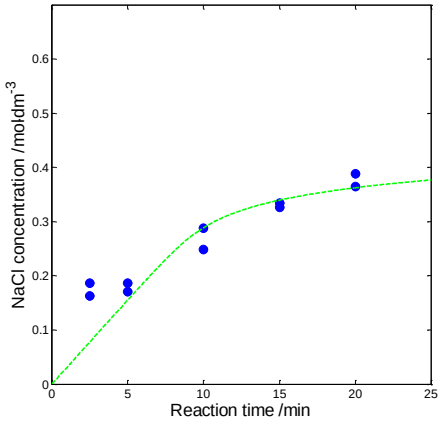

Figure 5-46. Concentration of NaCl produced vs. time for total fitting, at 303.15 K with an initial NaOH concentration of 2 mol·dm^{-3} and an R-22 partial pressure of 60 kPa (•, experimental; ---, model)

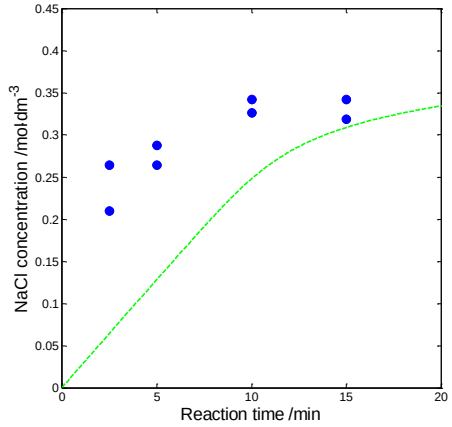

Figure 5-47. Concentration of NaCl produced vs. time for total fitting, at 303.15 K with an initial NaOH concentration of 1.5 mol·dm^{-3} and an R-22 partial pressure of 50 kPa (•, experimental; ---, model)

Figures 5-48 to 5-58 show the measured and predicted total salt mass in the sample as a function of time for all the experiments in the total fitting.

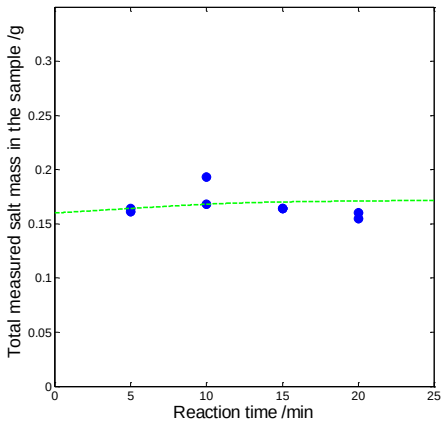

Figure 5-48. Total salt mass vs. time for total fitting at 283.15 K with an initial NaOH concentration of 2 mol·dm^{-3} and an R-22 partial pressure of 40 kPa (•, experimental; ---, model)

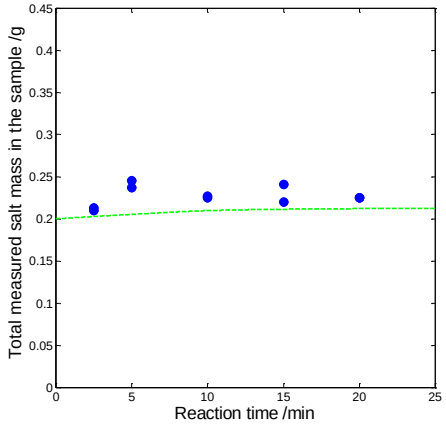

Figure 5-50. Total salt mass vs. time for total fitting at 283.15 K with an initial NaOH concentration of 2.5 mol·dm^{-3} and an R-22 partial pressure of 50 kPa (•, experimental; ---, model)

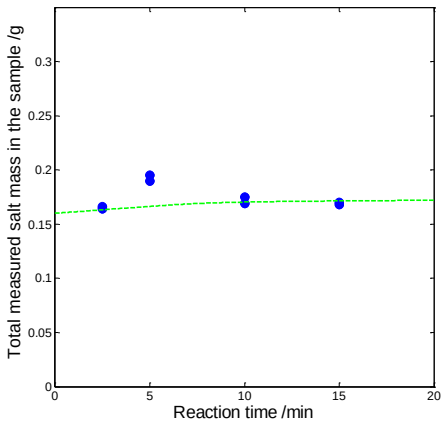

Figure 5-49. Total salt mass vs. time for total fitting at 283.15 K with an initial NaOH concentration of 2 mol·dm^{-3} and an R-22 partial pressure of 60 kPa (•, experimental; ---, model)

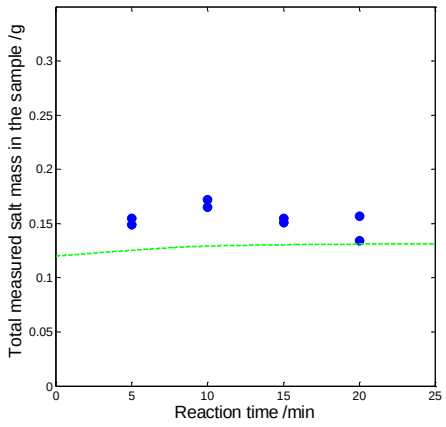

Figure 5-51. Total salt mass vs. time for total fitting at 283.15 K with an initial NaOH concentration of 1.5 mol·dm^{-3} and an R-22 partial pressure of 50 kPa (•, experimental; ---, model)

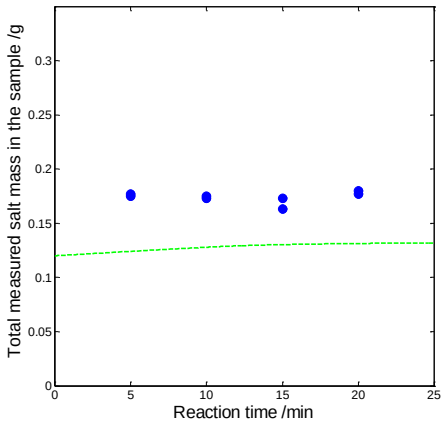

Figure 5-52. Total salt mass vs. time for total fitting at 293.15 K with an initial NaOH concentration of 1.5 mol·dm^{-3} and an R-22 partial pressure of 40 kPa (•, experimental; ---, model)

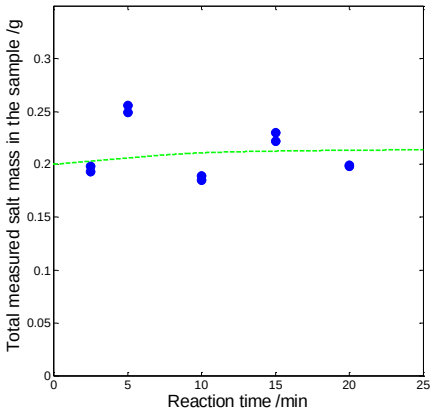

Figure 5-54. Total salt mass vs. time for total fitting at 293.15 K with an initial NaOH concentration of 2.5 mol·dm^{-3} and an R-22 partial pressure of 60 kPa (•, experimental; ---, model)

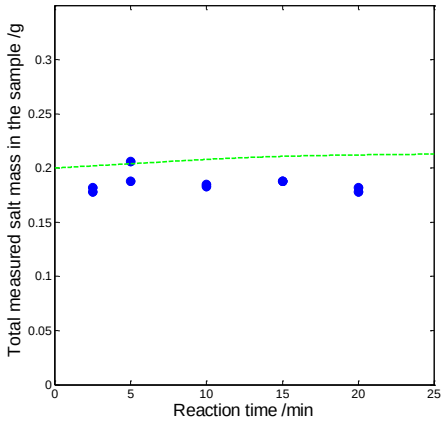

Figure 5-53. Total salt mass vs. time for total fitting at 293.15 K with an initial NaOH concentration of 2.5 mol·dm^{-3} and an R-22 partial pressure of 40 kPa (•, experimental; ---, model)

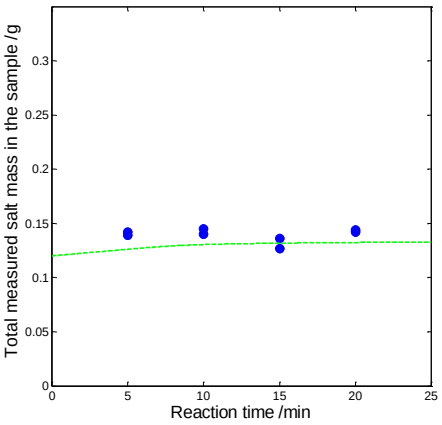

Figure 5-55. Total salt mass vs. time for total fitting at 293.15 K with an initial NaOH concentration of 1.5 mol·dm^{-3} and an R-22 partial pressure of 60 kPa (•, experimental; ---, model)

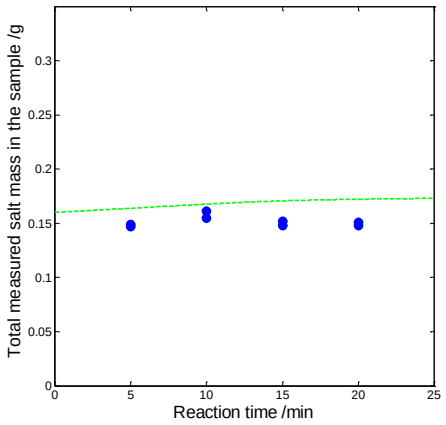

Figure 5-56. Total salt mass vs. time for total fitting at 303.15 K with an initial NaOH concentration of 2 mol·dm^{-3} and an R-22 partial pressure of 40 kPa (•, experimental; ---, model)

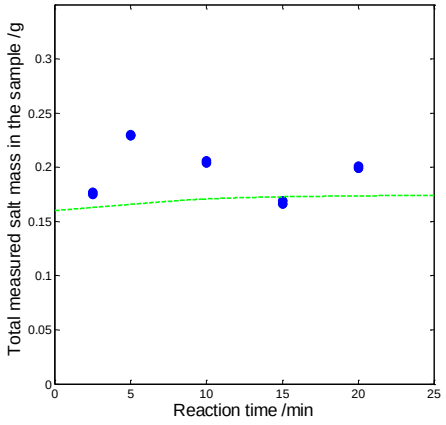

Figure 5-57. Total salt mass vs. time for total fitting at 303.15 K with an initial NaOH concentration of 2 mol·dm^{-3} and an R-22 partial pressure of 60 kPa (•, experimental; ---, model)

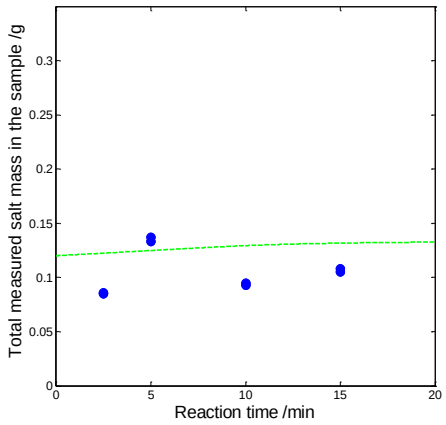

Figure 5-58. Total salt mass vs. time for total fitting at 303.15 K with an initial NaOH concentration of 1.5 mol·dm^{-3} and an R-22 partial pressure of 50 kPa (•, experimental; ---, model)

Figure 5-59 shows a simulated concentration-time profile for sodium methoxide for one set of operating conditions. Figure 5-60 shows the simulated profile of the cumulative superficial salt concentration in the liquid against time for the same set of operating conditions where the red and blue curves represent sodium chloride and sodium fluoride, respectively. The first figure clearly shows that there is only partial conversion of sodium methoxide. The change in the total mass of salt (predicted and dissolved) within the reactor vessel after 30 minutes would not be as great as the case if methoxide was completely consumed (as shown in section 5.4). This explains why for most of the experimental runs the total salt mass was found to be practically time independent, particularly towards the end of the run.

The amount of sodium fluoride produced is less than that of sodium chloride according to the simulated results.

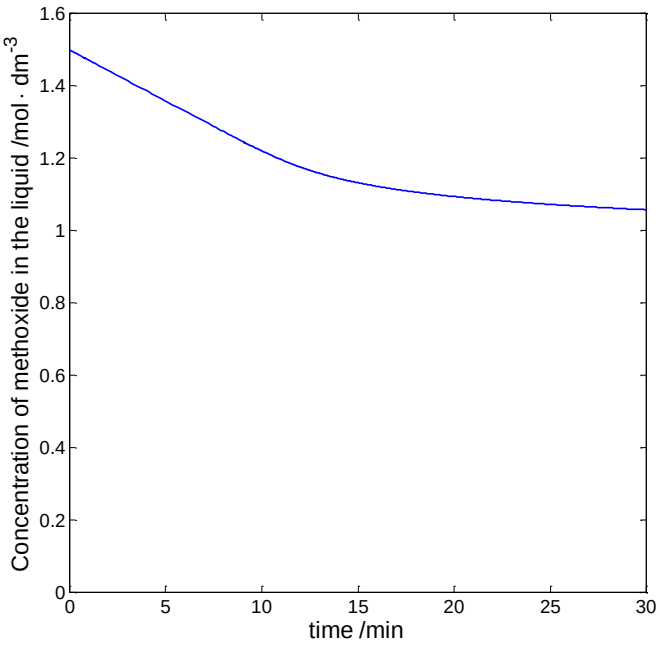

Figure 5-59. Simulated concentration vs. time profile for sodium methoxide at 293.15 K with an initial NaOH concentration of 2 mol·dm^{-3} and an R-22 partial pressure of 50 kPa

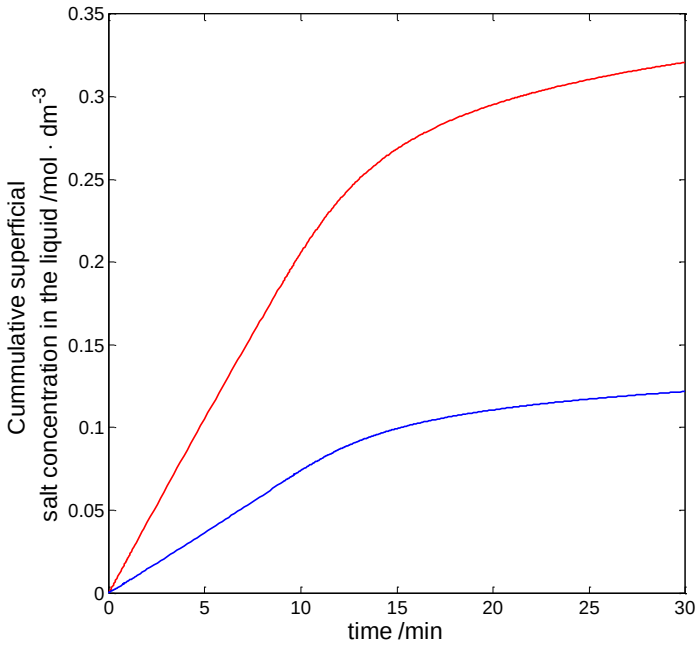

Figure 5-60. A profile of the simulated cumulative superficial salt concentration in the liquid vs. time at 293.15 K with an initial NaOH concentration of 2 mol·dm^{-3} and an R-22 partial pressure of 50 kPa (–, NaCl; –, NaF)

CHAPTER 6

CONCLUSIONS AND RECOMMENDATIONS

6.1. Conclusions

The reaction of R-22 with sodium methoxide is a well-established method of producing difluorodimethyl ether. The process serves as a means of converting existing reserves of R-22 into a useful replacement refrigerant with low ozone depleting potential. In this study, the gas-liquid reaction was carried out using a stirred semi-batch apparatus. To develop an understanding of the behaviour of the reaction system and to determine operating limits, a series of preliminary experiments was performed. It was found that the yield of difluorodimethyl ether increased substantially at higher reaction temperatures and higher initial concentrations of sodium hydroxide in methanol. However, the practical operating limits of the system were governed by the boiling point of the solvent at atmospheric pressure and the solubility limit of sodium hydroxide in methanol. A comparison of the results of identical experiments conducted separately in stainless steel and glass reactors showed that substantially better difluorodimethyl ether yields were obtained in the non-metallic apparatus. Such behaviour can be attributed to the possible catalytic action of the reactor surface, which accelerates the formation of a trimethyl orthoformate by-product. The presence of this by-product in the residual reactor liquid was confirmed in this study by GCMS analysis.

An extended Box-Behnken experimental design was subsequently employed using a glass semi-batch reactor to generate rate data for kinetic model identification purposes. Of the three design variables chosen, *viz*. initial sodium hydroxide concentration (1.5-2.5 $mol \cdot dm^{-3}$), R-22 partial pressure (40.5-60.8 kPa) and reaction temperature (283-303 K), the latter was found to have the most pronounced effect on the reaction rate and hence the yield of difluorodimethyl ether. A kinetic model for the gas-liquid reaction was developed based on the α-dehydrohalogenation mechanism of Hine and Porter (1957). Importantly, unlike previous kinetic studies reported in the literature (Nishiumi and Kato, 2003; Kato and Nishiumi, 2003), the side reaction involving the formation of trimethyl orthoformate and sodium fluoride was not completely ignored, but rather incorporated into the model.

In this system, the formation of sodium salts was found to have an inhibitory effect on gas-liquid mass transfer. Due to the relatively low solubilities of both sodium chloride and sodium fluoride in methanol, a large amount of precipitated salts were formed during the course of each experiment. The solid salt crystals appeared to change the rheological properties of the agitated fluid, resulting in inefficient mixing and lower mass transfer rates. In addition, the presence of dissolved salts resulted in lower gas solubility (i.e. higher Henry's law constants and a reduced driving force for mass transfer) through a phenomenon called 'salting-out'. The latter is a result of the solvation of salt ions by alcohol molecules (Nishiumi et al., 2010). Both of these salt effects were incorporated into the model of the semi-batch reactor. A gradual reduction in the mass transfer rates and gas solubility ultimately resulted in a very low dissolved gas concentration of R-22 toward the end of each experiment. The reaction rate was thus also greatly reduced, leading to the observed lower gradient of the cumulative superficial sodium chloride concentration-time curves. Mass transfer enhancement through reaction was not included in the modeling as it was estimated that the enhancement factor would be practically 1 at the beginning of the reaction, a point at which the effect of reaction on mass transfer is expected to have been the greatest.

For the kinetic model identification the following were included as fitting parameters:

- Pre-exponential factors and activation energies for reactions 1 and 2 (the difluorodimethyl ether and trimethyl orthoformate formation reactions, respectively).
- A single Sechenov 'salting-out' coefficient, K_{salt}, to account for the effect of dissolved sodium chloride and sodium fluoride on gas solubility.
- A mixing parameter, m, to account for the effect of precipitated salts on the volumetric mass transfer coefficient.

The activation energies for reactions 1 and 2 were estimated to be 89.12 and 45.83 $kJ \cdot mol^{-1}$, respectively. A Sechenov coefficient of 0.712 and mixing parameter of 22.43 were also identified. The Sechenov coefficient obtained in this study is of the same order of magnitude as those reported for sodium chloride in water and oxygen (Battino et al., 1983). It is important to note that the Sechenov coefficient for this gas-liquid-salt system cannot be easily determined directly as the measurements require a constant concentration of dissolved salts, a condition which cannot be maintained due to the continuous generation of sodium chloride and sodium fluoride by reaction.

It is unlikely that the production of difluorodimethyl ether on an industrial scale can be accomplished using a semi-batch apparatus due to the negative effects of dissolved and precipitated product salts on gas-liquid mass transfer. A brief look at the literature regarding industrial precipitation processes has indicted that large-scale implementation can possibly be achieved using continuous bubble column reactors (Rigopolous and Jones, 2001). In the latter, the precipitated salts are continuously removed from the apparatus and have little effect on mixing and mass transfer. A possibility exists that the 'salting-out' phenomenon associated with dissolved salts may not be influential at all points in this type of reactor, as is the case with an agitated tank. However, this needs to be verified independently through simulation and/or experimentation.

6.2. Recommendations for future work

Improvements in the kinetic data reported in this study can only be achieved through changes in the experimental techniques. In this investigation it was difficult to obtain a sample that was fully representative of all the salt that was present in the reactor at a particular time, due to the preferential accumulation of salt in certain regions within the reactor vessel (e.g. at the bottom). The experimental procedure used by Hine and Porter (1957) appears to be the best alternative for future investigations regarding this system. According to their method, the reaction is carried out for a prescribed time in a semi-batch apparatus similar to the one used in this study. The reaction is then quenched by rapidly lowering the temperature and sparging with an inert gas, after which the entire content of the vessel is used for gravimetric and titrimetric/spectrophotometric analysis. The application of this method ensures no losses during sampling.

To impose additional constraints on the objective function of the fitting algorithm, the total amount of precipitated salts can be obtained by filtering the residual reactor liquid and weighing the filter cake. This may improve the estimate of the Sechenov coefficient. In addition, the total quantity of difluorodimethyl ether produced during one experiment can be determined by condensing and trapping the product gas and thereafter undertaking gravimetric and gas chromatographic analysis of the collected material.

REFERENCES

Armstrong W.D. (1933). Colorimetric determination of fluorine. *Industrial and Engineering Chemistry*, **5**, pp. 300-302.

Armstrong W.D. (1936). Microdetermination of fluorine: Elimination of effect of chlorine. *Industrial and Engineering Chemistry*, **8**, pp. 384-387.

Banks R.E., Smart B.E., Tatlow J.C. (2000). *Organofluorine Chemistry: Principles and Commercial Applications*, New York, Plenum.

Barney J.E., Bertolacini R.J. (1957). Colorimetric determination of chloride with mercuric chlorinate. *Analytical Chemistry,* **29**, pp.1187-1188.

Baumol W.J., Blinder A.S. (2012). *Economics: Principles and Policy*, 12th Edition, Mason, South-Western, Cengage Learning.

Battino R., Rettich T.R., Tominaga T. (1983). The Solubility of Oxygen and Ozone in Liquids. *Journal of Physical and Chemical Reference Data*, **12**, pp.163-178.

Bond A.M., Murray M.M. (1953). Direct titrimetric determination of fluoride in natural waters. *Biochemical Journal*, **53**, pp. 642-645.

Box G.E.P., Behnken D.W. (1960). Some new three level designs for the study of quantitative variables. *Technometrics*, **2** (4), pp.455-475.

Bruice P.Y. (2004). *Organic Chemistry*, 4th Edition, NJ, Pearson/Prentice Hall.

Buzzi-Ferraris G., Manenti F. (2009). Kinetic Model Analysis. *Chemical Engineering Science,* **64**, pp. 1061-1074

Calm J.M. (2008). The next generation of refrigerants – Historical review, considerations, and outlook. *International Journal of Refrigeration*, **31**, pp. 1123-1133.

Chopey N.P. (2004). *Handbook of Chemical Engineering Calculations*, 3rd Edition, USA, McGraw-Hill.

Chu C., Wu S. (1973). Spectrophotometric determination for trace amount of chloride in uranium. *Journal of Chinese Chemical Society*, **21**, pp. 223-228.

Clarke F.E. (1950). Determination of chloride in water: Improved colorimetric and titrimetric methods. *Analytical Chemistry*, **22**, 553-555.

Couper J.R., Penney W.R., Fair J.R., Walas S.M. (2005). *Chemical Process Equipment: Selection and Design*, 2nd Edition, Amsterdam, Elsevier.

Cussler E.L. (1997). *Diffusion: Mass transfer in fluid systems*, 2nd Edition, Cambridge, Cambridge University Press.

Fahey J.J. (1939). Colorimetric Determination of Fluorine with Ferron. *Industrial and Engineering Chemistry, Analytical Edition*, pp. 362-363.

Falabella J.B., Kizzie A.C., Teja A.S. (2006). Henry's constants of gases and volatile organic compounds in aqueous solutions. *Fluid Phase Equilibria*, **241**, pp. 96-102.

Fritz J.S., Schenk G.H. (1987). *Quantitative analytical chemistry*, 5th Edition, Englewood Cliffs, Prentice Hall.

Gauthier L., Thibault J., LeDuy A. (1991). Measuring k_La with Randomly Pulsed Dynamic Method. *Biotechnology and Bioengineering*, **37**, pp. 889-893.

Garcia-Ochoa F., Gomez E. (2004). Theoretical prediction of gas-liquid mass transfer coefficient, specific area and hold-up in sparged stirred tanks. *Chemical Engineering Science*, **59**, pp. 2489-2501.

Halimic E., Ross D., Agnew B., Anderson A., Potts I. (2003). A comparison of the operating performance of alternative refrigerants. *Applied Thermal Engineering*, **23**, pp. 1441-1451.

Hine J., Porter J.J. (1957). Methylene derivatives as intermediates in polar reactions. VIII. Difluoromethylene in the reaction of chlorodifluoromethane with sodium methoxide. *Journal of the American Chemical Society,* **79**, pp. 5493-5496.

Incropera F.P., DeWitt D.P. (2001). *Introduction to heat transfer*, 4th Edition, New York, John Wiley and Sons.

Iwakura C., Hayashi T., Kikkawa S., Tamura H. (1972). Electrolytic behavior of non-aqueous systems in methanol. *Electrochimica Acta*, **17**, pp.1085-1093.

Jervis R.E., Muir D.R., Butler J.P., Gordon A.R. (1953). The conductance at 25 °C of Lithium Chloride, Sodium and Potassium Bromides and Potassium Iodide in Methanol, and of Lithium Chloride, Sodium Bromide and Potassium Iodide in Water, *Conductances of Alkaline Halides in Methanol and in Water*, **75**, pp. 2855-2858

Kato R., Nishiumi H. (2003). Stationary State Model in Reforming HCFC22 ($CHClF_2$) to Difluoromethyl ether (CH_3OCHF_2). *The Canadian Journal of Chemical Engineering*, **81**, pp. 1-6.

Kirsch P. (2004). *Modern Fluoroorganic Chemistry: Synthesis, Reactivity, Applications*, Weinheim, WILEY-VCH.

Kroschwitz J.I. (2007). *Kirk-Othmer Encyclopedia of Chemical Technology*, 5th Edition, New Jersey, John Wiley and Sons.

Lee H., Kim H.S., Lee S.D., Lee W.K., Kim H. (2001). Selective production of difluoromethyl methyl ether from chlorodifluoromethane using alkali metal carbonates. *Journal of Fluorine Chemistry*, **107**, pp.133-136.

Lemmon E.W., McLinden M.O., Friend D.G. (2003). *Thermophysical Properties of Fluid Systems* in **NIST Chemistry WebBook, NIST Standard Reference Database Number 69,** Eds. Linstrom P.J. and Mallard W.G., National Institute of Standards and Technology, Gaithersburg MD, 20899, http://webbook.nist.gov, accessed 19 November 2012.

Letzel H.M., Schouten J.C., Krishna R., van den Bleek C.M. (1999). Gas holdup and mass transfer in bubble column reactors operated at elevated pressure. *Chemical Engineering Science*, **54**, pp. 2237-2246.

Li G., Qui H., Zheng Z., Cai Z., Yang S. (1995). Effect of fluid rheological properties on mass transfer in a bioreactor. *Journal of Chemical Technology and Biotechnology*, **62**, pp. 385-391.

Mohanraj M., Jayaraj S., Muraleedharan C. (2009). Environment friendly alternatives to halogenated refrigerants – A review. *International Journal of Greenhouse Gas Control*, **3**, pp. 108-119.

Murthy C.P., Ali S.F.M., Ashok D. (1995). *University Chemistry*, New Delhi, New Age International (P) Ltd.

Nauman E.B. (1987). *Chemical reactor design*, New York, John Wiley and Sons Inc.

Nichols M.L., Olsen J.S. (1943). Determination of fluorine in organic compounds with cerous nitrate. *Industrial and Engineering Chemistry*, **15**, pp. 342-346.

Nishiumi H., Ogasawara H., Ago K. (2010). Effect of NaOH on the solubility of fluorocarbon in alcohol-NaOH systems. *Fluid Phase Equilibria*, **291**, pp. 159-165.

Nishiumi H., Kato R. (2003). Effect of NaCl precipitation on vapour-liquid dechlorination of $CHClF_2$. *Journal of Chemical Technology and Biotechnology*, **78**, pp. 298-302.

Omega. (1993). “ISE-8760 and ISE-8770 Chloride ion selective electrode operators manual”, Stamford, Omega Engineering Inc.

Omega. (1993). “ISE-8790 and ISE-8795 Fluoride ion selective electrodes operators manual”, Stamford, Omega Engineering Inc.

Parker L., Morrissey W.A. (2003). *Stratospheric ozone depletion*, New York, Nova Science Publishers.

PASCO Scientific, “Chloride ion selective electrode”, 2006-2012, California, USA, http://www.pasco.com/prodCatalog/CI/CI-6732_chloride-ion-selective-electrode/index.cfm#specificationsTab, accessed 16 November 2012.

PASCO Scientific. (1997). “Instruction manual and experiment guide for the PASCO Scientific model Cl-6728-Fluoride ion selective electrode”, California, USA, PASCO Scientific.

Perry R.H., Green D.W. (1999). *Perry’s Chemical Engineers’ Handbook*, New York, McGraw-Hill.

Radojević M., Bashkin V.N. (2006). *Practical environmental analysis*, 2nd Edition, Cambridge, RSC Publishing.

Rigopoulos S., Jones A.G. (2001). Dynamic modeling of a bubble column for particle formation via a gas-liquid reaction. *Chemical Engineering Science*, **56**, pp. 6177-6184.

Sapali S.N. (2009). *Refrigeration and air-conditioning.* New Delhi, PHI Learning Private Limited.

Satoh K., Nishiumi H., Kasatani T. (1998). Vapour pressure of CH_3OCHF_2 synthesized from HCFC22. *Fluid Phase Equilibria*, **144**, pp. 211-216.

Schumpe A. (1993). The estimation of gas solubilities in salt solutions. *Chemical Engineering Science*, **48**, pp. 153-158.

Seader J.D., Henley E.J. (2006). *Separation process principles*, 2nd Edition, NJ, John Wiley and Sons.

Sekiya A., Misaki S. (2000). The potential of hydrofluoroethers to replace CFCs, HCFCs and PFCs. *Journal of Fluorine Chemistry*, **101**, pp. 215-221.

Shu-Chuan L., Ch'eng-Yü C. (1956). On the colorimetric determination of fluoride. *Scientia Sinica*, **6**, pp. 259-263.

Smith O.M., Dutcher H.A. (1934). Colorimetric Determination of Fluorine. *Industrial and Engineering Chemistry, Analytical Edition*, **6**, pp.61-62.

Stenger V.A. (1996). Solubilities of Various Alkali Metal and Alkaline Earth Metal Compounds in Methanol. *Journal of Chemical Engineering Data*, **41**, pp.1111-1113.

Takenouchi M., Kato R., Nishiumi H. (2001). Henry's law constant measurements of CCl_2F_2, $CHClF_2$, CH_2F_2, C_2ClF_5, CH_2FCF_3, and CH_3CHF_2 in methanol, ethanol, and 2-propanol. *Journal of Chemical Engineering Data*, **46**, pp. 746-749.

Teledyne Analytical Instruments. (2006). *Teledyne LXT 220-Fluoride ion electrode operators manual*, California, USA, Teledyne Analytical Instruments.

Thermo Scientific. (2008). *Orion CIE operators manual*, Waltham, Massachusetts, USA, Thermo Fisher Scientific Inc.

Tiepel E.W., Gubbins K.E. (1973). Thermodynamic properties of gases dissolved in electrolyte solutions. *Industrial Engineering Chemical Fundamentals*, **12**, pp. 18-25.

Tiwary A., Colls J. (2010). *Air Pollution: Measurement, modelling and mitigation*, 3rd Edition, Oxon, Routledge.

Tsai W. (2005). Environmental risk assessment of hydrofluoroethers (HFEs). *Journal of Hazardous Materials*, **A119**, pp.69-78.

van Swaaij W.P.M., Versteeg G.F. (1992). Mass transfer accompanied with complex reversible chemical reactions in gas-liquid systems: An overview. *Chemcial Engineering Science*, **47**, pp. 3181-3195

Venkatesan P., Subrahmanyam P.V.R.S., Raghu Pratap D. (2010). Spectrophotometric determination of pure amitriptyline hydrochloride through ligand exchange on mercuric ion. *International Journal of ChemTech Research*, **2**, pp. 54-56.

Vining G., Kowalski S.M. (2011). *Statistical methods for engineers*, United States, Brookes/Cole.

Whitman W.C., Johnson W.M., Tomczyk J.A. (2005). *Refrigeration and Air Conditioning Technology*, New York, Thomson Delmark Learning.

Willard H.H., Winter O.B. (1933). Volumetric method for determination of fluorine. *Industrial and Engineering Chemistry, Analytical Edition*, **5**, pp. 7-10.

Wojciechowski B.W., Rice N.M. (2003). *Experimental methods in kinetic studies,* Amsterdam, Elsevier.

Yoe J.H., Hall R.T. (1937). A study of 7-Iodo-8-hydroxyquinoline-5-sulfonic acid as a reagent for the colorimetric determination of ferric iron. *Journal of American Chemical Society*, **54**, pp.872-879.

Zall D.M., Fisher D., Garner M.Q. (1956). Photometric determination of chlorides in water. *Analytical Chemistry*, **28**, pp. 1665-1668.

Zhu C., Chen J., Zheng H., Wu Y., Xu J. (2005). A colorimetric method for fluoride determination in aqueous samples based on the hydroxyl deprotection reaction of a cyanine dye. *Analytica Chimica Acta*, **539**, pp.311-316.

APPENDIX A

The determination of the necessary minimum heat transfer area of the reactor coil

The purpose of the heat transfer calculation undertaken during the reactor design was to determine the coil area required to provide adequate cooling for the exothermic reactions in the reactor, as well as to estimate the external convective heat transfer coefficient. The heat of reaction is generally defined as the sum of the heat of formation of product less the sum of the heat of formation of reactants (Chopey, 2004).

$$\Delta H_r^0 = \Delta H_{f,products}^0 - \Delta H_{f,reactants}^0 \qquad \text{(A-1)}$$

However, in the case of aqueous solutions, this definition is not applicable. The enthalpy of solution of the dissolved reactant/product must be accounted for. ΔH_s^0 represents the standard integral heat of solution at infinite dilution (Chopey, 2004).

$$\Delta H_r^0 = \Delta H_{f,products}^0 + \Delta H_{s,dissolved\ products}^0 - \Delta H_{f,reactants}^0 - \Delta H_{s,dissolved\ reactants}^0 \qquad \text{(A-2)}$$

Using Equation A-2 the heats of reactions for reaction 1 and reaction 2 (presented in Table 3-1) were calculated to be -119.58 kJ·mol^{-1} and -1183.64 kJ·mol^{-1} respectively. Kinetic data is only available in literature for reaction 1. Therefore, for reaction 2, the reaction rate was assumed to be 10% of the first reaction. The rate was a maximum when the greatest concentration of reactant was present. The 'maximum rate' was calculated using the upper limit of conditions so as to present the worst case scenario. Nishiumi and Kato (2003) reported a reaction rate constant of 1.10 MPa^{-1}·min^{-1}. A maximum R-22 partial pressure of 25 kPa was used together with a maximum methoxide concentration of 2.5 mol·dm^{-3}. Defining the rates of reaction as:

$$r_{\max}^{I} = k_1 P_{R-22} C_{CH_3ONa} \qquad \text{(A-3)}$$

$$r_{\max}^{II} = 0.1 r_{\max}^{I} \qquad \text{(A-4)}$$

The heat released from the reaction, denoted as Q in kJ·min^{-1}, was determined by the summation of the product of the reaction rate with the heat of reaction for each reaction respectively.

$$Q = V\sum_i r_i \Delta H_{ri} \tag{A-5}$$

The heat transfer coefficient was calculated using an appropriate correlation from Incropera and DeWitt (2001). d_{imp} and n_{imp} are the diameter and speed of the impeller blade respectively. The speed range for the impeller blade was 0-1700 rpm. The maximum speed was used in the calculation.

.

$$\frac{h_i d_t}{k_l} = 0.36\left(\frac{d_{imp}^2 n_{imp}\rho_L}{\mu_L}\right)^{0.67}\left(\frac{C_{p,L}\mu_L}{k_l}\right)^{1/3} \tag{A-6}$$

The area of the coil can be calculated using the following form of Newton's law of cooling (Incropera and De Witt, 2001).

$$Q = UA_c\Delta T_{LM} \tag{A-7}$$

A_c represents the coil area and ΔT_{LM} is the logarithmic mean temperature difference.

$$\Delta T_{LM} = \frac{\left(T_{coil,in} - T_L\right) - \left(T_{coil,out} - T_L\right)}{\ln\left[\dfrac{T_{coil,in} - T_L}{T_{coil,out} - T_L}\right]} \tag{A-8}$$

The logarithmic mean temperature difference provides a more accurate determination of the driving force as opposed to using the temperature difference between the fluid and surface (Incropera and DeWitt, 2001). The length of the coil was calculated from the area by fixing the diameter of the coil tube to 8mm and using the equation for the surface area of a coil.

$$A_c = \pi d_c L \tag{A-9}$$

Using an overall energy balance, the mass flow rate of coolant can be calculated from:

$$Q = \dot{m} C_p \Delta T_{coil} \tag{A-10}$$

The volumetric flow rate is then calculated from the mass flow rate using the density of the coolant.

The calculation procedure described above yielded the following results:

$Q = -545 \ \mathrm{J \cdot s^{-1}}$

$U = 370 \ \mathrm{W \cdot m^{-2} \cdot K^{-1}}$

$A_c = 0.028 \ \mathrm{m^2}$

$\dot{V} = 1.87 \ \mathrm{dm^3 \cdot min^{-1}}$

APPENDIX B

Converting between the different forms of the Henry's law constant for the R-22/methanol system

Henry's law states that the solubility of a gas in a liquid is directly proportional to the partial pressure of the gas in equilibrium with that liquid. Various mathematical representations of Henry's law exist, incorporating different units of measure. For example, one form of Henry's law is given by:

$$H^{pc} = \frac{P_a}{C_{i,L}} \tag{B-1}$$

where H^{pc} is the Henry's law constant or partition coefficient defined as the partial pressure of solute *i* in the gas phase (P_a) divided by the concentration of the solute in the liquid phase ($C_{i,L}$). The mass transfer term in the reactor model presented in section 3.3.3 required that the Henry's law constant be defined as:

$$H^{cc} = \frac{C_{i,G}}{C_{i,L}} \tag{B-2}$$

where H^{cc} is the concentration-based Henry's law constant, $C_{i,G}$ is the concentration of the solute in the gas phase and $C_{i,L}$ is the concentration of the solute in the liquid phase. In this appendix, a method of extracting the appropriate form of the Henry's law constant for the R22/methanol system from available solubility data is presented.

Experimental vapour-liquid equilibrium data at infinite dilution for R22 in methanol were reported by Takenouchi et al (2001) and were used to obtain Henry's law constants for this system. The measured data are given in Table B-1, where x_a and x_b are defined as the solute (R-22) and solvent (methanol) mole fractions in the liquid phase respectively and y_a is the mole fraction of the solute in the vapour in equilibrium with the liquid.

Table B-1. Experimental vapour-liquid equilibrium data for R-22 (a) and methanol (b) (Takenouchi et al., 2001)

Temperature / K	x_a	y_a
283.15	0.0856	0.9326
293.15	0.0609	0.8757
303.15	0.0401	0.7792

Assuming that $V^E = 0$, the molar volume of the mixture is given by:

$$V^m = \sum_i x_i V_i \tag{B-2}$$

$$= x_a V_a + x_b V_b \tag{B-3}$$

$$= x_a \frac{M_a}{\rho_a} + x_b \frac{M_b}{\rho_b} \tag{B-4}$$

Physical properties for this system are listed in Table B-2.

Table B-2. Physical properties of liquid methanol and R-22 gas

Property		Methanol	R-22	Reference
Density / kg·m^{-3}	ρ	781.69	1171	Lemmon et al. (2003)
Molecular weight / g·mol^{-1}	M	32.04	86.48	-

For a basis of 1 mole of mixture, the total volume is given by:

$$V^T = nV^m \tag{B-5}$$

The concentration of component *i* in the liquid is defined as:

$$C_{i,L} = \frac{n_a}{V^T} \tag{B-6}$$

The partial pressure of component *i* is given by:

$$P_i = y_i P \tag{B-7}$$

where P is the total system pressure. Once $C_{i,L}$ and P_i are known, the Henry's law constant can be calculated according to Equation B-1. The concentration-based Henry's law constants are given by:

$$H^{cc} = \frac{H^{pc}}{RT} \tag{B-8}$$

Two forms of the Henry's law constant for the R-22/methanol system at each of the three temperatures considered in this study are given in Table B-3.

Table B-3. Two forms of the Henry's law constant for the R-22/methanol system at the temperatures of interest

	Temperature / K		
	283.15	**293.15**	**303.15**
H^{pc} /kPa·dm^3·mol^{-1}	48.18	62.33	82.92
H^{cc}	0.020	0.026	0.033

APPENDIX C

Calculations for preliminary experiments

The results for experiments conducted in both the stainless steel reactor and the single-jacketed glass reactor during the initial investigations of the project were analyzed in an identical manner. The calculation procedure for a single experiment in the stainless steel reactor is described in explicit detail. The calculation procedure was followed identically for the single jacketed glass reactor. For the case of the single jacketed glass reactor, the calculation method involving the cold traps do not apply and must therefore be omitted.

The calculation procedure is detailed for the following set of conditions:

Reaction temperature / K	276.94
NaOH concentration / mol·dm^{-3}	2
Volumetric flow rate / dm^3·min^{-1}	0.65
Feed temperature / K	296.12
Set 1 Δt / min	10

C.1. Reactor feed

$$\dot{n}_{R-22,tot} = \frac{PV_G}{RT}$$

$$= \frac{101325 \bullet 0.65}{1000000 \bullet 8.314 \bullet 296.12}$$

$$= 2.69 \times 10^{-02}\ \text{mol} \cdot \text{min}^{-1}$$

$$n_{R-22} = \frac{\dot{n}_{R-22}}{t}$$

$$= \frac{2.69 \times 10^{-02}}{44.8}$$

$$= 1.21\ \text{mols}$$

C.2. Reactor effluent

- ***Residual gas***

The volumetric flow rate and molar flow rate of the residual gas is:

$$\dot{V}_{res} = \frac{V}{t}$$
$$= \frac{100 \text{ ml}}{7.215 \text{ min}}$$
$$= 13.86 \text{ ml} \cdot \text{min}^{-1}$$

$$\dot{n}_{res} = \frac{P\dot{V}_{res}}{RT}$$
$$= \frac{101325 \text{ Pa} \bullet 13.86 \times 10^{-06} \text{ m}^3 \cdot \text{min}^{-1}}{8.314 \text{ J} \cdot \text{mol}^{-1} \cdot \text{K}^{-1} \bullet 294.05 \text{ K}}$$
$$= 5.74 \times 10^{-04} \text{ mol} \cdot \text{min}^{-1}$$

The moles of each component were calculated using the GC peak areas in Table C-1.

Table C-1. Peak areas obtained from gas chromatograms for the residual gas

Component	Peak area
R-22	42730470.5
Difluorodimethyl Ether	1679208.3
Trimethyl orthoformate	52790254.8
Total	**97199933.6**

$$x_{R-22} = \frac{\text{peak area for R-22}}{\text{Total peak area}} = \frac{42730470.5}{97199933.6} = 0.44$$

$$x_{DFDME} = \frac{\text{peak area for difluorodimethyl ether}}{\text{Total peak area}} = \frac{1679208.3}{97199933.6} = 0.02$$

$$\dot{n}_{R-22} = x_{R-22} \bullet \dot{n}_{res} = 0.44 \bullet 5.74 \times 10^{-04} \text{ mol} \cdot \text{min}^{-1} = 2.53 \times 10^{-04} \text{ mol} \cdot \text{min}^{-1}$$

$$\dot{n}_{DFDME} = x_{DFDME} \bullet \dot{n}_{res} = 0.02 \bullet 5.74 \times 10^{-04} \text{ mol} \cdot \text{min}^{-1} = 9.92 \times 10^{-06} \text{ mol} \cdot \text{min}^{-1}$$

The above procedure was repeated for the remainder of the data sets obtained under this condition. Once the molar flow rates of R-22 and difluorodimethyl ether were calculated for each data set, the total accumulative moles of each of the two components was evaluated.

The accumulative moles of R-22 was obtained by the summation of the product of R-22 molar flow rate and Δt (time elapsed) for each set of data points measured.

$$\text{Total accumulative R-22}_{residualgas} = \sum_i \left(\dot{n}_{R-22} \bullet \Delta t\right)_i$$
$$= \left(\dot{n}_{R-22} \bullet \Delta t\right)_{set1} + \left(\dot{n}_{R-22} \bullet \Delta t\right)_{set2} + \left(\dot{n}_{R-22} \bullet \Delta t\right)_{set3} + \left(\dot{n}_{R-22} \bullet \Delta t\right)_{set4}$$
$$= \left(2.53 \times 10^{-04}\ \text{mol} \cdot \text{min}^{-1} \times 10\ \text{min}\right) + \left(8.89 \times 10^{-04}\ \text{mol} \cdot \text{min}^{-1} \times 10\ \text{min}\right)$$
$$+ \left(1.79 \times 10^{-03}\ \text{mol} \cdot \text{min}^{-1} \times 10\ \text{min}\right) + \left(2.60 \times 10^{-03}\ \text{mol} \cdot \text{min}^{-1} \times 10\ \text{min}\right)$$
$$= 5.50 \times 10^{-02}\ \text{mol}$$

The accumulative moles of difluorodimethyl ether was obtained by the summation of the product of difluorodimethyl ether molar flow rate and Δt (time elapsed) for each set of data points measured.

$$\text{Total accumulative DFDME}_{residualgas} = \sum_i \left(\dot{n}_{DFDME} \bullet \Delta t\right)_i$$
$$= \left(\dot{n}_{DFDME} \bullet \Delta t\right)_{set1} + \left(\dot{n}_{DFDME} \bullet \Delta t\right)_{set2} + \left(\dot{n}_{DFDME} \bullet \Delta t\right)_{set3} + \left(\dot{n}_{DFDME} \bullet \Delta t\right)_{set4}$$
$$= \left(9.92 \times 10^{-06}\ \text{mol} \cdot \text{min}^{-1} \times 10\ \text{min}\right) + \left(5.83 \times 10^{-06}\ \text{mol} \cdot \text{min}^{-1} \times 10\ \text{min}\right)$$
$$+ \left(2.87 \times 10^{-05}\ \text{mol} \cdot \text{min}^{-1} \times 10\ \text{min}\right) + \left(5.39 \times 10^{-05}\ \text{mol} \cdot \text{min}^{-1} \times 10\ \text{min}\right)$$
$$= 9.84 \times 10^{-04}\ \text{mol}$$

- ***Cold trap gas***

Two identical samples were analyzed from the cold trap. The average values of the two samples were used for improved accuracy.

Mass of gas collected in cold trap = 25.3 g

The peak areas of each component in both the samples are given in Table C-2.

Table C-2. Peak areas obtained from the gas chromatograph for the cold trap gas

Component	Peak area: sample 1	Peak area: sample 2
R-22	1597085128	1908166678
Difluorodimethyl Ether	66657590.1	87071801.5
Trimethyl orthoformate	6221032.5	8175346.3
Ethanol	1275971.2	1996374.4
Total	**1671239722**	**2005410200**

For sample 1, the mole fraction of R-22, difluorodimethyl ether, trimethyl orthoformate and ethanol is:

$$x_{R-22,1} = \frac{\text{peak area for R-22}}{\text{Total peak area}} = \frac{1597085128}{1671239722} = 0.956$$

$$x_{DFDME,1} = \frac{\text{peak area for difluorodimethyl ether}}{\text{Total peak area}} = \frac{66657590.1}{1671239722} = 0.040$$

$$x_{TMOF,1} = \frac{\text{peak area for trimethyl orthoformate}}{\text{Total peak area}} = \frac{6221032.5}{1671239722} = 0.0037$$

$$x_{ETHANOL,1} = \frac{\text{peak area for ethanol}}{\text{Total peak area}} = \frac{1275971.2}{1671239722} = 0.00076$$

Repeating the calculation for sample 2 we obtain:

$$x_{R-22,2} = 0.952, x_{DFDME,2} = 0.043, x_{TMOF,2} = 0.0041 \text{ and } x_{ETHANOL,2} = 0.001$$

Taking the average mole fraction of sample 1 and 2 for each component we get:

$$x_{R-22,av} = 0.954, x_{DFDME,2} = 0.042, x_{TMOF,2} = 0.0039 \text{ and } x_{ETHANOL,2} = 0.00088$$

Using these average mole fractions, the average molar mass of the gas collected was calculated as:

$$\begin{aligned} MM_{av} &= \sum_i x_{i,av} MM_i \\ &= x_{R-22,av} \bullet MM_{R-22,av} + x_{DFDME,av} \bullet MM_{DFDME,av} + x_{TMOF,av} \bullet MM_{TMOF,av} + x_{ETHANOL,av} \bullet MM_{ETHANOL,av} \\ &= 0.954 \bullet 86.45 + 0.042 \bullet 82 + 0.0039 \bullet 106 + 0.00088 \bullet 46 \\ &= 86.31 \text{ g} \cdot \text{mol}^{-1} \end{aligned}$$

The moles of gas collected are calculated by:

$$n_{G,c} = \frac{m_{G,c}}{MM_{av}} = \frac{25.3}{86.31} = 0.293 \text{mols}$$

$$n_{R-22,}^{tot,acc}(coldtrap) = x_{R-22,av} \bullet n_{G,c} = 0.954 \bullet 0.293 \text{mols} = 0.280 \text{ mols}$$

$$n_{DFDME}^{tot,acc}(coldtrap) = x_{DFDME,av} \bullet n_{G,c} = 0.042 \bullet 0.293 \text{mols} = 0.012 \text{ mols}$$

C.3. Total outlet stream

Now combining the total accumulative moles of R-22 from the residual gas with the total accumulative moles of R-22 from the gas collected in the cold trap gives the moles of each component in the total outlet stream.

$$n_{R-22}^{out} = n_{R-22,}^{tot,acc}(res.gas) + n_{R-22,}^{tot,acc}(coldtrap) = 0.055 + 0.280 = 0.335 \text{ mols}$$

$$n_{DFDME}^{out} = n_{DFDME}^{tot,acc}(res.gas) + n_{DFDME}^{tot,acc}(coldtrap) = 9.84 \times 10^{-4} + 0.012 = 0.013 \text{ mols}$$

C.4. Performance calculations

$$X = 100 \frac{(moles\ R-22\ in) - (moles\ R-22\ out)}{moles\ R-22\ in} = 100 \bullet \frac{1.206 - 0.335}{1.206} = 72.23\%$$

$$S = 100 \frac{moles\ fluoroether\ produced}{(moles\ R-22\ in) - (moles\ R-22\ out)} = 100 \bullet \frac{0.013}{1.206 - 0.013} = 1.515\%$$

$$Y = \frac{XS}{100} = 100 \frac{moles\ fluoroether\ produced}{moles\ R-22\ in} = 100 \bullet \frac{0.013}{1.206} = 1.094\%$$

APPENDIX D

Calculations: Volumetric mass transfer coefficient,

Interfacial area and Hatta number

D.1. Volumetric mass transfer coefficient (k_La) for oxygen and R-22

Using the Wilke-Chang correlation to determine the diffusivity of oxygen in methanol at, for example, 283.15 K:

$$D_A = 1.1728\times10^{-16}\frac{T\left(\chi_{CH_3ONa}M_{CH_3OH}\right)^{1/2}}{\mu_{CH_3OH}\hat{V}_{O_2}^{0.6}}$$

$$= 1.1728\times10^{-16}\frac{283.15\bullet1.9\bullet32.04^{1/2}}{0.000701\bullet0.135^{0.6}} = 1.23\times10^{-09}\ \mathrm{m^2\cdot s^{-1}}$$

Using the Wilke-Chang correlation to determine the diffusivity of R-22 in methanol at, for example, 283.15 K:

$$D_A = 1.1728\times10^{-16}\frac{T\left(\chi_{CH_3ONa}M_{CH_3OH}\right)^{1/2}}{\mu_{CH_3OH}\hat{V}_{R-22}^{0.6}}$$

$$= 1.1728\times10^{-16}\frac{283.15\bullet1.9\bullet32.04^{1/2}}{0.000701\bullet0.0524^{0.6}} = 2.17\times10^{-09}\ \mathrm{m^2\cdot s^{-1}}$$

Now, using Equation 3-50 with a measured $(\mathbf{k_La})_{\mathbf{oxygen}}$ of 0.445 $\mathrm{min^{-1}}$, we get:

$$\left(k_La\right)_{R-22} = \frac{D_{R-22}}{D_{oxygen}}\left(k_La\right)_{oxygen} = \frac{2.17\times10^{-09}}{1.23\times10^{-09}}\bullet0.445 = 0.786\ \mathrm{min^{-1}}$$

D.2. Interfacial area

Table D-1 lists the properties of methanol and impeller dimensions. The properties were obtained from Lemmon et al. (2003). Table D-2 lists the dimensions of the reactor vessel.

Table D-1. Properties of methanol and dimensions of impeller

Impeller diameter / m	d_{imp}	0.06
Impeller speed / rps	N	17
Gravitational constant / m·s^{-2}	g	9.81
Surface tension / N·m^{-1}	σ	0.0218
Liquid density / kg·m^{-3}	ρ_L	781.69
Vapour density / kg·m^{-3}	ρ_G	0.31
Liquid viscosity / Pa·s	μ_L	0.000521
Vapour viscosity / Pa·s	μ_G	0.0000098

Table D-2. Reactor vessel dimensions

Volume / cm^3	1000
Diameter / cm	8
Height / cm	19.89

The gas hold-up was estimated using Equation 3-61 as:

$$\frac{\Phi}{1-\Phi} = \frac{0.819 V_s^{2/3} N^{2/5} d_{imp}^{4/15}}{g^{1/3}} \left(\frac{\rho_L}{\sigma}\right)^{1/15} \left(\frac{\rho_L}{\rho_L - \rho_G}\right) \left(\frac{\rho_L}{\rho_G}\right)^{-1/15} = 0.0957$$

$$\Rightarrow \quad \Phi = 0.0874$$

Using Equation 3-63 to calculate the Reynolds number:

$$\mathrm{Re} = \frac{N d_{imp}^2 \rho_L}{\mu_L} = 91822.32$$

Reading off the power number from Figure 3-2 at a Reynolds number of 91822.32 gives: $Pw = 0.98$. Using Equation 3-64 the power input under gassed conditions was calculated to be 0.298.With a liquid volume of 700 ml, the diameter of the bubble was calculated using Equation 3-62.

$$d_b = \frac{0.7\sigma^{0.6}}{\left(P/V_L\right)^{0.4}\rho_L^{0.2}}\left(\frac{\mu_L}{\mu_G}\right)^{0.1} = 2.46\ \text{mm}$$

The interfacial area is therefore calculated from Equation 3-60 as:

$$a = \frac{6\Phi}{d_b} = \frac{6 \bullet 0.087}{0.00246} = 213.44\ \text{m}^2/\text{m}^3$$

D.3. Hatta-number

Table D-3 lists the general data obtained from Nishiumi et al. (2003).

Table D-3. Data obtained from Nishiumi et al. (2003)

m	1
n	2
$k / (\text{m}^3)^2 \cdot \text{mol}^{-2} \cdot \text{s}^{-1}$	1.372E-09
$C^*_{R-22,L} / \text{mol} \cdot \text{dm}^{-3}$	125
$C_{CH_3OH,L} / \text{mol} \cdot \text{dm}^{-3}$	500
ν_{CH_3OH}	1
$k_L a / \text{min}^{-1}$	0.0911

The diffusivity of R-22 gas in liquid methanol was calculated using Equation 3-56. The diffusivity of sodium methoxide in liquid methanol was calculated using Equation 3-57.

$$D_A = 1.1728\times10^{-16}\frac{T\left(\chi_{CH_3ONa}M_{CH_3OH}\right)^{1/2}}{\mu_{CH_3OH}\hat{V}_{R-22}^{0.6}} = 1.1728\times10^{-16}\frac{303.15\bullet1.9\bullet32.04^{1/2}}{0.000521\bullet0.0524^{0.6}}$$
$$= 3.122\times10^{-09}\ \mathrm{m^2\cdot s^{-1}}$$

Table D-4. Limiting ionic conductance and molar conductance for CH_3ONa in methanol at 298.15 K

Variable		Reference
A_0 at 298.15 K / ohm·cm^2	98.3	Iwakura et al. (1972)
λ_+ at 298.15 K / A·cm^{-2}	45.22	Jervis et al. (1953)
λ_- at 298.15 K / A·cm^{-2}	53.08	-

λ_- in Table was calculated using Kohlrausch's law defined by as $A_0 = \lambda_+ + \lambda_-$. The corrected values of λ_+ and λ_- at 303.15 K are listed in Table C-7. Equation 3-58 was used for the temperature correction.

Table D-5. Limiting ionic conductances at 303.15 K for CH_3ONa in methanol

Variable	Conductance	Equation
λ_+ at 303 K/ A·cm^{-2}	78.74	3-58
λ_- at 303 K/ A·cm^{-2}	92.42	3-58

$$D_B = \frac{RT}{F^2}\frac{\left|\frac{1}{n_+}\right|+\left|\frac{1}{n_-}\right|}{\frac{1}{\lambda_+^0}+\frac{1}{\lambda_-^0}} = \frac{8.314\bullet303.15}{96500^2}\frac{\left|\frac{1}{1}\right|+\left|\frac{1}{17}\right|}{\frac{1}{78.74}+\frac{1}{92.42}} = 1.22\times10^{-09}\ \mathrm{m^2\cdot s^{-1}}$$

The Hatta number was calculated using Equation 3-59.

$$Ha = \frac{\sqrt{\frac{2}{m+1}k_{m,n}C_{R-22,L}^{*m-n}C_{CH_3ONa,L}^{n}D_A}}{k_L} = \frac{\sqrt{\frac{2}{1+1}\bullet1.37\times10^{-09}\bullet125^{1-1}\bullet500^2\bullet3.12\times10^{-09}}}{7.11\times10^{-06}} = 0.145$$

Using the sum of squares error minimization technique to solve for E_A in Equation 3-54 gives an enhancement factor E_A value of 1.007.

APPENDIX E

CHEMICAL DATA

Table E.1. List of chemical data for materials used

Chemical name	CAS Number	Supplier	Purity
Chlorodifluoromethane (R-22)	75-45-6	AFROX	>98%
Ethanol	64-17-5	MERCK	95%
Ethylene glycol	107-21-1	Laboratory Supplies Co.	99%
Ferric chloride hexahydrate	10025-77-1	Laboratory Supplies Co.	60%
Ferron	547-91-1	Laboratory Supplies Co.	98%
Iron (II) perchlorate hydrate	335159-18-7	Laboratory Supplies Co.	98%
Mercury (II) thiocyanate	592-85-8	Laboratory Supplies Co.	98%
Methanol	67-56-1	MERCK	99.5%
Nitrogen	7727-37-9	AFROX	99.9999%
perchloric acid	7601-90-3	Laboratory Supplies Co.	60%
Sodium chloride	7647-14-5	Laboratory Supplies Co.	99%
Sodium fluoride	7681-49-4	Laboratory Supplies Co.	97%
Sodium hydroxide	1310-73-2	MERCK	99%

APPENDIX F

RAW DATA FOR OXYGEN MASS TRANSFER MEASUREMENTS

F.1. Sensor lag measurements

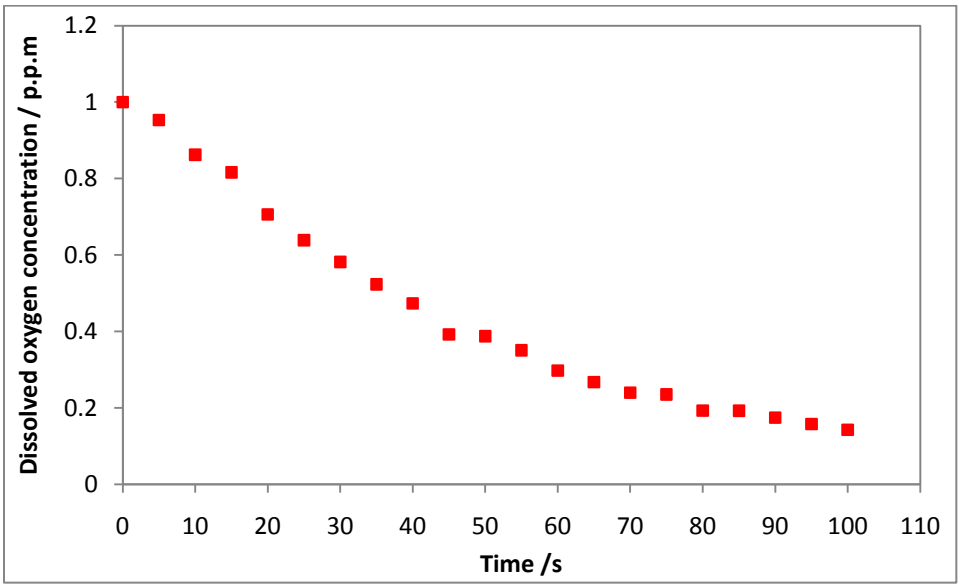

Figure F-1. Sensor lag plot: repeat measurement I

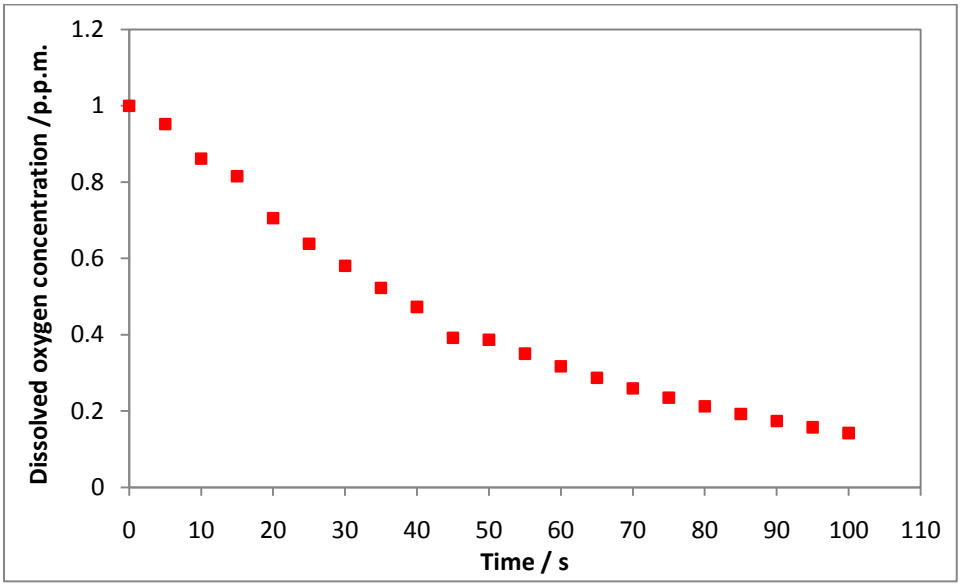

Figure F-2. Sensor lag plot: repeat measurement II

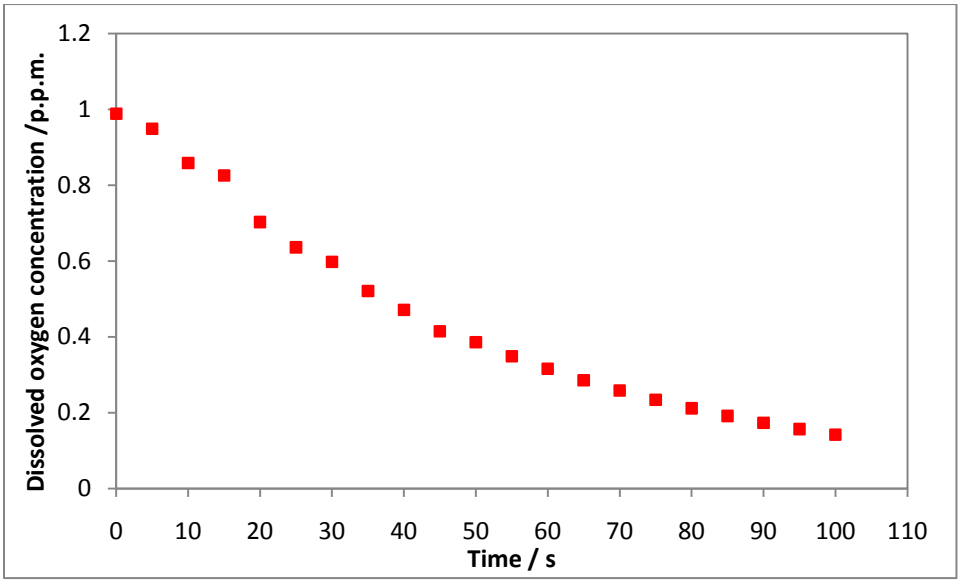

Figure F-3. Sensor lag plot: repeat measurement III

F.2. k_La measurements

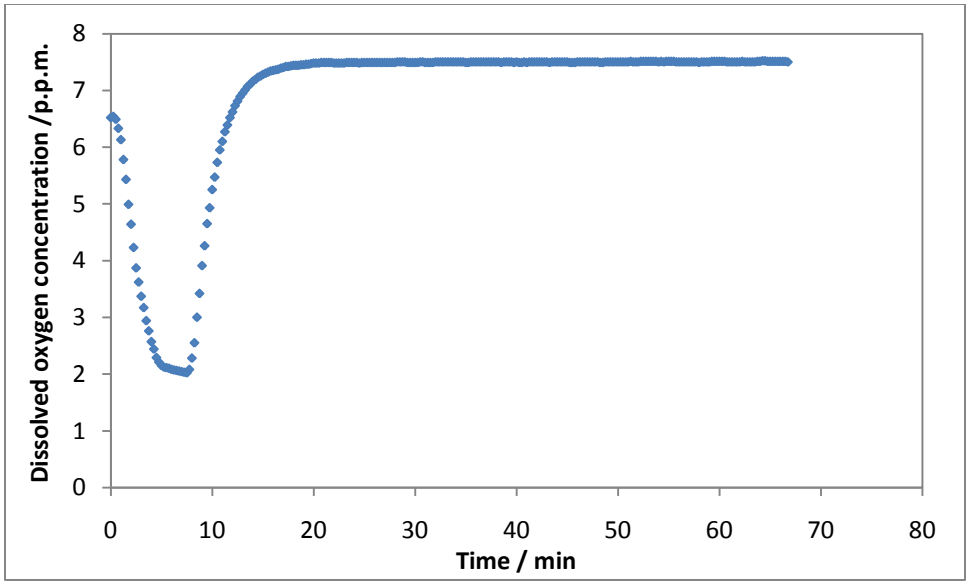

Figure F-4. k_La measurements for oxygen at 283.15 K: measurement I

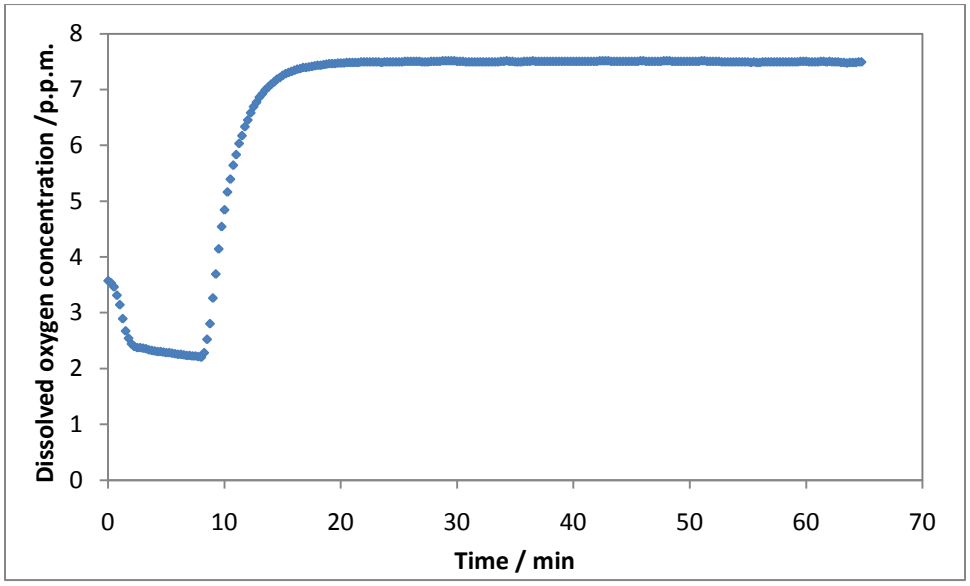

Figure F-5. k_La measurements for oxygen at 283.15 K: measurement II

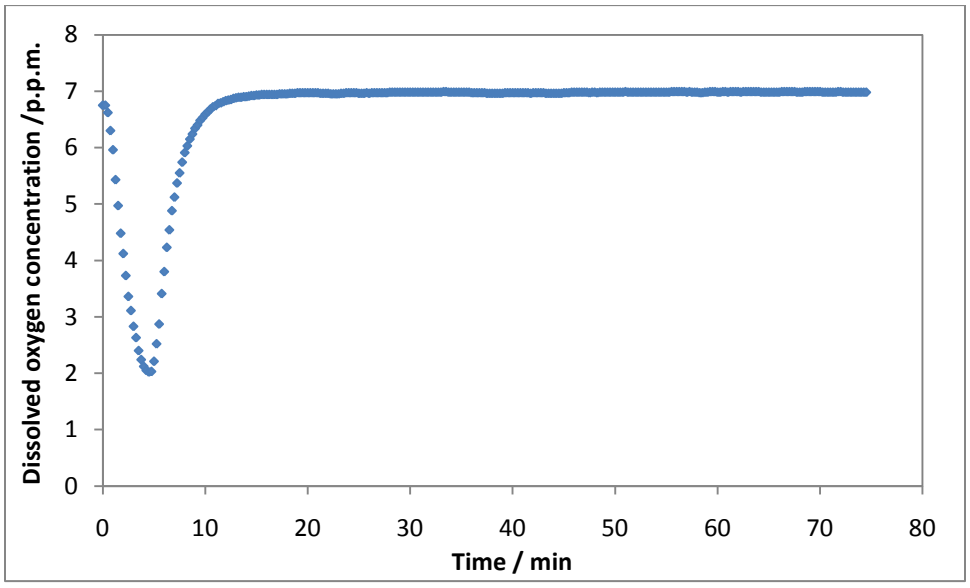

Figure F-6. k_La measurements for oxygen at 293.15 K: measurement I

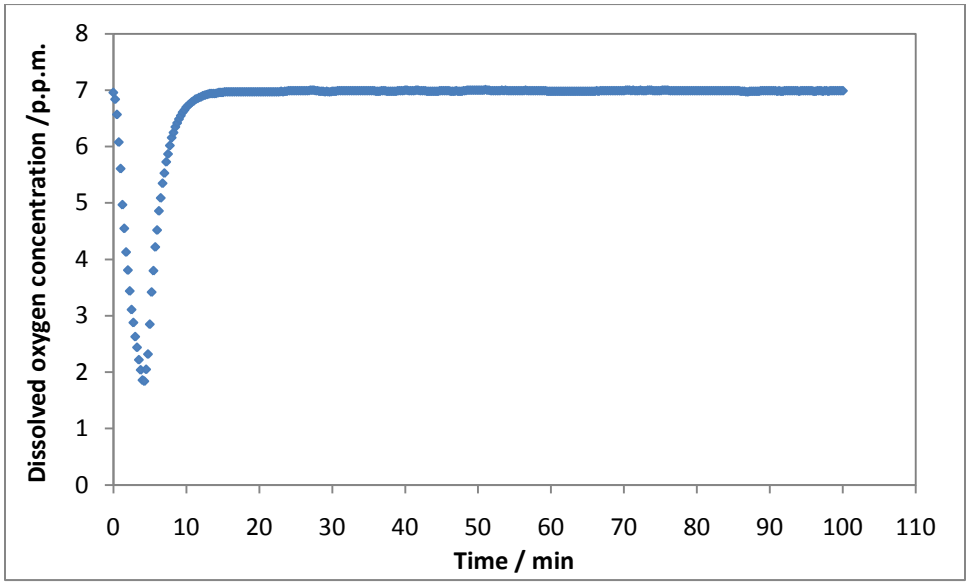

Figure F-7. k_La measurements for oxygen at 293.15 K: measurement II

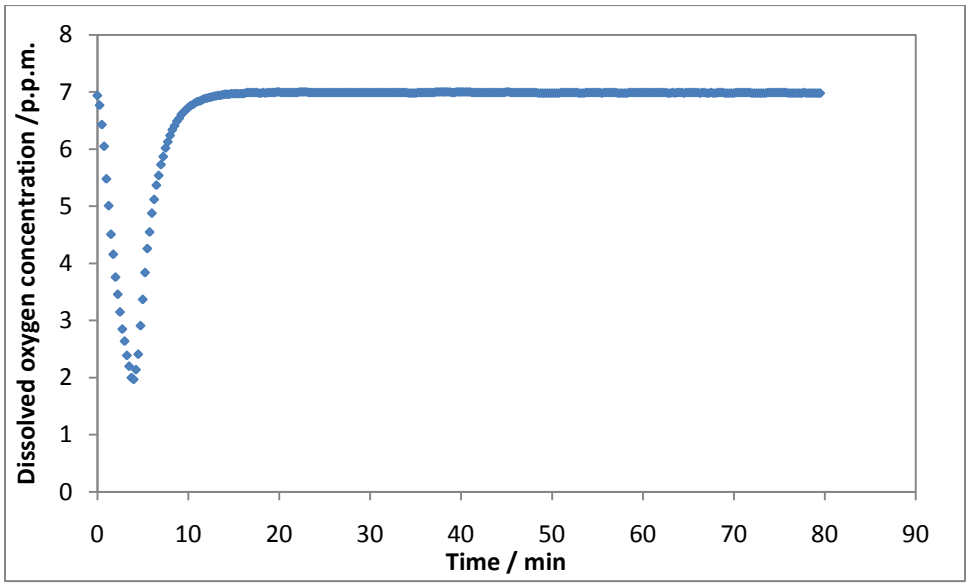

Figure F-8. k_La measurements for oxygen at 293.15 K: measurement III

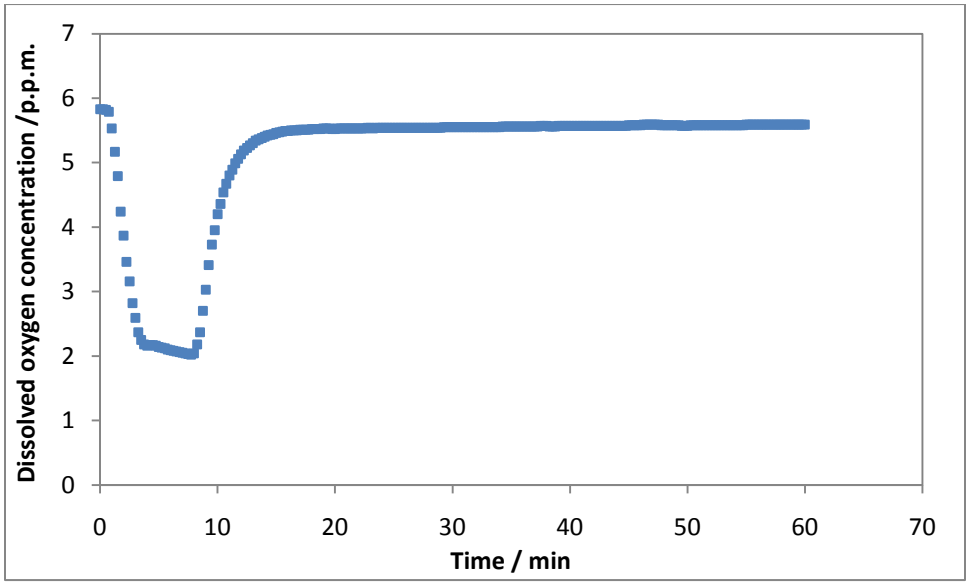

Figure F-9. k_La measurements for oxygen at 303.15 K: measurement I

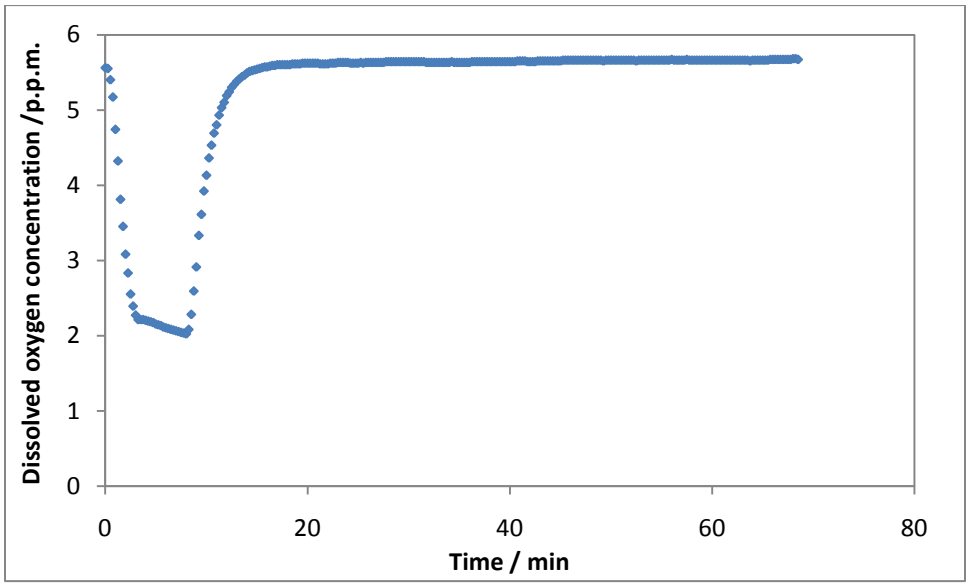

Figure F-10. k_La measurements for oxygen at 303.15 K: measurement II

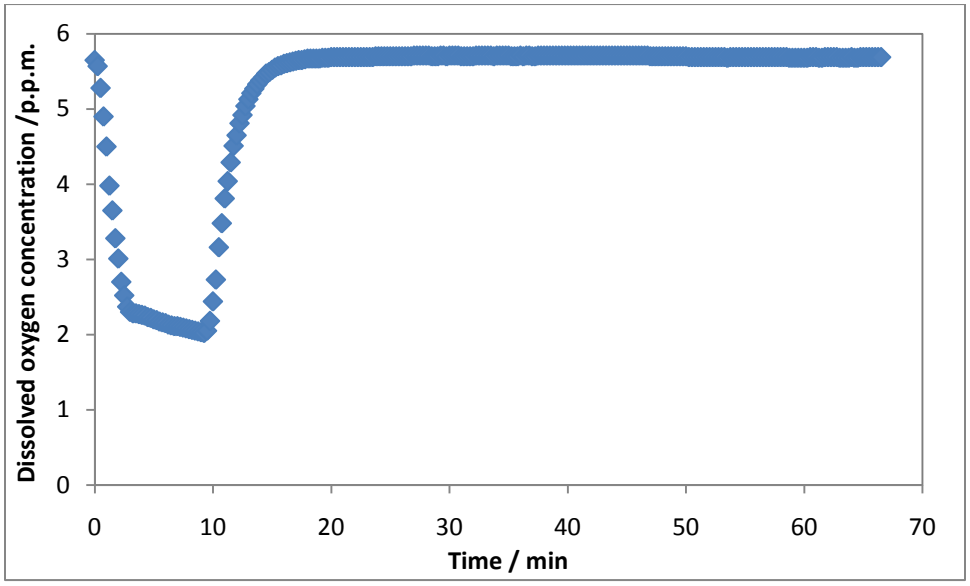

Figure F-11. k_La measurements for oxygen at 303.15 K: measurement III

APPENDIX G

Gas chromatograms

G.1. Experiments conducted at constant temperature

G.1.1. Stainless steel reactor

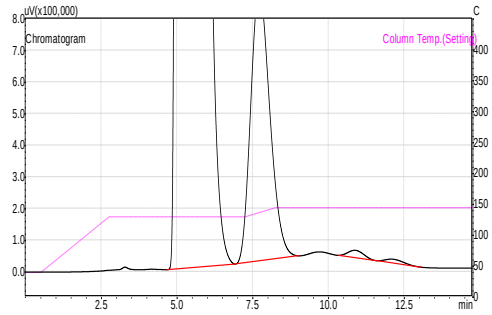

Set			1
Temperature / K			298.15
Concentration / mol·L^{-1}			0.586
Peak No.	**Retention time**	**Area**	**Compound**
1	5.177	1899566819	R-22
2	7.712	37871937.1	CH_3OCHF_2
3	10.865	833058.1	$(CH_3O)_3CH$
4	12.069	486382.6	C_2H_6O

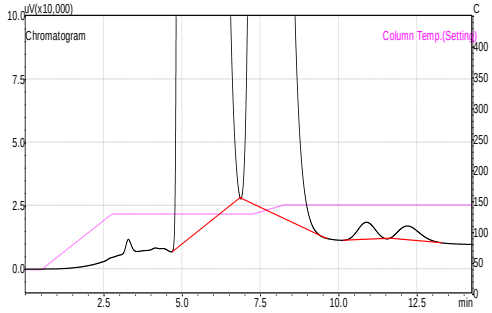

Set			2
Temperature / K			298.15
Concentration / mol·L^{-1}			0.586
Peak No.	**Retention time**	**Area**	**Compound**
1	5.152	2030888552	R-22
2	7.686	74336772.1	CH_3OCHF_2
3	10.883	246719.9	$(CH_3O)_3CH$
4	12.19	249349	C_2H_6O

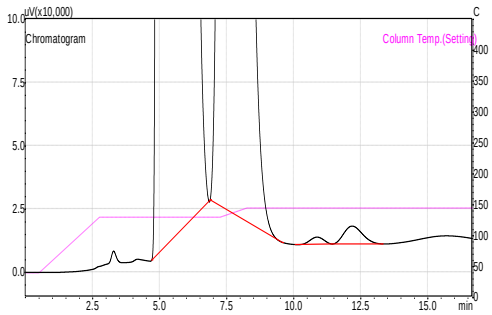

Set			3
Temperature / K			298.15
Concentration / mol·L^{-1}			0.586
Peak No.	**Retention time**	**Area**	**Compound**
1	5.165	1884615178	R-22
2	7.679	72974278.1	CH_3OCHF_2
3	10.867	96569.3	$(CH_3O)_3CH$
4	12.178	339841	C_2H_6O

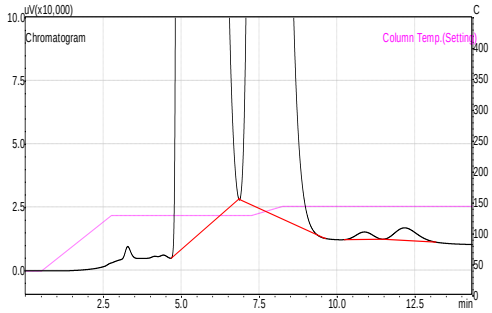

Set			4
Temperature / K			298.15
Concentration / mol·L^{-1}			0.586
Peak No.	**Retention time**	**Area**	**Compound**
1	5.151	2000193790	R-22
2	7.68	76135410	CH_3OCHF_2
3	10.871	105654.9	$(CH_3O)_3CH$
4	12.159	236500.8	C_2H_6O

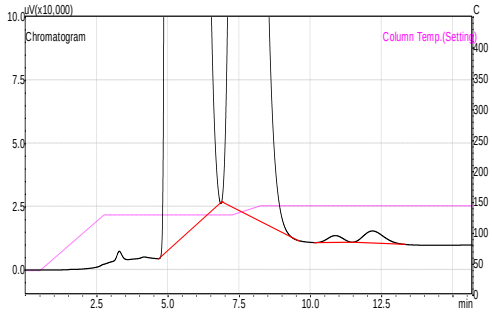

Set			5
Temperature / K			298.15
Concentration / mol·L^{-1}			0.586
Peak No.	**Retention time**	**Area**	**Compound**
1	5.208	1566836269	R-22
2	7.684	56843080.9	CH_3OCHF_2
3	10.872	95484.2	$(CH_3O)_3CH$
4	12.177	231098.4	C_2H_6O

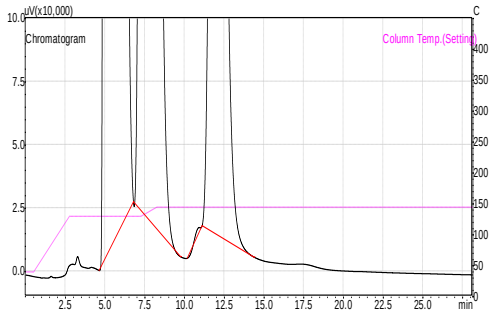

Cold trap			1
Temperature / K			298.15
Concentration / mol·L^{-1}			0.586
Peak No.	**Retention time**	**Area**	**Compound**
1	5.163	1781034858	R-22
2	7.662	121158545.1	CH_3OCHF_2
3	11.103	36229.2	$(CH_3O)_3CH$
4	12.022	31218042	C_2H_6O

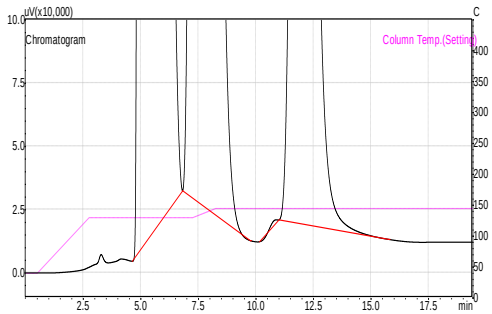

Cold trap			2
Temperature / K			298.15
Concentration / mol·L^{-1}			0.586
Peak No.	**Retention time**	**Area**	**Compound**
1	5.149	1919399870	R-22
2	7.648	133585903.1	CH_3OCHF_2
3	10.879	22847	$(CH_3O)_3CH$
4	11.996	40060702	C_2H_6O

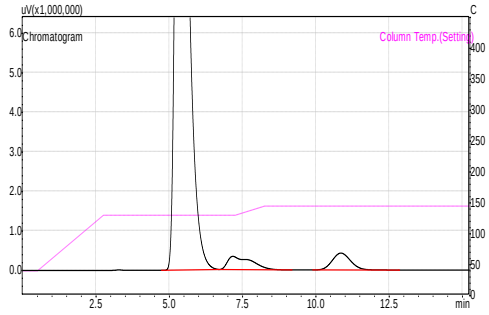

Set			1
Temperature / K			298.15
Concentration / mol·L^{-1}			2
Peak No.	Retention time	Area	Compound
1	5.362	537208385	R-22
2	7.168	18873887	CH_3OCHF_2
3	10.856	18700074	$(CH_3O)_3CH$

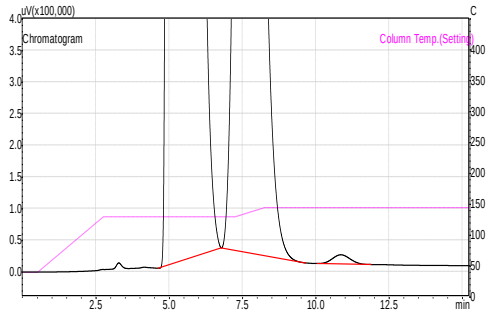

Set			2
Temperature / K			298.15
Concentration / mol·L^{-1}			2
Peak No.	Retention time	Area	Compound
1	5.154	1916011295	R-22
2	7.648	128885391	CH_3OCHF_2
3	10.853	609250.7	$(CH_3O)_3CH$

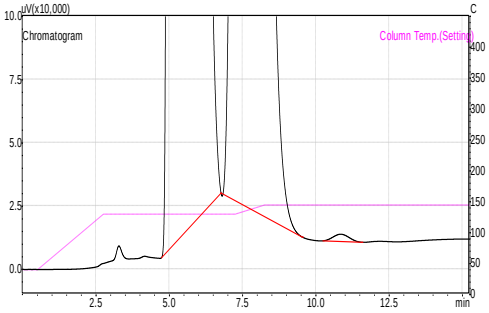

Set			3
Temperature / K			298.15
Concentration / mol·L^{-1}			2
Peak No.	Retention time	Area	Compound
1	5.237	1291749933	R-22
2	7.659	103283714	CH_3OCHF_2
3	10.848	108452.8	$(CH_3O)_3CH$

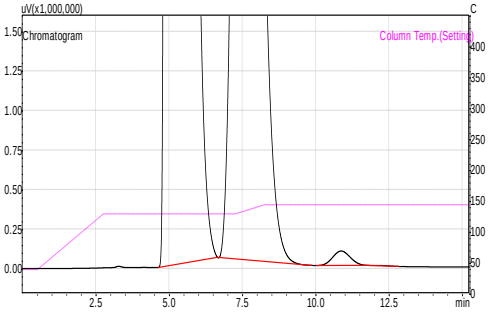

Cold trap			1
Temperature / K			298.15
Concentration / mol·L^{-1}			2
Peak No.	Retention time	Area	Compound
1	5.044	2843909145	R-22
2	7.571	524480651.7	CH_3OCHF_2
3	10.865	3752318.7	$(CH_3O)_3CH$
4	11.738	54243.6	C_2H_6O

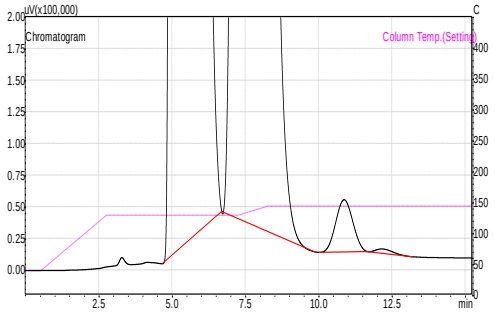

Cold trap			2
Temperature / K			298.15
Concentration / mol·L^{-1}			2
Peak No.	Retention time	Area	Compound
1	5.175	1744876256	R-22
2	7.619	293491756.3	CH_3OCHF_2
3	10.862	1677168.1	$(CH_3O)_3CH$
4	12.153	137845.4	C_2H_6O

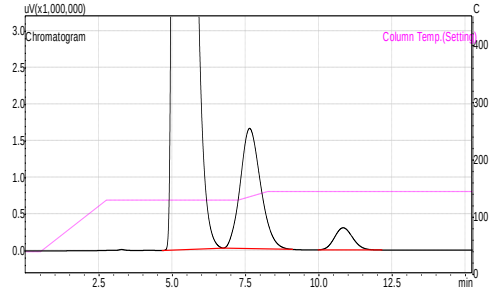

Set			1
Temperature / K			298.15
Concentration / mol·L^{-1}			3.414
Peak No.	Retention time	Area	Compound
1	5.201	1451304982	R-22
2	7.638	79062237	CH_3OCHF_2
3	10.829	13101636	$(CH_3O)_3CH$

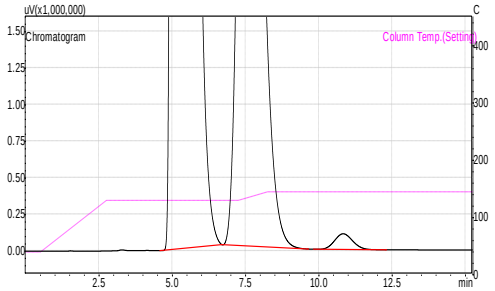

Set			2
Temperature / K			298.15
Concentration / mol·L^{-1}			3.414
Peak No.	Retention time	Area	Compound
1	5.155	1812008724	R-22
2	7.591	307788679	CH_3OCHF_2
3	10.83	4586386.1	$(CH_3O)_3CH$

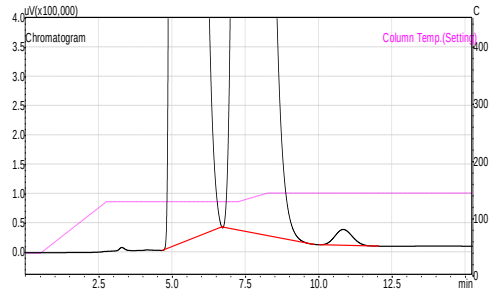

Set			3
Temperature / K			298.15
Concentration / mol·L^{-1}			3.414
Peak No.	Retention time	Area	Compound
1	5.18	1612377023	R-22
2	7.583	364702635	CH_3OCHF_2
3	10.832	1135264.9	$(CH_3O)_3CH$

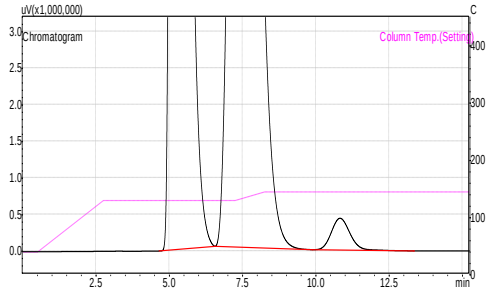

Cold trap			1
Temperature / K			298.15
Concentration / mol·L^{-1}			3.414
Peak No.	**Retention time**	**Area**	**Compound**
1	5.2	1276481680	R-22
2	7.435	1077899819	CH_3OCHF_2
3	10.825	19050388.6	$(CH_3O)_3CH$

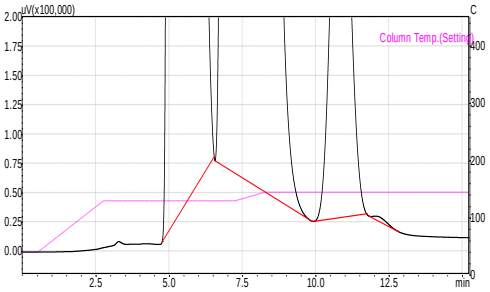

Cold trap			2
Temperature / K			298.15
Concentration / mol·L^{-1}			3.414
Peak No.	**Retention time**	**Area**	**Compound**
1	5.212	1304180212	R-22
2	7.447	1058265477	CH_3OCHF_2
3	10.829	17696799.6	$(CH_3O)_3CH$
4	12.04	118326.4	C_2H_6O

G.1.2. Jacketed glass reactor

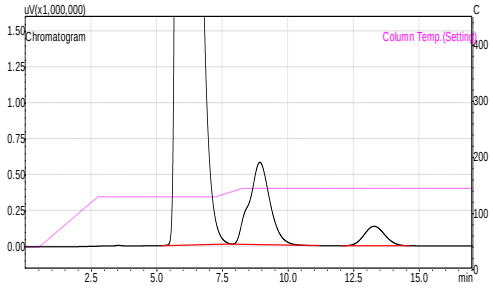

Set			1
Temperature / K			298.15
Concentration / mol·L^{-1}			0.586
Peak No.	Retention time	Area	Compound
1	5.969	902521349	R-22
2	8.921	31376965	CH_3OCHF_2
3	13.276	7469712.5	$(CH_3O)_3CH$

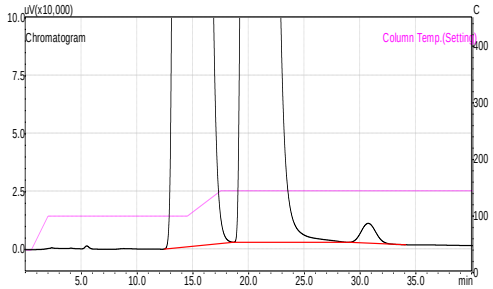

Set			1
Temperature / K			298.15
Concentration / mol·L^{-1}			2
Peak No.	Retention time	Area	Compound
1	14.153	504373110	R-22
2	20.639	444317213	CH_3OCHF_2
3	30.728	783849.3	$(CH_3O)_3CH$

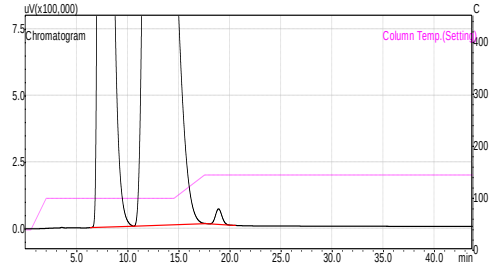

Set			1
Temperature / K			298.15
Concentration / mol·L^{-1}			3.414
Peak No.	Retention time	Area	Compound
1	7.475	593167807	R-22
2	12.472	1125082280	CH_3OCHF_2
3	18.87	2576082.8	$(CH_3O)_3CH$

G.2. Experiments conducted at constant base concentration

G.2.1. Stainless steel reactor

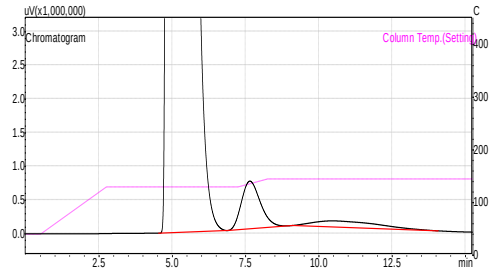

Set			1
Temperature / K			313.15
Concentration / mol·L^{-1}			2
Peak No.	**Retention time**	**Area**	**Compound**
1	4.979	3406855227	R-22
2	7.648	31801633.1	CH_3OCHF_2
3	10.465	14547672.2	$(CH_3O)_3CH$

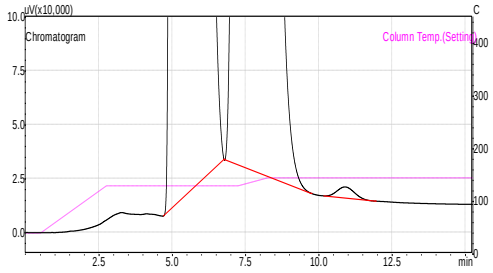

Set			2
Temperature / K			298.15
Concentration / mol·L^{-1}			2
Peak No.	**Retention time**	**Area**	**Compound**
1	5.21	1425012713	R-22
2	7.636	233362301	CH_3OCHF_2
3	10.889	211270.9	$(CH_3O)_3CH$

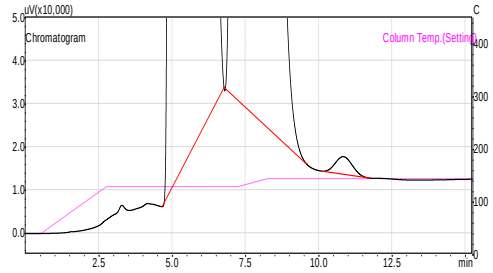

Set			3
Temperature / K			298.15
Concentration / mol·L^{-1}			2
Peak No.	**Retention time**	**Area**	**Compound**
1	5.179	1640209929	R-22
2	7.626	173003877	CH_3OCHF_2
3	10.83	164618.8	$(CH_3O)_3CH$

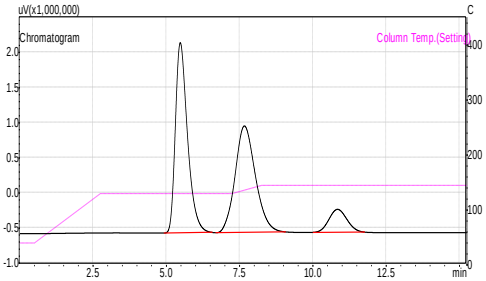

Set			1
Temperature / K			298.15
Concentration / mol·L^{-1}			2
Peak No.	Retention time	Area	Compound
1	5.477	77784544	R-22
2	7.666	72974192	CH_3OCHF_2
3	10.843	13793577	$(CH_3O)_3CH$

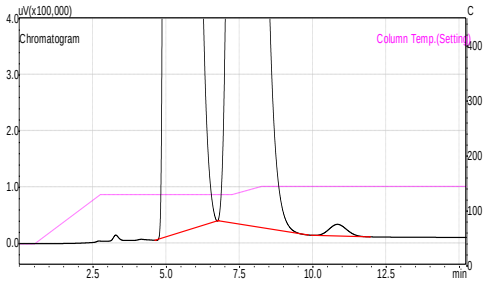

Set			2
Temperature / K			313.15
Concentration / mol·L^{-1}			2
Peak No.	Retention time	Area	Compound
1	5.175	1651483974	R-22
2	7.604	286120975.7	CH_3OCHF_2
3	10.84	868802.1	$(CH_3O)_3CH$

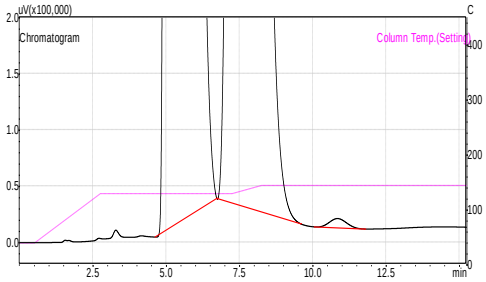

Set			3
Temperature / K			313.15
Concentration / mol·L^{-1}			2
Peak No.	Retention time	Area	Compound
1	5.194	1531494015	R-22
2	7.609	282322175.8	CH_3OCHF_2
3	10.842	334837.9	$(CH_3O)_3CH$

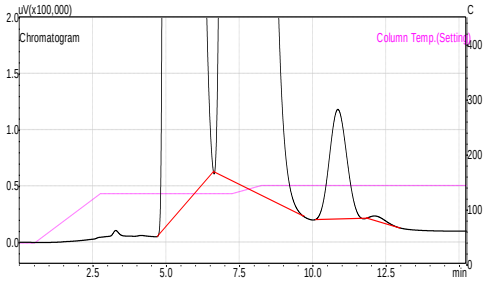

Cold trap			1
Temperature / K			313.15
Concentration / mol·L^{-1}			2
Peak No.	Retention time	Area	Compound
1	5.189	1541338225	R-22
2	7.541	636657585.2	CH_3OCHF_2
3	10.854	3967090.7	$(CH_3O)_3CH$

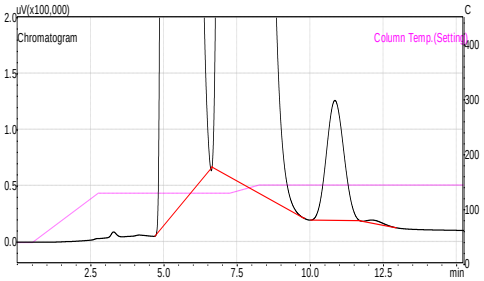

Cold trap			2
Temperature / K			313.15
Concentration / mol·L^{-1}			2
Peak No.	Retention time	Area	Compound
1	5.185	1563685559	R-22
2	7.523	691221148.5	CH_3OCHF_2
3	10.841	4410241.5	$(CH_3O)_3CH$
4	12.096	101788.4	C_2H_6O

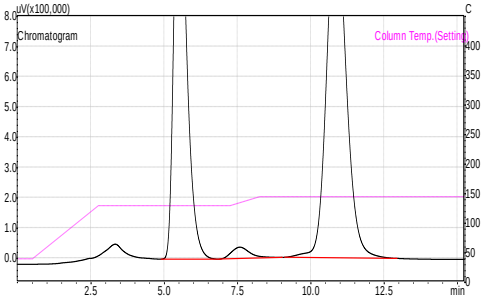

Set			1
Temperature / K			276.94
Concentration / mol·L^{-1}			2
Peak No.	Retention time	Area	Compound
1	5.5	42730471	R-22
2	7.578	1679208	CH_3OCHF_2
3	10.851	52790255	$(CH_3O)_3CH$

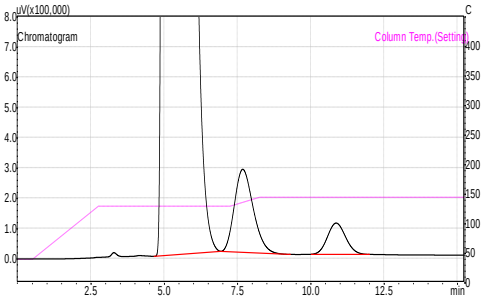

Set			2
Temperature / K			276.94
Concentration / mol·L^{-1}			2
Peak No.	Retention time	Area	Compound
1	5.158	1870522163	R-22
2	7.677	12273690	CH_3OCHF_2
3	10.863	4449710	$(CH_3O)_3CH$

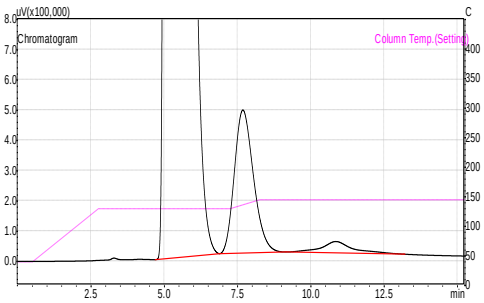

Set			3
Temperature / K			276.94
Concentration / mol·L^{-1}			2
Peak No.	Retention time	Area	Compound
1	5.228	1339275271	R-22
2	7.681	21471219.7	CH_3OCHF_2
3	10.853	2848507.8	$(CH_3O)_3CH$

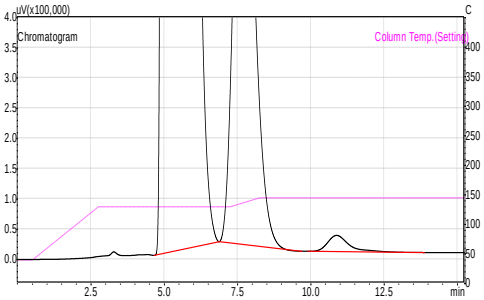

Set			4
Temperature / K			276.94
Concentration / mol·L^{-1}			2
Peak No.	**Retention time**	**Area**	**Compound**
1	5.146	2020630769	R-22
2	7.676	41981185	CH_3OCHF_2
3	10.881	1357740.9	$(CH_3O)_3CH$

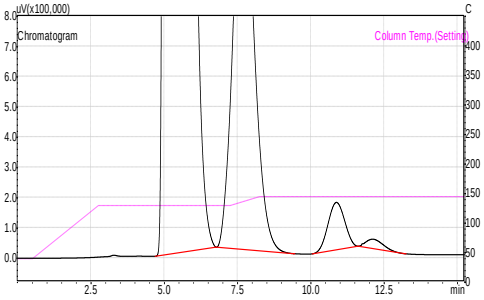

Cold trap			1
Temperature / K			276.94
Concentration / mol·L^{-1}			2
Peak No.	**Retention time**	**Area**	**Compound**
1	5.2	1597085128	R-22
2	7.673	66657590.1	CH_3OCHF_2
3	10.874	6221032.5	$(CH_3O)_3CH$
4	12.105	1275971	C_2H_6O

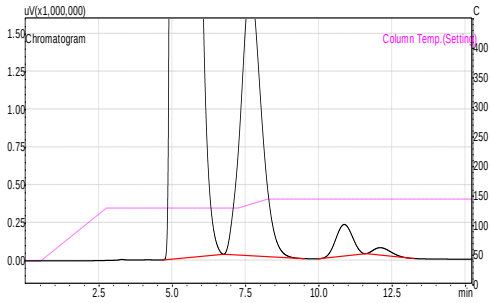

Cold trap			2
Temperature / K			276.94
Concentration / mol·L^{-1}			2
Peak No.	**Retention time**	**Area**	**Compound**
1	5.162	1908166678	R-22
2	7.665	87071801.5	CH_3OCHF_2
3	10.867	8175346.3	$(CH_3O)_3CH$
4	12.096	1996374	C_2H_6O

G.2.2. Jacketed glass reactor

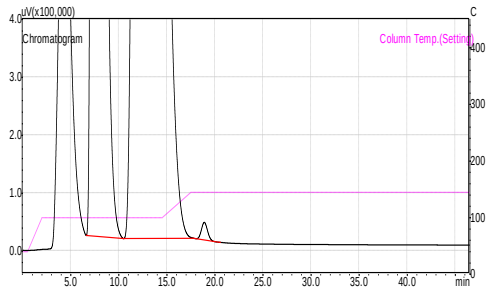

Set			1
Temperature / K			313.15
Concentration / mol·L^{-1}			2
Peak No.	Retention time	Area	Compound
1	7.527	510566961.6	R-22
2	12.478	1190057655	CH_3OCHF_2
3	18.889	1315086.1	$(CH_3O)_3CH$

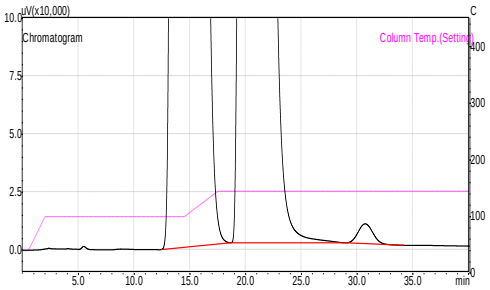

Set			1
Temperature / K			298.15
Concentration / mol·L^{-1}			2
Peak No.	Retention time	Area	Compound
1	14.153	504373110.2	R-22
2	20.639	444317213.2	CH_3OCHF_2
3	30.728	783849.3	$(CH_3O)_3CH$

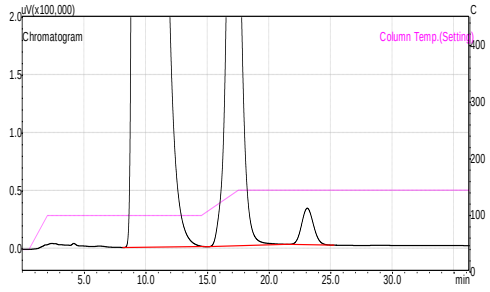

Set			1
Temperature / K			276.94
Concentration / mol·L^{-1}			2
Peak No.	Retention time	Area	Compound
1	9.553	737766821.9	R-22
2	17.081	38853610.8	CH_3OCHF_2
3	23.087	2096197.7	$(CH_3O)_3CH$

APPENDIX H

MATLAB CODE

H.1. Single temperature data-fitting code

H.1.1. Main MATLAB m-file

```
close all
clear all
clc

global c1 time T P_R22 C_methox_0 C_NaCl Ms_tot WF Var_C_NaCl Var_Ms_tot FN2

%----------Read in experimental data


time=xlsread('datafile.xls','data','B25:AI25');          % reaction time for all data points (min)

T=xlsread('datafile.xls','data','B27:AI27');             % temperatures for all data points (Kelvin)
P_R22=xlsread('datafile.xls','data','B29:AI29');         % inlet partial pressure of R22 for all data points
(Pascals)
C_methox_0=xlsread('datafile.xls','data','B31:AI31');    % initial concentration of sodium methoxide for all
data points (mol/m3)
C_NaCl=xlsread('datafile.xls','data','B33:AI33');        % final measured NaCl concentrations for all data
points (mol/m3)
Ms_tot=xlsread('datafile.xls','data','B35:AI35');        % final measured total salt mass in the sample for
all data points (g)
Var_C_NaCl=xlsread('datafile.xls','data','B38:AI38');    % variance of final measured NaCl concentrations
for all data points
Var_Ms_tot=xlsread('datafile.xls','data','B39:AI39');    % variance of final measured total salt mass in the
sample for all data points
```

```
WF=xlsread('datafile.xls','data','B41:AI42');            % Weighting factor for all data points
FN2=xlsread('datafile.xls','data','B30:AI30');             % inlet molar flow-rate of nitrogen for all data
points

P_R22=P_R22/1000;
C_methox_0=C_methox_0/1000;
C_NaCl=C_NaCl/1000;
Var_C_NaCl=Var_C_NaCl/1e+06;

%----------count number of data points

c1=length(T);

%---------set bounds and initial parameter estimates

lb=[0 0 0 0];                                                  % lower bounds for parameter estimates
ub=[inf inf inf inf];                                              % upper bounds for parameter estimates
k0=[18.78 10.47 0.71 22.43];                                   % initial values for parameter estimates


options=optimset('Display','iter','MaxIter',100,'MaxFunEvals',1000,'TolFun',1e-20,'TolX',1e-
20,'LargeScale','on');

[k,resnorm,residual,exitflag,output,lambda,jacobian]=lsqnonlin(@objectivefun1,k0,lb,ub,options);

ci=nlparci(k,residual,jacobian);

%--------Post processing and regression evaluation

C_NaCl_pred=zeros(1,c1);
Ms_tot_pred=zeros(1,c1);
Cfinal_pred=zeros(c1,4);

for c4=1:c1

    tp=time(c4);                    % reaction time for one data point
```

```
    T_p=T(c4);                          % reaction temperature for one data point
    P_R22_p=P_R22(c4);                  % inlet partial pressure of R22 for one data point
    C_methox_0_p=C_methox_0(c4);        % initial concentration of sodium methoxide for one data point
    C_NaCl_p=C_NaCl(c4);                % final measured NaCl concentration for one data point
    Ms_tot_p=Ms_tot(c4);                % final measured total salt mass in the sample for one data point
    WF_p=WF(:,c4);                      % Weighting factors for one data point
    FN2_p=FN2(c4);                      % inlet molar flow-rate of nitrogen for one data point

    C0=[0 C_methox_0_p 0 0];            % set initial conditions

    %------set relative and absolute tolerance for ode solver

    reltol=1e-11;
    abstol=1e-11;


    %-----integrate differential equations
    % note that concentrations cannot be
    % negative, hence set NonNegative for all species

    options=odeset('RelTol',reltol,'AbsTol',abstol,'NonNegative',[1 2 3 4]);
    [t,C]=ode15s(@(t,C) ratefile(t,C,k,T_p,P_R22_p,FN2_p),[0 tp],C0,options);

    c5=length(C);

    Cfinal_pred(c4,:)=C(c5,:);              % final concentrations of all species predicted by the model

    C_NaCl_pred(1,c4)=(WF_p(1))*Cfinal_pred(c4,3);         % predicted final NaCl concentration for one data
point


    Ms_tot_pred(1,c4)=(WF_p(2))*(2e-03*39.997*Cfinal_pred(c4,2) + 2e-03*58.443*Cfinal_pred(c4,3)...
        + 2e-03*41.988*Cfinal_pred(c4,4));                 % predicted final total salt mass in the sample
for one data point
```

```
end


%--------plotting the results

%------------regression results, direct comparision

C_NaCl=C_NaCl.*WF(1,:);
Ms_tot=Ms_tot.*WF(2,:);

figure(1)

plot(C_NaCl,C_NaCl_pred,'o','Marker','o','MarkerEdgeColor','r','MarkerFaceColor','r','MarkerSize',10);

hold on

FFDx=linspace(0,0.6,50);                    % HAVE TO CHECK LIMITS OF CONCENTRATIONS AND ENTER THEM HERE,
this is a 45 degree line
FFDy=linspace(0,0.6,50);

plot(FFDx,FFDy,'k-','LineWidth',2)

axis square

xlabel('Measured NaCl concentration [mol/L]','FontName','Arial','FontSize',20,'FontWeight','normal')
ylabel('Predicted NaCl concentration [mol/L]','FontName','Arial','FontSize',20,'FontWeight','normal')
ylim([0 0.5])
xlim([0 0.5])
set(gca,'FontName','Arial','FontSize',14)
hold off


figure(2)

plot(Ms_tot,Ms_tot_pred,'o','Marker','o','MarkerEdgeColor','b','MarkerFaceColor','b','MarkerSize',10);
```

```
hold on

FFDx=linspace(0,0.8,50);                    % HAVE TO CHECK LIMITS OF MASSES AND ENTER THEM HERE, this is a
45 degree line
FFDy=linspace(0,0.8,50);

plot(FFDx,FFDy,'k-','LineWidth',2)

axis square

xlabel('Measured total salt mass in sample [g]','FontName','Arial','FontSize',20,'FontWeight','normal')
ylabel('Predicted total salt mass in sample [g]','FontName','Arial','FontSize',20,'FontWeight','normal')
ylim([0 0.5])
xlim([0 0.5])
set(gca,'FontName','Arial','FontSize',14)
hold off

%------------regression results, comparison of model profiles with measured
%data


%------Plotting results for run 1

figure(3)

plot(time(1:4),C_NaCl(1:4),'o','Marker','o','MarkerEdgeColor','b','MarkerFaceColor','b','MarkerSize',10);
hold on
plot(time(18:21),C_NaCl(18:21),'o','Marker','o','MarkerEdgeColor','b','MarkerFaceColor','b','MarkerSize',10)
;

%--simulation
tp=25;            % minutes
T_p=283.15;       % Kelvin
P_R22_p=40;       % kPa
C_methox_0_p=2.0;  % mol/L
FN2_p=0.05165;    % mol/min
C0=[0 C_methox_0_p 0 0];
```

```
options=odeset('RelTol',reltol,'AbsTol',abstol,'NonNegative',[1 2 3 4]);
[t,C]=ode15s(@(t,C) ratefile(t,C,k,T_p,P_R22_p,FN2_p),[0 tp],C0,options);

plot(t,C(:,3),'LineStyle','--','Color','g','LineWidth',2);
%-end simulation


axis square

xlabel('Reaction time [min]','FontName','Arial','FontSize',20,'FontWeight','normal')
ylabel('NaCl concentration [mol/L]','FontName','Arial','FontSize',20,'FontWeight','normal')

ylim([0 0.45])
xlim([0 25])
set(gca,'FontName','Arial','FontSize',14)
hold off


%------Plotting results for run 2

figure(4)

plot(time(5:8),C_NaCl(5:8),'o','Marker','o','MarkerEdgeColor','b','MarkerFaceColor','b','MarkerSize',10);
hold on
plot(time(22:25),C_NaCl(22:25),'o','Marker','o','MarkerEdgeColor','b','MarkerFaceColor','b','MarkerSize',10)
;

%--simulation
tp=25;            % minutes
T_p=283.15;       % Kelvin
P_R22_p=60;       % kPa
C_methox_0_p=2.0;  % mol/L
FN2_p=0.034433;    % mol/min
C0=[0 C_methox_0_p 0 0];
```

```
options=odeset('RelTol',reltol,'AbsTol',abstol,'NonNegative',[1 2 3 4]);
[t,C]=ode15s(@(t,C) ratefile(t,C,k,T_p,P_R22_p,FN2_p),[0 tp],C0,options);

plot(t,C(:,3),'LineStyle','--','Color','g','LineWidth',2);
%-end simulation

axis square

xlabel('Reaction time [min]','FontName','Arial','FontSize',20,'FontWeight','normal')
ylabel('NaCl concentration [mol/L]','FontName','Arial','FontSize',20,'FontWeight','normal')
set(gca,'FontName','Arial','FontSize',14)
hold off

ylim([0 0.45])
xlim([0 25])

%--------Plotting results for run 3

figure(5)

plot(time(9:13),C_NaCl(9:13),'o','Marker','o','MarkerEdgeColor','b','MarkerFaceColor','b','MarkerSize',10);
hold on
plot(time(26:30),C_NaCl(26:30),'o','Marker','o','MarkerEdgeColor','b','MarkerFaceColor','b','MarkerSize',10)
;

%--simulation
tp=25;            % minutes
T_p=283.15;       % Kelvin
P_R22_p=50;       % kPa
C_methox_0_p=2.5;  % mol/L
FN2_p=0.043042;    % mol/min
C0=[0 C_methox_0_p 0 0];

options=odeset('RelTol',reltol,'AbsTol',abstol,'NonNegative',[1 2 3 4]);
[t,C]=ode15s(@(t,C) ratefile(t,C,k,T_p,P_R22_p,FN2_p),[0 tp],C0,options);

plot(t,C(:,3),'LineStyle','--','Color','g','LineWidth',2);
```

```
%-end simulation

axis square

xlabel('Reaction time [min]','FontName','Arial','FontSize',20,'FontWeight','normal')
ylabel('NaCl concentration [mol/L]','FontName','Arial','FontSize',20,'FontWeight','normal')
set(gca,'FontName','Arial','FontSize',14)
hold off
ylim([0 0.45])
xlim([0 25])

%-------Plotting results for run 4

figure(6)

plot(time(14:17),C_NaCl(14:17),'o','Marker','o','MarkerEdgeColor','b','MarkerFaceColor','b','MarkerSize',10)
;
hold on
plot(time(31:34),C_NaCl(31:34),'o','Marker','o','MarkerEdgeColor','b','MarkerFaceColor','b','MarkerSize',10)
;

%--simulation
tp=25;            % minutes
T_p=283.15;       % Kelvin
P_R22_p=50;       % kPa
C_methox_0_p=1.5;  % mol/L
FN2_p=0.043042;    % mol/min
C0=[0 C_methox_0_p 0 0];

options=odeset('RelTol',reltol,'AbsTol',abstol,'NonNegative',[1 2 3 4]);
[t,C]=ode15s(@(t,C) ratefile(t,C,k,T_p,P_R22_p,FN2_p),[0 tp],C0,options);

plot(t,C(:,3),'LineStyle','--','Color','g','LineWidth',2);
%-end simulation

axis square
```

```
xlabel('Reaction time [min]','FontName','Arial','FontSize',20,'FontWeight','normal')
ylabel('NaCl concentration [mol/L]','FontName','Arial','FontSize',20,'FontWeight','normal')
set(gca,'FontName','Arial','FontSize',14)
hold off

ylim([0 0.45])
xlim([0 25])
```

H.1.2. Objective function m-file

```
function Fob=objectivefun1(k)

global c1 time T P_R22 C_methox_0 C_NaCl Ms_tot WF Var_C_NaCl Var_Ms_tot FN2

Fob=zeros(2,c1);                    % two rows, and number of columns equal to number of data points
Cfinal_pred=zeros(c1,4);


for c2=1:c1;                        % cycle through data points

    % set conditions for one data point
    tp=time(c2);                    % reaction time for one data point (seconds)
    T_p=T(c2);                      % reaction temperature for one data point
    P_R22_p=P_R22(c2);              % inlet partial pressure of R22 for one data point
    C_methox_0_p=C_methox_0(c2);    % initial concentration of sodium methoxide for one data point
    C_NaCl_p=C_NaCl(c2);            % final measured NaCl concentration for one data point
    Ms_tot_p=Ms_tot(c2);            % final measured total salt mass in the sample for one data point
    Var_C_NaCl_p=Var_C_NaCl(c2);    % variance of final measured NaCl concentration for one data point
    Var_Ms_tot_p=Var_Ms_tot(c2);    % variance of final measured total salt mass in the sample for one data
point
    WF_p=WF(:,c2);                  % Weighting factors for one data point
    FN2_p=FN2(c2);                  % inlet molar flow-rate of nitrogen for one data point
```

```
    C0=[0 C_methox_0_p 0 0];        % set initial conditions for integration, R22, methoxide, Nacl, NaF


    %------set relative and absolute tolerance for ode solver

    reltol=1e-11;
    abstol=1e-11;


    %-----integrate differential equations
    %-----note that concentrations cannot be negative

    options=odeset('RelTol',reltol,'AbsTol',abstol,'NonNegative',[1 2 3 4]);
    [t,C]=ode15s(@(t,C) ratefile(t,C,k,T_p,P_R22_p,FN2_p),[0 tp],C0,options);


    c3=length(C);       % count the number of elements in the C matrix returned by the ODE solver


    Cfinal_pred(c2,:)=C(c3,:);                    % final concentrations of all species predicted by the
model.
                                                  % Rows are data points, columns are species

    %-----compute error between measured and predicted final NaCl concentration

    Fob(1,c2)=(WF_p(1))*10*(Cfinal_pred(c2,3)- C_NaCl_p)/((Var_C_NaCl_p)^0.5);


    %----compute error between measured and predicted final total salt mass in
    %the sample.


    Fob(2,c2)=(WF_p(2))*((2e-03*39.997*Cfinal_pred(c2,2) + 2e-03*58.443*Cfinal_pred(c2,3)...
       + 2e-03*41.988*Cfinal_pred(c2,4))- Ms_tot_p)/((Var_Ms_tot_p)^0.5);
```

```
end

Fob=reshape(Fob,1,[]);
Fob=Fob';
```

H.1.3. Reaction rate m-file

```
function dC=ratefile(t,C,k,T_p,P_R22_p,FN2_p)

global H0 H klAl

dC=zeros(4,1);


k1=k(1);                        % rate constant for first reaction
k2=k(2);                        % rate constant for second reaction
Ksalt=k(3);                     % Stechenov constant for sodium chloride
m=k(4);
% m=20;
% Ksalt=0.87;

if T_p==283.15;
    H0=0.020466;                  % Henry's constant at 10 degrees (dimensionless)
    klAl=0.786;                 % volumetric mass transfer coefficient (1/min)
elseif T_p==293.15;
    H0=0.025574;                  % Henry's constant at 20 degrees
    klAl=0.860;                 % volumetric mass transfer coefficient (1/min)
else
    H0=0.032900;                  % Henry's constant at 30 degrees
    klAl=0.973;                 % volumetric mass transfer coefficient (1/min)
end
```

```
r1=k1*(C(1)^1)*(C(2))^(2);
r2=k2*(C(1)^1)*(C(2))^(1);



% Mixing effects

if (C(3)>=0.18968) && (C(4)>=0.005657)

    klAl=(klAl)*exp(-m*((C(3)-0.18968)+(C(4)-0.005657)));


elseif (C(3)<=0.1896) && (C(4)>=0.005657)

    klAl=(klAl)*exp(-m*(C(4)-0.005657));


end



Cnacl=C(3);
Cnaf=C(4);

%Salting-out effects (three conditions)

%Condition 1

if (Cnacl>=0.18968) && (Cnaf>=0.005657)

    H=H0*exp(Ksalt*(0.18968 + 0.005657));
end
```

```
%Condition 2

if (Cnacl<=0.18968) && (Cnaf>=0.005657)

    H=H0*exp(Ksalt*(Cnacl + 0.005657));
end

%Condition 3

if (Cnacl<=0.18968) && (Cnaf<=0.005657)

    H=H0*exp(Ksalt*(Cnacl + Cnaf));
end



% Gas-phase balance

CRgas_in=(P_R22_p/(8.314*T_p));          % inlet concentration of R22 (mol/L)

alpha=(klAl*1.5)/(2*CRgas_in);           % (L/mol)

beta=(FN2_p)/(2*CRgas_in);               % (dimensionless)

gamma=101.325/(8.314*T_p);               % (mol/L)


delta=(gamma + (H/alpha)*(1+beta) + H*C(1))^2 - 4*gamma*(H/alpha)*(1+alpha*C(1));


CRgas_out=(gamma +(H/alpha)*(1+beta)+ H*C(1) - (delta)^(0.5))/(2);
```

```
% Liquid-phase balances

dC(1)=(klAl/1)*((CRgas_out/H)-C(1))-r1-r2;
dC(2)=-r1-3*r2;
dC(3)=r1+r2;
dC(4)=2*r2;
```

H.2. Total data-fitting code

H.2.1. Main MATLAB m-file

```
close all
clear all
clc

global c1 time T P_R22 C_methox_0 C_NaCl Ms_tot WF Var_C_NaCl Var_Ms_tot Tcent FN2

%----------Read in experimental data


time=xlsread('datafile.xls','totaldata','B4:DC4');          % reaction time for all data points (min)

T=xlsread('datafile.xls','totaldata','B6:DC6');             % temperatures for all data points (Kelvin)
P_R22=xlsread('datafile.xls','totaldata','B8:DC8');         % inlet partial pressure of R22 for all data
points    (Pascals)
C_methox_0=xlsread('datafile.xls','totaldata','B10:DC10');    % initial concentration of sodium methoxide
for all data points (mol/m3)
C_NaCl=xlsread('datafile.xls','totaldata','B12:DC12');        % final measured NaCl concentrations for all
data points (mol/m3)
Ms_tot=xlsread('datafile.xls','totaldata','B14:DC14');        % final measured total salt mass in the sample
for all data points (g)
Var_C_NaCl=xlsread('datafile.xls','totaldata','B17:DC17');    % variance of final measured NaCl
concentrations for all data points
```

```
Var_Ms_tot=xlsread('datafile.xls','totaldata','B18:DC18');    % variance of final measured total salt mass
in the sample for all data points
WF=xlsread('datafile.xls','totaldata','B20:DC21');            % Weighting factor for all data points
FN2=xlsread('datafile.xls','totaldata','B9:DC9');             % inlet molar flow-rate of nitrogen for all
data points

P_R22=P_R22/1000;
C_methox_0=C_methox_0/1000;
C_NaCl=C_NaCl/1000;
Var_C_NaCl=Var_C_NaCl/1e+06;


Tcent=293.15;

%----------count number of data points

c1=length(T);

%---------set bounds and initial parameter estimates

lb=[0 0 0 0 0 0];                                                % lower bounds for parameter estimates
ub=[inf inf inf inf inf inf];                                          % upper bounds for parameter
estimates
A0=[5.6270e+17 6.3476e+09];                                         % initial guess of pre-exonential
factor
Ea=[89114 47620];                                              % initial guess of activation energy (from
Arrhenius plots)

A_prime=A0.*exp(-Ea./(8.314*Tcent));

k0=[A_prime Ea 0.71 22.43];

options=optimset('Display','iter','MaxIter',20,'MaxFunEvals',1000,'TolFun',1e-20,'TolX',1e-
20,'LargeScale','on');

[k,resnorm,residual,exitflag,output,lambda,jacobian]=lsqnonlin(@objectivefun1,k0,lb,ub,options);
```

```
ci=nlparci(k,residual,jacobian);

%--------Post processing and regression evaluation


C_NaCl_pred=zeros(1,c1);
Ms_tot_pred=zeros(1,c1);
Cfinal_pred=zeros(c1,4);

for c4=1:c1

    tp=time(c4);                    % reaction time for one data point
    T_p=T(c4);                      % reaction temperature for one data point
    P_R22_p=P_R22(c4);              % inlet partial pressure of R22 for one data point
    C_methox_0_p=C_methox_0(c4);    % initial concentration of sodium methoxide for one data point
    C_NaCl_p=C_NaCl(c4);            % final measured NaCl concentration for one data point
    Ms_tot_p=Ms_tot(c4);            % final measured total salt mass in the sample for one data point
    WF_p=WF(:,c4);                  % Weighting factors for one data point
    FN2_p=FN2(c4);                  % inlet molar flow-rate for all data points

    C0=[0 C_methox_0_p 0 0];        % set initial conditions

    %------set relative and absolute tolerance for ode solver

    reltol=1e-11;
    abstol=1e-11;



    %-----integrate differential equations
    % note that concentrations in the temporal plane cannot be
    % negative, hence set NonNegative for all species

    options=odeset('RelTol',reltol,'AbsTol',abstol,'NonNegative',[1 2 3 4]);
    [t,C]=ode15s(@(t,C) ratefile(t,C,k,T_p,P_R22_p,FN2_p),[0 tp],C0,options);
```

```
    c5=length(C);

    Cfinal_pred(c4,:)=C(c5,:);              % final concentrations of all species predicted by the model

    C_NaCl_pred(1,c4)=(WF_p(1))*Cfinal_pred(c4,3);         % predicted final NaCl concentration for one data
point


    Ms_tot_pred(1,c4)=(WF_p(2))*(2e-03*39.997*Cfinal_pred(c4,2) + 2e-03*58.443*Cfinal_pred(c4,3)...
        + 2e-03*41.988*Cfinal_pred(c4,4));                 % predicted final total salt mass in the sample
for one data point


end


%--------plotting the results

%------------regression results, direct comparision

C_NaCl=C_NaCl.*WF(1,:);
Ms_tot=Ms_tot.*WF(2,:);

figure(1)

plot(C_NaCl,C_NaCl_pred,'o','Marker','o','MarkerEdgeColor','r','MarkerFaceColor','r','MarkerSize',10);

hold on

FFDx=linspace(0,0.6,50);                    % HAVE TO CHECK LIMITS OF CONCENTRATIONS AND ENTER THEM HERE,
this is a 45 degree line
FFDy=linspace(0,0.6,50);
ylim([0 0.6])
xlim([0 0.6])
plot(FFDx,FFDy,'k-','LineWidth',2)
```

```
axis square

xlabel('Measured NaCl concentration [mol l^{-1}]','FontName','Arial','FontSize',20,'FontWeight','normal')
ylabel('Predicted NaCl concentration [mol/L]','FontName','Arial','FontSize',20,'FontWeight','normal')
set(gca,'FontName','Arial','FontSize',14)
hold off


figure(2)

plot(Ms_tot,Ms_tot_pred,'o','Marker','o','MarkerEdgeColor','b','MarkerFaceColor','b','MarkerSize',10);

hold on

FFDx=linspace(0,0.5,50);                    % HAVE TO CHECK LIMITS OF MASSES AND ENTER THEM HERE, this is a
45 degree line
FFDy=linspace(0,0.5,50);

plot(FFDx,FFDy,'k-','LineWidth',2)

axis square

xlabel('Measured total salt mass in sample [g]','FontName','Arial','FontSize',20,'FontWeight','normal')
ylabel('Predicted total salt mass in sample [g]','FontName','Arial','FontSize',20,'FontWeight','normal')
set(gca,'FontName','Arial','FontSize',14)
hold off

%------------regression results, comparison of model profiles with measured
%data

Activation_energy=k(3:4)

Preexponential=k(1:2)./(exp(-k(3:4)./(8.314*Tcent)))
```

H.2.2. Reaction rate m-file

```
function dC=ratefile(t,C,k,T_p,P_R22_p,FN2_p)

global H Tcent

dC=zeros(4,1);


if T_p==283.15;
    H0=0.020466;                    % Henry's constant at 10 degrees (dimensionless)
    klAl=0.786;                    % volumetric mass transfer coefficient (1/min)
elseif T_p==293.15;
    H0=0.025574;                    % Henry's constant at 20 degrees
    klAl=0.860;                    % volumetric mass transfer coefficient (1/min)
else
    H0=0.032900;                    % Henry's constant at 30 degrees
    klAl=0.973;                    % volumetric mass transfer coefficient (1/min)
end

k1=k(1)*exp((-k(3)/8.314)*(1/T_p - 1/Tcent));                      % rate constant for first reaction
k2=k(2)*exp((-k(4)/8.314)*(1/T_p - 1/Tcent));                     % rate constant for second reaction

r1=k1*(C(1)^1)*(C(2))^(2);
r2=k2*(C(1)^1)*(C(2))^(1);

Knacl=k(5);                     % Stechenov constant for sodium chloride
m=k(6);


if (C(3)>=0.18968) && (C(4)>=0.005657)

    klAl=(klAl)*exp(-m*((C(3)-0.18968)+(C(4)-0.005657)));
```

```
elseif (C(3)<=0.1896) && (C(4)>=0.005657)

    klAl=(klAl)*exp(-m*(C(4)-0.005657));


end


Cnacl=C(3);

if Cnacl >= 0.18968

    H=H0*exp(Knacl*0.18968);
else
    H=H0*exp(Knacl*C(3));
end


CRgas_in=(P_R22_p/(8.314*T_p));          % inlet concentration of R22 (mol/L)

alpha=(klAl*1.5)/(2*CRgas_in);           % (L/mol)

beta=(FN2_p)/(2*CRgas_in);               % (dimensionless)

gamma=101.325/(8.314*T_p);               % (mol/L)


delta=(gamma + (H/alpha)*(1+beta) + H*C(1))^2 - 4*gamma*(H/alpha)*(1+alpha*C(1));


if delta<=0
    delta=0;
end
```

```
CRgas_out=(gamma +(H/alpha)*(1+beta)+ H*C(1) - (delta)^(0.5))/(2);


dC(1)=(klAl/1)*((CRgas_out/H)-C(1))-r1-r2;
dC(2)=-r1-3*r2;
dC(3)=r1+r2;
dC(4)=2*r2;
```